UNIVERSITÄTSKLINIKUM HAMBURG-EPPENDORF

Institut für Medizinische Mikrobiologie, Virologie und Hygiene

Prof. Dr. med. Martin Aepfelbacher

Super-resolved and live visualization of *Yersinia* type three secretion system components

Dissertation

zur Erlangung des Doktorgrades Dr. rer. biol. hum.
an der Medizinischen Fakultät der Universität Hamburg

vorgelegt von:
Alexander Carsten
aus Einbeck

Hamburg 2023

Für Paps

Table of contents

1 Abstract

1.1 Abstract

Yersinia enterocolitica harbors a type 3 secretion system (T3SS) to translocate effector proteins into host cells. This complicated macromolecular nanomachine has dimensions of approximately 120 nm length and up to 30 nm width. To visualize components of the T3SS and resolve them from each other, (live-) super-resolution fluorescence microscopy is the preferred tool. However, to date only a handful of studies have been published employing super-resolution fluorescence microscopy to gain insights into the T3SS. Furthermore, the established super-resolution microscopy techniques STED and STORM do not provide enough resolution to resolve single T3SS components or even proteins.

In this work the recently introduced MINFLUX microscopy, which offers resolutions and localization precisions down to single-digit nanometers, was used to visualize various T3SS components *in situ*, i.e., in contact with infected cells. MINFLUX in combination with nanobody labeling of a tagged translocation pore protein enabled for the first time the visualization of translocation pores down to the single molecular level. The data indicated that the size of the *Y. enterocolitica* T3SS translocation pore is approximately 18 nm. Furthermore, a T3SS sorting platform complex formed by a single component was visualized at the actual size within a whole bacterium. For this, 3D-MINFLUX reaching isotropic localization precisions in the single digit nanometer range was established. It revealed that the majority of sorting platforms are localized in the periphery of the bacteria. In addition, 2 color MINFLUX microscopy was used to co-visualize a sorting platform and a translocation pore protein of the same T3SS. Finally, live cell 2D- and 3D-STED microscopy were used to visualize single translocation pores during a cell infection over a long time frame. Altogether this work provided new insights into the organization and distribution of the translocation pore and sorting platform in the *Y. enterocolitica* T3SS. The new MINFLUX technology, applied here for the first time to a bacterial molecular machine, will enable unprecedented opportunities for imaging molecular details and movements in bacteria end eukaryotes alike.

1.2 Zusammenfassung

Yersinia enterocolitica besitzt ein Typ 3 Sekretionssystem (T3SS) um Effektorproteine in Wirtszellen zu injizieren. Diese komplexe makromolekulare Nanomaschine hat Abmessungen von etwa 120 nm Länge und bis zu 30 nm Breite. Um die Komponenten des T3SS voneinander aufgelöst sichtbar zu machen, ist hochauflösende (Live-) Fluoreszenzmikroskopie die bevorzugte Technologie. Bislang gibt es jedoch nur wenige veröffentlichte Studien, in denen hochauflösende Fluoreszenzmikroskopie zur Untersuchung des T3SS eingesetzt wurde. Darüber hinaus haben die etablierten hochauflösenden Mikroskopietechniken STED und STORM nicht genügend Auflösungsvermögen, um einzelne T3SS-Komponenten oder sogar Proteine aufzulösen. In dieser Arbeit wurde die kürzlich eingeführte MINFLUX-Mikroskopie verwendet, die eine Auflösung und Lokalisierungspräzision bis in den einstelligen Nanometerbereich erreicht, um verschiedene T3SS-Komponenten *in situ*, d. h. in Kontakt mit infizierten Zellen, sichtbar zu machen. MINFLUX in Kombination mit einer Nanobody-Färbung eines markierten Proteins der T3SS Translokationspore ermöglichte zum ersten Mal die Visualisierung von Translokationsporen bis auf Einzelmolekülebene. Diese Daten zeigten, dass die Größe der T3SS-Translokationspore von *Y. enterocolitica* etwa 18 nm beträgt. Darüber hinaus wurde ein Proteinkomplex der T3SS „sorting platform", der aus einer einzigen Komponente besteht, in seiner tatsächlichen Größe innerhalb eines ganzen Bakteriums sichtbar gemacht. Hierfür wurde 3D-MINFLUX etabliert, die isotrope Lokalisierungsgenauigkeiten im einstelligen Nanometerbereich erreichte. Es zeigte sich, dass die Mehrzahl der „sorting platforms" in der Peripherie des Bakteriums lokalisiert ist. Darüber hinaus wurde 2-Farben-MINFLUX-Mikroskopie verwendet, um eine „sorting platform" und ein Protein der Translokationspore im selben T3SS darzustellen. Zusätzlich wurden 2D- und 3D-STED-Mikroskopie in lebenden Zellen eingesetzt, um einzelne Translokationsporen über einen langen Zeitraum zu visualisieren.

Insgesamt lieferte diese Arbeit neue Erkenntnisse über die Organisation und Verteilung der Translokationspore und der „sorting platform" im T3SS von *Y. enterocolitica.* Die neue MINFLUX-Technologie, die hier zum ersten Mal auf eine bakterielle molekulare Maschine angewandt wurde, wird nie dagewesene Möglichkeiten für die Darstellung molekularer Details und Dynamiken in Bakterien und Eukaryoten gleichermaßen bieten.

2 Introduction

2.1 Pathogenic *Yersinia*

Belonging to the family of Yersiniaceae, the genus *Yersinia* includes 28 different species of which three are human pathogens: the enteropathogenic species *Yersinia enterocolitica* and *Yersinia pseudotuberculosis* and the causative agent of the bubonic plague *Yersinia pestis* (Adeolu et al., 2016, Parte et al., 2020). The latter species was first isolated by A. Yersin and S. Kitasato in 1894 from human tissue (Treille and Yersin, 1894, Kitasato, 1894). *Yersinia* are gram-negative pleomorphic rods and have a facultative anaerobe lifestyle. They are catalase positive, oxidase negative, do not form endospores and have the ability to grow at 0-4 °C, although their optimal growth takes place at 24-27 °C (Fredriksson-Ahomaa, 2007). After *Campylobacter* spp. and *Salmonella* spp. the enteropathogenic *Yersinia* species are the third most common bacterial agent of gastroenteritis in Europe (Rosner et al., 2010, van Pelt, 2003, McNally et al., 2016). *Y. enterocolitica* and *Y. pseudotuberculosis* are mostly transmitted via contaminated food, especially contaminated pork meat (Jalava et al., 2006, Bottone, 1997) and cause an often self-limiting infection called yersiniosis, which is restricted to the gastrointestinal tract and the intestinal lymphatic system most of the time.

In contrast, *Y. pestis* is transmitted via aerosols or via a bite of the rat flea. Today this disease is no acute threat anymore as it can be treated with antibiotics, but it is fatal in most cases if left untreated (Brubaker, 2003).

Evolutionary, *Y. pestis* and *Y. pseudotuberculosis* are closely related. *Y. enterocolitica* split off from their common ancestor about 200 million years ago, whilst *Y. pestis* developed from *Y. pseudotuberculosis* about 5,700 – 6,000 years ago (Achtman et al., 1999, Andrades Valtuena et al., 2017, Rascovan et al., 2019, Rasmussen et al., 2015, Spyrou et al., 2018).

Despite the different routes of infection, all *Yersinia* species share a tropism for lymphatic tissue. Furthermore, the human pathogenic *Yersinia* can replicate extracellularly in micro abscesses and impair the hosts innate immune response (Cornelis and Wolf-Watz, 1997). The *Yersinia* virulence is mediated through multiple chromosomal and plasmid associated factors. All human pathogenic *Yersinia* species harbor a 70 kb virulence plasmid called pYV (plasmid of *Yersinia* virulence) which encodes for all proteins of the Ysc (*Yersinia* secretion) type 3 secretion

system (T3SS) and its Yop (*Yersinia* outer protein) effectors. The Yop effectors get translocated from the bacterium through the T3SS into the host cells cytoplasm and inhibit phagocytosis and impair the host cells immune response (Viboud and Bliska, 2005, Pha and Navarro, 2016).

2.2 Yersinia enterocolitica

Y. enterocolitica is the more common causative agent of yersiniosis and enters the gastrointestinal tract of humans mostly via contaminated food products such as pork meat, but also contaminated milk, tofu and water (Jones et al., 2003, Fredriksson-Ahomaa et al., 2006, Lynch et al., 2006, Bonardi et al., 2010).

2.2.1 Classification

Y. enterocolitica is a heterogenous species and can be divided into six biovars (1A, 1B, 2-5) by biochemical reactions. It can be further divided into more than 50 different serotypes by differentiation of specific presented antigens on the bacterial surface (Wauters et al., 1987, Aleksic and Bockemuhl, 1984, Sabina et al., 2011). Most relevant serotypes for research are O:4, O:8, O:13, O:18, O:20 and O:21 of biovar 1B, which are medically relevant and spread in Northern America, as well as the European biovars 2 and 4 with their serotypes O:3, O:5 and O:9.

The serotypes O:3, O:8 and O:9 are the most abundant ones in clinical isolates (Fredriksson-Ahomaa, 2007, Galindo et al., 2011). Strains of the biovar 1A do not harbor a virulence plasmid and are thus considered as apathogenic (Bottone, 1999). *Yersinia* of biovar 1B show the highest pathogenicity (Wren, 2003). The *Y. enterocolitica* strain WA-314 that was investigated in this study belongs to this biovar and serotype O:8 (Heesemann and Laufs, 1983). Bacteria belonging to this serotype show a specifically strong binding to mucus and the colonialization of peyer plaques (Mantle and Husar, 1993, Grutzkau et al., 1990). These bacteria also contain yersiniabactin, a siderophore-dependent iron absorption system which is encoded at the *High-Pathogenicity island (HPI)* of the virulence plasmid. This system allows *Yersinia* growth also under iron limiting conditions (Sabina et al., 2011, Perry and Fetherston, 2011).

2.2.2 Yersiniosis

Enteropathogenic *Yersinia* cause an enterocolitis with the mostly self-regulating symptoms of abdominal pain, diarrhea caused by the enterotoxin Yst and mild fever (Pai and Mors, 1978, Takao et al., 1984, Bottone, 1997, Drummond et al., 2012). These symptoms are caused by a gastrointestinal infection including enteritis, terminal ileitis or mesenteric lymphadenitis (Gurry, 1974, Lee et al., 1990, Galindo et al., 2011). Only in rare cases post-infectious immunopathologic complications such as reactive arthritis or erythema nodosum can follow (Fredriksson-Ahomaa et al., 2006, Galindo et al., 2011). The infectious dose of *Y. enterocolitica* is not exactly known, numbers vary between 10^4 to 10^6 (Food and Drug Administration, 2012) and 10^9 (Schaake et al., 2014). In general, the highest infection rates can be seen with small children under 4 years. The majority of the 7,000 cases of yersiniosis in Europe occurs in Germany (Galindo et al., 2011, European Centre for Disease Prevention and Control, 2022), likely due to frequency and method of diagnosis, but also due to the higher consumption of raw pork meat in Germany (Rosner et al., 2010). The overall fatality rate of yersiniosis is around 0.05 % (European Centre for Disease Prevention and Control, 2022), caused by septicemia occurring in immunocompromised patients or patients with states of iron overload such as reactive hemolytic anemia (Bottone, 1997).

2.2.3 Pathogenesis and route of infection

Y. enterocolitica infections usually occur because of consumption of contaminated food or water, rarely directly via blood transfusions. The bacteria survive the acidic environment of the stomach by expressing urease (de Koning-Ward et al., 1995, Agrain et al., 2005, Bhagat and Virdi, 2009). The crucial pathogen-host cell interaction takes place in the follicle associated epithelium (FAE) of the ileum (Autenrieth and Firsching, 1996) where *Yersinia* have to pass the gastrointestinal mucus. The expressed invasin (inv) and attachment invasion locus (ail) proteins are used by *Yersinia* to invade M (microfold)-cells overlaying Peyer's patches (Pepe and Miller, 1993, Fredriksson-Ahomaa et al., 2006, Grutzkau et al., 1990). Invasin activates integrins of the M-cells, followed by restructuring of the cells cytoskeleton in a way that *Yersinia* get internalized (Wong and Isberg, 2005). After *Yersinia* get released from M-cells they come into contact with immune cells such as macrophages or neutrophils (Jepson and Clark, 1998). The translocation of anti-

phagocytic bacterial effector proteins through the T3SS allows *Y. enterocolitica* to impair the hosts immune system and to replicate extracellularly in lymphatic tissue and to form microcolonies (Cornelis et al., 1998, Viboud and Bliska, 2005, Aepfelbacher et al., 2007). *In vivo* studies in mice showed that *Y. enterocolitica* destroys the FAE and Peyer's patches five to seven days after infection (Autenrieth and Firsching, 1996). From there on, *Yersinia* spread to mesenterial lymph nodes to further disseminate to inner organs such as spleen and liver (Pepe and Miller, 1993, Pepe et al., 1995, Cornelis and Wolf-Watz, 1997).

2.3 *Yersinia* virulence factors

The infection strategy of *Y. enterocolitica* is based on a variety of virulence factors that allow survival and replication inside the host (Atkinson and Williams, 2016). Both chromosomal- and plasmid-encoded virulence factors come into play during different stages of infection.

2.3.1 Chromosomal and plasmid encoded virulence factors

Chromosomal virulence factors such as *ail* and *inv* play an important role in the early stages of the infection process, namely host cell attachment (Atkinson and Williams, 2016, Pepe and Miller, 1993) and invasion of the intestinal epithelium (Miller and Falkow, 1988). Invasin is a bacterial protein covering the bacterial surface (Grosdent et al., 2002). Invasin allows efficient and highly affine binding to the host cells integrin proteins, resulting in a restructuring of the cytoskeleton and, ultimately, internalization of bacteria (Van Nhieu and Isberg, 1991, Atkinson and Williams, 2016). The highest expression of integrin takes place at 26 °C whilst its expression is lowered at 37 °C (Simonet and Falkow, 1992). In contrast, the bacterial surface protein Ail (attachment invasion locus) is expressed at 37 °C (Miller and Falkow, 1988) and plays a role in binding to epithelial cells (Chauhan et al., 2016). Additionally, Ail is important for serum resistance of Yersinia (Miller et al., 1989, Pierson and Falkow, 1993) and protects the bacteria from complement killing by the host (Kirjavainen et al., 2008).

In contrary, the plasmid encoded virulence factors play an important role in the later stage of infection, e.g. to establish and maintain the actual infection. The 70 kb pYV (plasmid of *Yersinia* virulence) plasmid encodes for all structural Ysc (*Yersinia*

secretion) proteins of the T3SS, Yop (*Yersinia* effector protein) effector proteins that get translocated through the T3SS, their regulatory proteins such as chaperones and also the adhesin YadA (*Yersinia* adhesin A). YadA forms a fibrillary matrix on the bacterial surface and mediates binding to host cell integrins (Muhlenkamp et al., 2015, Deuschle et al., 2016). Plasmid encoded virulence factors are highly expressed at 37 °C and low Calcium concentrations (Cornelis et al., 1998), in vivo secretion and translocation of effector proteins are triggered by cell contact (Rosqvist et al., 1994, Nordfelth and Wolf-Watz, 2001). Controlled blocking of secretion is caused by a protein complex ("calcium plug") formed by YopN, TyeA, YscB and SycN (Day and Plano, 1998, Ferracci et al., 2005, Joseph and Plano, 2013).

2.3.2 The type three section system (T3SS)

Throughout various bacterial species there are numerous types of secretion systems (Filloux, 2022, Green and Mecsas, 2016). A recent study proposed a type 11 secretion system, which also reflects the number of different types of secretion systems (Grossman et al., 2021). This study focusses solely on the type 3 secretion system, consequently this is the only one that will be described in the next paragraphs.

The T3SS, which is also called injectisome, is a complex bacterial nanomachine consisting of more than 20 different proteins with a total molecular weight of around 6 MDa (Dey et al., 2019, Torres-Vargas et al., 2019). It is an essential bacterial virulence factor, necessary for the translocation of effector proteins into host cells in *Y. enterocolitica*. From proximal to distal end it has a length of approximately 120 nm and the maximal width of some components is around 30 nm. It was first described in 1994 in *Yersinia* spp. (Rosqvist et al., 1994). Evolutionary, it is related to bacterial flagella needed for bacterial motility, which can also be seen in structural and functional similarities (Diepold and Armitage, 2015). Among the up to eleven known different secretion systems, the T3SS is the best studied and also most abundant one among numerous bacterial species (Tseng et al., 2009, Costa et al., 2015, Green and Mecsas, 2016). In general, three different classes of T3SSs can be distinguished: The Ysc-injectisome present in *Yersinia* spp., *Pseudomonas* spp. and *Aeromonas* spp. (Troisfontaines and Cornelis, 2005, Cornelis, 2006), the Inv-Mxi-Spa-injectisome in *Salmonella* SPI-1, *Shigella* spp. and *Chlamydia* spp.

(Cornelis and Van Gijsegem, 2000, Mota et al., 2005) and the Ssa-Esc-injectisome present in *Escherichia coli* and *Salmonella* SPI-2 (Diepold et al., 2015). A bacterial species can not only have different variants of the same secretion system class, but also different types of secretion systems. For example, *Y. enterocolitica* biovar 1B not only harbors the plasmid encoded Ysc-T3SS and the chromosomically encoded Ysa-T3SS but in addition a type 2 secretion system and a type 6 secretion system (Foultier et al., 2003, Young and Young, 2002, Bent et al., 2015, Yang et al., 2018). The published number and distribution of present T3SSs per bacterium are highly variable, depending on organism and also most likely experimental conditions. Numbers range from 10-30 injectisomes in *Y. enterocolitica* to 50-100 injectisomes in *Shigella* or also 10-100 injectisomes for *Salmonella* SPI-1 (Diepold and Armitage, 2015, Blocker et al., 1999, Notti et al., 2015).

2.3.2.1 Components of the type 3 secretion system

The structure of the majority of injectisome components is well known and resolved by cryo-electron microscopy and –tomography in various bacteria (e.g. Park et al., 2018, Berger et al., 2021, Marlovits and Stebbins, 2010, Torres-Vargas et al., 2019). In Fig. 1 a schematic illustration of the T3SS is depicted (derived from Torres-Vargas et al., 2019). Here, the proposed unified nomenclature using the prefix Sct of T3SS components is shown in parallel to the *Yersinia* specific Ysc nomenclature (Wagner and Diepold, 2020). Throughout this thesis the *Yersinia* specific Ysc nomenclature is used. A translation table between Sct and Ysc nomenclature is provided in Fig. 1. The T3SS can generally be divided into basal body, export apparatus, sorting platform, needle filament and needle tip/translocon.

The basal body (Fig. 1, orange) is the basis of the whole T3SS and forms concentric rings that span the inner and outer bacterial membranes. While YscC, the first secreted component of the injectisome, forms a protein ring in the outer bacterial membrane, YscD and YscJ create a ring in the inner bacterial membrane (Diepold et al., 2010, Koster et al., 1997, Ross and Plano, 2011). The insertion of these protein rings into the bacterial membranes takes place in the Sec dependent phase, characterized by cleavable amino-terminal secretion signals (Kubori et al., 2000, Kimbrough and Miller, 2000, Deng et al., 2017).

The export apparatus (Fig. 1, red) serves as a gate for effector proteins that need to pass the bacterial inner membrane during the process of translocation (Butan et

al., 2019). This complex is composed of the proteins YscR, YscS, YscT, YscU and YscV (Wagner et al., 2010).

The sorting platform (Fig. 1, light blue) is a dynamic intrabacterial injectisome component consisting of the proteins YscN, YscL, YscQ and YscK. The sorting platform can be found both injectisome bound and also freely diffusing. Additionally, several intermediate protein complexes of the sorting platform are proposed (Rocha et al., 2018, Prindle et al., 2022). Generally, the sorting platform is responsible for the recruitment of chaperone substrate complexes and the regulation of the export order of those complexes (Lara-Tejero et al., 2011). For this, the ATPase complex formed by YscN localizes to the C-ring and export apparatus (TTSS phase) which enables the secretion of the early substrates essential for needle formation and the secretion of middle substrates (translocators) and late substrates (effector proteins) (Dewoody et al., 2013). In addition, the ATPase complex detaches the substrates from their chaperones and unfolds the proteins which is necessary for protein export (Neyt and Cornelis, 1999, Akeda and Galan, 2005, Foultier et al., 2003, Wattiau et al., 1994, Roblin et al., 2015). While YscQ is forming the cytoplasmic ring of the sorting platform, YscK seems to function as a connection between the ATPase complex (formed by YscN and YscL) and YscQ, apart from that its function remains unknown (Diepold et al., 2017). YscL functions as a negative regulator of the ATPase YscN (Blaylock et al., 2006).

In the early stages of secretion, YscI forms a tunnel that allows substrates to pass the inner bacterial membrane (Allaoui et al., 1995, Sukhan et al., 2003, Marlovits et al., 2004, Wood et al., 2008, Sal-Man et al., 2012). The needle filament (Fig. 1, green) itself is formed by helical polymerization of YscF (Hoiczyk and Blobel, 2001, Hu et al., 2018, Achtman et al., 1999). It has a diameter of only 2 – 3 nm and, in *Y. enterocolitica,* an average length of 58 nm, but the needle length can vary between species ranging from 30 – 80 nm in different species (Kubori et al., 1998, Blocker et al., 2001, Hoiczyk and Blobel, 2001, Poyraz et al., 2010, Cordes et al., 2003, Marlovits et al., 2006, Miletic et al., 2020, Journet et al., 2003). The needle length is defined by the inner rod protein YscP (Marlovits et al., 2006). After the formation of the needle, a substrate switch takes place and the tip complex protein LcrV is attached to the distal end of the needle (Mueller et al., 2005). LcrV forms a pentameric protein platform (Fig. 1, dark blue 1) for the formation of a translocation pore also called translocon, comprised of the hydrophobic transmembrane proteins

YopB and YopD within the host cell membrane (Broz et al., 2007, Mueller et al., 2008). So far, the structure and precise composition of the pore complex is not exactly known. Anyhow, there are studies that suggest that the translocon forms a putatively 8:8 hexadecameric ring-structure with an inner opening of approximately 1.2 - 3.5 nm (Hakansson et al., 1996, Romano et al., 2016, Neyt and Cornelis, 1999, Park et al., 2018).

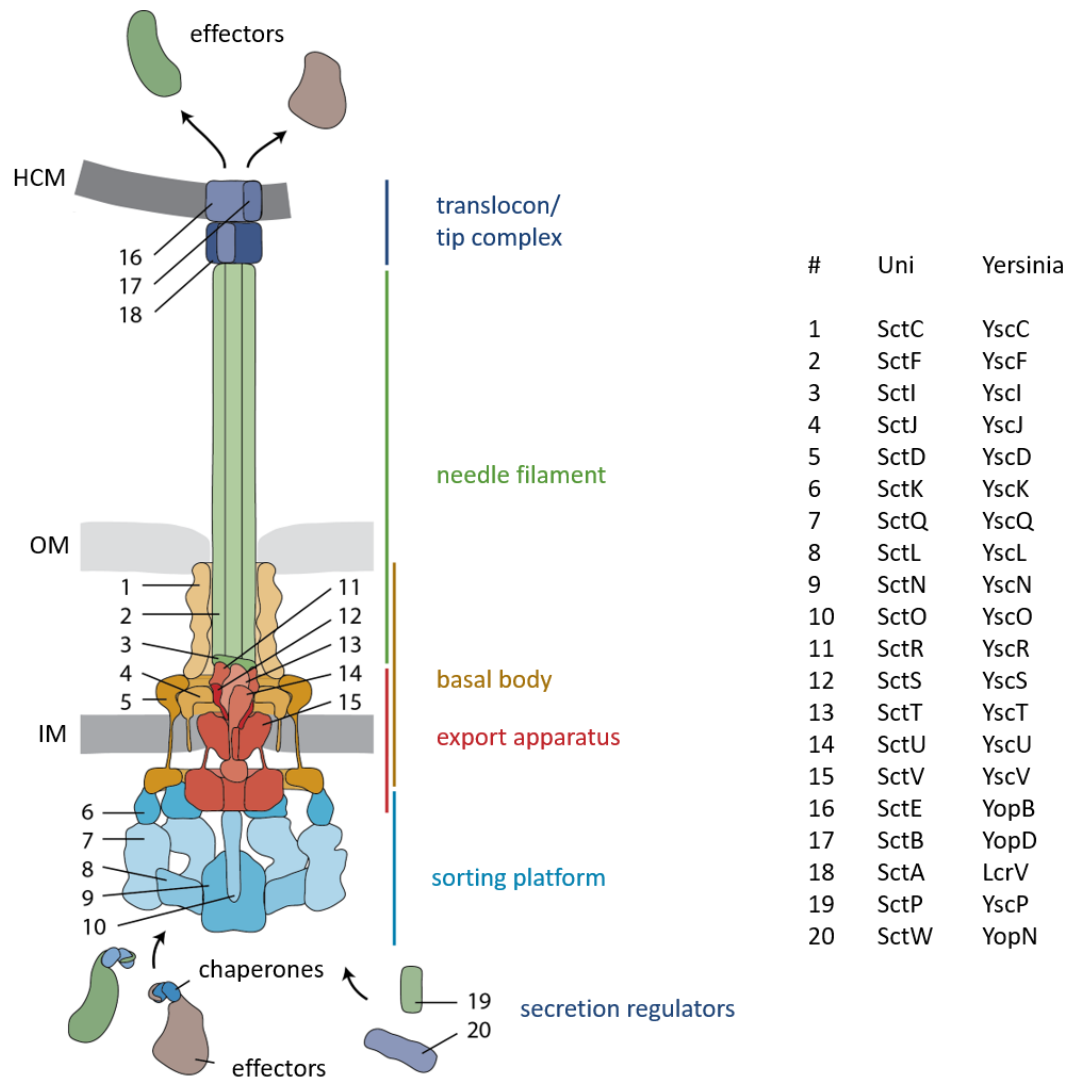| #	Uni	Yersinia
1	SctC	YscC
2	SctF	YscF
3	SctI	YscI
4	SctJ	YscJ
5	SctD	YscD
6	SctK	YscK
7	SctQ	YscQ
8	SctL	YscL
9	SctN	YscN
10	SctO	YscO
11	SctR	YscR
12	SctS	YscS
13	SctT	YscT
14	SctU	YscU
15	SctV	YscV
16	SctE	YopB
17	SctB	YopD
18	SctA	LcrV
19	SctP	YscP
20	SctW	YopN

Fig. 1 Schematic overview of the type 3 secretion system. Unified and *Yersinia* nomenclature of proteins are provided in the table (Wagner and Diepold, 2020). HCM: host cell membrane; OM: outer membrane; IM: inner membrane. Adapted from: Wagner et al., 2018.

2.3.2.2 Effector proteins

As soon as the T3SS is completely formed, the six *Yersinia* effector proteins YopH, YopO, YopP, YopE, YopM and YopT get translocated into the host cell as late substrates and directly interact with host proteins (Rosqvist et al., 1994, Cornelis, 2002, Isaksson et al., 2009, Dewoody et al., 2013, Bliska et al., 2013, Pha and Navarro, 2016). The effector proteins mimic the function of host cell proteins in a more efficient way then their native counterparts, which results in an inhibited phagocytosis activity by manipulating the actin cytoskeleton and a downregulation of proinflammatory responses (Pha and Navarro, 2016, Atkinson and Williams, 2016). Generally, YopH, YopO, YopE and YopT inhibit phagocytosis of *Yersinia* by modulating the cytoskeleton. Except YopH, the effectors accomplish that by direct interaction with Rho-GTPases (Barbieri et al., 2002, Grosdent et al., 2002, Aepfelbacher, 2004). YopH, YopP and YopM modulate the inflammatory response (Cornelis, 2002). Apart from the aforementioned effectors, YopQ (termed YopK in *Y. pseudotuberculosis* and *Y. pestis*) and YopN are also translocated into host cells (Lee et al., 1998, Garcia et al., 2006, Thorslund et al., 2011). In contrast to the other effectors it seems, that those two effectors do not affect cellular factors directly, but rather regulate secretion and translocation (Forsberg et al., 1991, Holmstrom et al., 1997). Anyhow in the case of YopQ it has been shown that limiting the translocation rate of other effectors by interaction with the translocators also prevents activation of the host cells inflammasome (Brodsky et al., 2010, Bliska et al., 2013).

2.3.2.3 Regulation of effector translocation

While YopQ seems to limit the effector translocation rate by interaction with the translocators as mentioned above, there are also other bacterial and host cellular factors involved in effector translocation regulation. YopN (Calcium plug) prevents too early secretion and translocation by blocking the secretion channel (Iriarte et al., 1998, Amer et al., 2016). YopN itself and thus also indirectly effector translocation is regulated via an RNA thermometer that silences yopN mRNA at low environmental temperatures (Pienkoss et al., 2021, Pienkoss et al., 2022).
YopO, YopE and YopT also reduce effector translocation but, in contrast to YopQ, by manipulating and inactivating Rho GTPase activity (Aili et al., 2006, Viboud et al., 2006, Mejia et al., 2008, Isaksson et al., 2009, Gaus et al., 2011).

In general, both the formation of the T3SS and effector translocation are tightly regulated processes.

2.4 Super-resolution microscopy

Super-resolution microscopy is the term for all microscopy approaches that overcome the diffraction limit defined by Abbe (Abbe, 1873). In this thesis only super-resolution microscopy approaches that reach resolutions/localization precisions lower than 100 nm were used, consequently these are the methods that will be described in the next paragraphs. These microscopy techniques are sometimes also called nanoscopy techniques. In general, there are many more super-resolution microscopy techniques achieving resolutions in the range of 100-150 nm, e.g. structured illumination microscopy (SIM), super-resolution optical fluctuation imaging (SOFI) and many more (Guerra, 1995, Dertinger et al., 2009). Overall, there are two groups of methods for super-resolution microscopy methods: 1. Targeted super-resolution, in which a directed focused laser-beam is used for on/off switching of fluorophores (e.g. STED) (Hell and Wichmann, 1994) and 2. Stochastic super-resolution, in which emission of nearby fluorophores is randomly separated by time and thereby becomes resolvable (e.g. STORM) (Rust et al., 2006, Betzig et al., 2006, Schermelleh et al., 2019).

2.4.1 STED microscopy

STED (stimulated emission depletion) microscopy was first developed in 1994 by Stefan W. Hell and Jan Wichmann, whilst the first successful experiments were demonstrated in 1999 (Hell and Wichmann, 1994, Klar and Hell, 1999). It is a laser-scanning microscope that uses an excitation laser to excite fluorophores, i.e. like a confocal microscope. In addition, it uses a second donut-shaped STED laser with a zero intensity point at its center. This red-shifted laser suppresses fluorescence emission from the fluorophores that are not located at the center of the excitation (Fig. 2). This process is called stimulated emission in which an excited-state fluorophore jumps back to its ground state by emitting another photon identical to the incoming photon, effectively resulting in a depleted excitation-state of the fluorophore (Hell and Wichmann, 1994). In the end, resolutions of down to 20-30 nm can be achieved which is, amongst other factors, depending on the laser power

that was used (Westphal and Hell, 2005). Polarizing the STED laser not only in XY but also in Z enables 3D-STED microscopy. Using this, some XY-resolution is lost, but resolution in Z is increased from the confocal Z-resolution of ~600 nm to typically ~75 nm (Schmidt et al., 2008). As scanning microscopy methods are generally suitable for live-cell imaging, also live-STED experiments can be performed. The positions of the fluorophores are very well known using STED microscopy (in the center of the depletion laser), but the microscope does not necessarily work on a single molecule level, as the zero point (Fig. 2) cannot be made infinitely small. This means that also two or more fluorescent molecules could still be present in the center of the depletion laser.
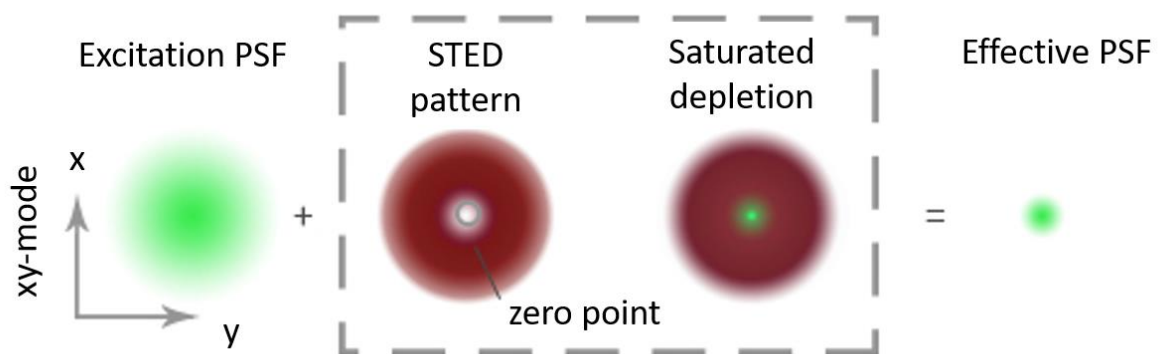
Fig. 2 Principle of 2D-STED microscopy. In 2D-STED a red-shifted, donut-shaped depletion laser is applied with its zero overlapping the maximum of the excitation laser focus, resulting in depletion of fluorescence in the excitation PSF periphery. PSF: point spread function. Adapted from: Huang et al., 2009.

2.4.2 STORM/PALM microscopy

STORM (stochastic optical reconstruction microscopy) and PALM (photo-activated localization microscopy) were first proposed in 2006 (Betzig et al., 2006, Rust et al., 2006). Both methods share the same fundamental principle which relies on the fact that fluorophores can have an on- and an off-state which can be controlled to a certain level. As depicted in Fig. 3, only a sparse pool of the fluorophores is activated at a given time point and thus emitting fluorescence. The microscope's camera takes a picture of this state, in which only few, but in the best case clearly resolvable

fluorophores are activated. Due to the on-/off-switching behavior of fluorophores in STORM, the next time a picture is taken, other fluorophores are activated. Performing this for many cycles (e.g. 10,000 pictures), a reconstructed image can be produced by a software algorithm. This algorithm calculates the center of each emitting molecule in the images, as shown by the red cross in Fig. 3. Overlaying all calculated centers of emission results in a super-resolved reconstruction image of the sample (van de Linde et al., 2011). To enable 3D-STORM imaging, an astigmatism is introduced in the point spread function (PSF). The distorted PSF can later be reassigned to a position in Z by an algorithm (Huang et al., 2008). Belonging to the family of SMLM (single molecule localization microscopy) techniques, STORM already operates on a single molecule level, but the precise position of a single fluorophore cannot be determined, as the center of the PSF is not necessarily the position of the emitting molecule, for example when its orientation is not precisely in plane. There are approaches that show examples of Live-STORM microscopy, anyhow this microscopy technique is very limited towards this direction (Klein et al., 2011, Shim et al., 2012). Samples often need to be embedded in a specific "blinking-buffer" (e.g. glucose-oxidase containing buffer) that supports the on-/off-switching behavior of the fluorescent molecules, which is not a physiological environment for living organisms. Furthermore, usually a lot of images have to be recorded before a proper super-resolved image can be reconstructed. Acquiring these amounts of data takes a lot of time, which makes it difficult to visualize fast molecular processes in whole living cells.
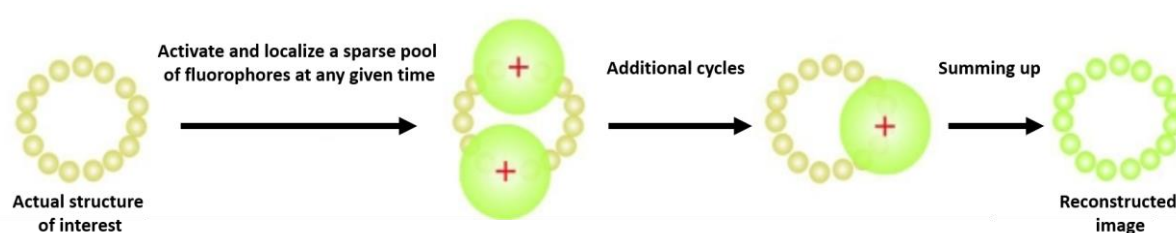
Fig. 3 Principle of STORM microscopy. Only a subset of fluorescent molecules is activated at any given time, resulting in diffraction-limited emission signals that do not overlap each other. The center of each recorded PSF can be determined (red cross). Repeating this cycle often enough, superimposing the determined centers of PSF results in a reconstructed super-resolved image of the actual structure of interest. Adapted from: Chiu and Leake, 2011.

2.4.3 MINFLUX microscopy

Recently, minimal photon fluxes (MINFLUX) microscopy has been introduced (Balzarotti et al., 2017). Combining features of both STORM/PALM and STED microscopy, MINFLUX achieves resolutions down to 1 nm or in other words: the size of a molecule. Like in STORM/PALM microscopy MINFLUX separates single fluorophore over time, by switching them on and off individually. Once a single activated fluorophore is detected, the precise position of this fluorophore is determined with a donut-shaped excitation beam with an excitation zero in its center. This excitation zero is brought to the fluorescent molecule in several iterations, until the detected fluorescence rate is equal to the background noise (Schmidt et al., 2021). Optically injecting a coordinate using a donut zero is already present in the original STED concept (Hell and Wichmann, 1994). The imaging scheme for 2D-MINFLUX is depicted in Fig. 4 A. This concept allows the precise localization of a molecule with a comparatively low number of photons, as the precise localization of a fluorophore is exactly known once it is in the excitation zero center of the donut laser, thus not getting excited anymore. 3D-MINFLUX with an isotropic localization precision of below 5 nm is enabled by shaping the two-dimensional excitation donut into a 3D "bottle beam" donut. The imaging pattern is adapted in this imaging mode to an octahedron-shaped coordinate set, depicted in Fig. 4 B (Schmidt et al., 2021). Reaching localization precisions in the few nanometer range requires a precise stabilization of the sample and the whole system, which is accomplished by an active-feedback position stabilization. Positional changes are constantly measured using backscattered light from immobilized gold nanorods on the sample at a rate higher than 40 Hz. The positional deviations are immediately corrected by a piezo-driven sample stage in all three dimensions (Schmidt et al., 2021). The studies performed so far with MINFLUX have been mainly proof-of-principle studies on different MINFLUX modalities (Balzarotti et al., 2017, Gwosch et al., 2020, Schmidt et al., 2021), description of the development of MINFLUX-suitable dyes and labeling approaches (Butkevich et al., 2021, Ostersehlt et al., 2022, Mihaila et al., 2022, Gerasimaite et al., 2021) or first MINFLUX imaging of components in eukaryotic cells, e.g. mitochondrial proteins (Pape et al., 2020) or the active site of the photoreceptor (Grabner et al., 2022). The first study on bacterial molecular complexes with MINFLUX was published within the framework of this thesis (Carsten et al., 2022).
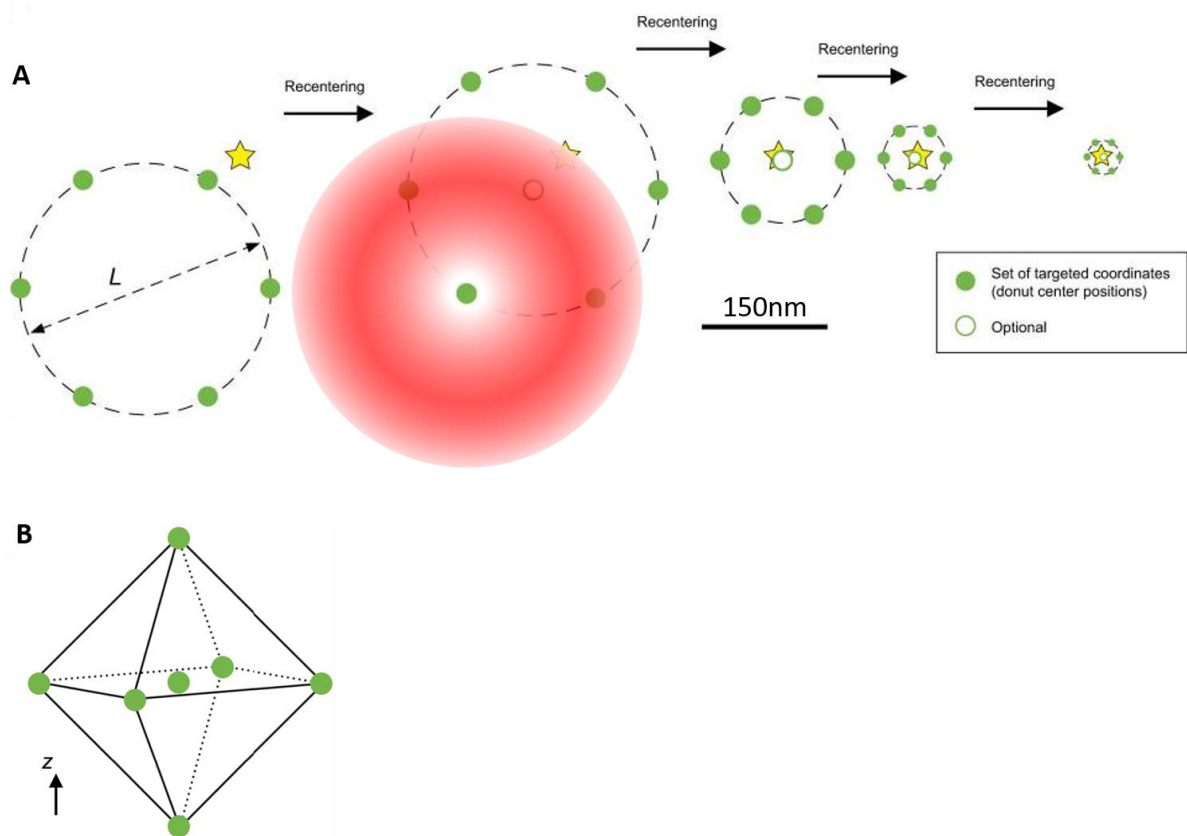
Fig. 4 Principle of MINFLUX imaging. The targeted coordinate pattern is depicted for 2D-MINFLUX (Fig. 4 A) and 3D-MINFLUX (Fig. 4 B) microscopy. The green dots depict the donut center positions in a localization iteration. (A): The yellow star depicts a fluorescent molecule. The red circle depicts the donut shaped MINFLUX excitation beam with zero excitation power at its center. After each iteration, the targeted coordinate pattern is re-centered based on the localization information of the fluorophore obtained in the prior iteration. (B): Coordinates that are not in the focal plane are addressed by defocusing using a deformable mirror. Adapted from: Schmidt et al., 2021.

2.4.4 Super-resolution microscopy and the type 3 secretion system

Super-resolution microscopy seems to be the perfect tool to visualize type 3 secretion system components during different stages of infection. The dimensions (length: approximately 120 nm; width: up to 30 nm) of this molecular machine already indicate that diffraction limited microscopy with a resolution of at least 200 nm cannot resolve any of its components. And although structures of many T3SS components throughout different organisms, such as the sorting platform (Berger et

al., 2021), the basal body (Spreter et al., 2009, Miletic et al., 2021), the export apparatus (Kuhlen et al., 2018, Butan et al., 2019) the needle filament (Habenstein et al., 2020) and the tip complex (Guo and Galan, 2021) are known, only few studies show super-resolved fluorescence data of the T3SS. The majority of data from cryo-imaging methods are based on purified T3SSs. These data provide highly resolved structures of numerous T3SS components mentioned above. Despite this fact, purified T3SSs do not contain translocation pore complexes as they need to be inserted into a host cell membrane. This is one of the reasons why there are so few data available about T3SS translocation pores. Furthermore, cryo-imaging methods do not allow live-imaging of biological processes, so no conclusions about dynamics of certain processes can be drawn. In addition, most of the cryo-imaging methods providing high resolution information rely on averaging of large amounts of data, so that no biological variabilities between single protein complexes within the same experimental approach or even the same organism can be seen. These limitations can be overcome by (super-resolution) fluorescence microscopy, which allows to visualize T3SS components *in situ* within a whole bacterium.

Barlag and colleagues provide STORM microscopy visualizations of the *Salmonella* T3SS ATPase InvC and the export apparatus component SpaS labeled with Halo- and SNAP-tags. In addition, they performed single molecule tracking of SpaS-Halo, expectably showing no diffusion, as it is a static T3SS component. Also, dual color STORM experiments were performed showing parallel visualizations of SpaS and the flagellar motor subunit FliN (Barlag et al., 2016).

Several publications using single molecule tracking gave insights into sorting platform dynamics and composition during secretion conditions (Rocha et al., 2018, Prindle et al., 2022). In these studies, the sorting platform components YscQ, YscN and YscL of *the Y. enterocolitica* T3SS were analyzed, indicating that sorting platform components diffuse in different compositions within the bacterial cytosol. It was also shown in other studies using diffraction-limited fluorescence microscopy, PALM and fluorescence correlation spectroscopy that soluble proteins from sorting platforms form complexes both at the injectisome and in the cytosol (Diepold et al., 2017, Diepold et al., 2015). A combination of *in vivo* fluorescent imaging and high-resolution *in situ* visualizations of *Y. enterocolitica* injectisomes showed clustering of T3SSs under secreting conditions (Kudryashev et al., 2015).

Using 2D and 3D PALM microscopy and live *Salmonella* Typhimurium bacteria, Zhang and colleagues obtained insights into the assembly, distribution and function of T3SS component complexes, reflected by clusters in the images. Clusters in this study are grouped fluorescence signals that are supposed to reflect the labeled protein subunits of a single T3SS. In general, T3SS components were either labeled with a primary and secondary antibody staining and the genetically encoded photo-switchable fluorophore mEos3.2. They analyzed the number of clusters (mostly between 5 and 20), the cluster size (mostly between 40 and 50 nm) and the distance between the tip complex protein SipD and the basal body component PrgH (mostly between 50 to 125 nm) in *Salmonella* Typhimurium. The same analyses were performed for the sorting platform component SpaO and PrgH (10 to 30 clusters; cluster size between 40 and 55 nm; distance between 25 and 125 nm). Furthermore, visualizations and stoichiometry data for the sorting platform components OrgA, OrgB, InvC and InvI and the export apparatus component InvA were provided. Their cluster sizes were about 40 nm and the number of clusters ranged from 10 to 20, depending on the protein. Also, localization and number of clusters of the effector protein SopB was shown and compared in different deletion mutants. The number of clusters ranged from 6 to 10, depending on the strain that was used for analysis. (Zhang et al., 2017). Before this present thesis, Zhang and colleagues provided the highest-resolved insights into T3SS components using super-resolution fluorescence microscopy. Nevertheless, fluorescence clusters cannot always be necessarily resolved from each other, possibly due to the limitations given by the chosen labeling approach and the resolution of approximately 20-35 nm of the used microscopes (Zhang et al., 2017).

The first visualization of a translocon during cell infection using super-resolution microscopy was shown in *Yersinia enterocolitica* by Nauth and colleagues using STED microscopy. Both components YopB and YopD were labeled with antibodies. It was shown that YopB and YopD decorate the bacterial surface after secretion by the T3SS. Translocon-associated YopB was shown during infection and the number of translocon clusters in STED microscopy (n=30) was compared to the one in confocal microscopy (n=10). Additionally, the distance between the basal body component YscD and the translocon protein YopB was measured to be roughly 90 nm (Nauth et al., 2018). Two more publications providing super-resolved insights into the T3SS by STED, STORM and MINFLUX and also live-microscopy were

published within the framework of this thesis (Rudolph et al., 2022, Carsten et al., 2022). For the first time, Rudolph and colleagues showed the formation and also the further fate of the T3SS translocation pore using live-cell microscopy in combination with different cellular immune-markers such as galectin-3 and GBP-1. The same labeling approach also allowed the translocation pore visualization down to the single molecular level and live-STED microscopy and are further described in this thesis and in Carsten et al., 2022.

2.5 Protein tags for fluorescence microscopy

Any fluorescent microscope uses fluorescence to detect and localize proteins. To analyze the localization of any protein under a fluorescence microscope it is crucial to tag that protein of interest (POI) with a fluorescent marker. The first described fluorescent protein was GFP (green fluorescent protein) by Osamu Shimomura (Shimomura et al., 1962). Since then, an increasing number of fluorescent labels, proteins and tags have been developed and nowadays there is a huge number of fluorescent markers researchers can choose from. As one of the goals of this work was to identify a fluorescent label that allows the super-resolution visualization of different T3SS components and especially the translocon, the next paragraphs will focus on labels that allow and are beneficial for super-resolution microscopy.

2.5.1 Fluorescent labeling for super-resolution microscopy

Super-resolution microscopy allows to overcome the limit that defines resolution of light microscopes (Abbe, 1873). MINFLUX microscopy allows for the first time to achieve localization precisions and resolutions down to 1 nm (Balzarotti et al., 2017). To take full benefit of the localization power of super-resolution microscopes and especially MINFLUX microscopy, researchers need to particularly take care about the fluorescent label they choose for their experiments.

Reducing the size of the label and the resulting linkage error between the protein of interest and the fluorescent label is becoming more important the more precise the microscopy method is. A common immunofluorescent labeling approach using a primary antibody against the protein of interest and a fluorescently labeled secondary antibody against the primary antibody displaces the fluorophore up to 25 nm from the actual protein of interest (Fig. 5). This is due to the large size of the

antibodies (10-15 nm). Consequently, also direct labeling of the primary antibody results in a linkage error of up to 13 nm (Fruh et al., 2021).

Another approach is the direct genetic fusion of the POI to a fluorescent marker which reduces the linkage error down to 2-3 nm. Most of the commonly used genetically encoded fluorophores lack properties important for super-resolution microscopy. Either they are too dim, bleach too fast or they do not show on-/off-switching behavior. Anyhow, there are exceptions, for example photoactivatable dyes (Lippincott-Schwartz and Patterson, 2009). In addition, once the genetically encoded fluorophore is cloned to the protein of interest, a potential flexibility for choosing different fluorescent markers for specific purposes is missing. In contrast, the self-labeling enzymes called SNAP-/CLIP- and Halo-tag give researchers more flexibility on the choice of fluorophores: These tags are not intrinsically fluorescent. Only by addition of a substrate/dye with a specific reactive group (SNAP-tag: Benzylguanine; CLIP-tag: Benzylcytosine; Halo-tag: Chloroalkane) a covalent bond between the substrate/dye the label becomes fluorescent (Los et al., 2008, Keppler et al., 2003, Gautier et al., 2008). A drawback of the above mentioned genetically fused fluorescent labels is the size of 20-35 kDa that may have influences on the structure and biological function of the protein of interest (see also chapter 2.5.2).

To avoid massive influence on the biological function of the protein of interest, genetically encoded tags such as Spot-tag (1.4 kDa) and ALFA-tag (1.9 kDa) can be used. These tags can be specifically stained with fluorescently labeled nanobodies (Virant et al., 2018, Gotzke et al., 2019). These nanobodies (~ 15 kDa) reduce the linkage error to below 5 nm (Gotzke et al., 2019).

For some proteins/structures of interest there are specific small molecules that stain them directly, e.g. paclitaxel for microtubules or DAPI for DNA (Barasoain et al., 2010, Wilson et al., 1990). These small molecules minimize the linkage error but are not available for a large variety of targets.

Lastly, site-specific labeling by insertion of an unnatural amino acid into the POI and staining with a dye via click chemistry can be performed. This approach minimizes linkage error and disruption of protein function but is currently challenging to perform in a biological wet lab (Beliu et al., 2019).
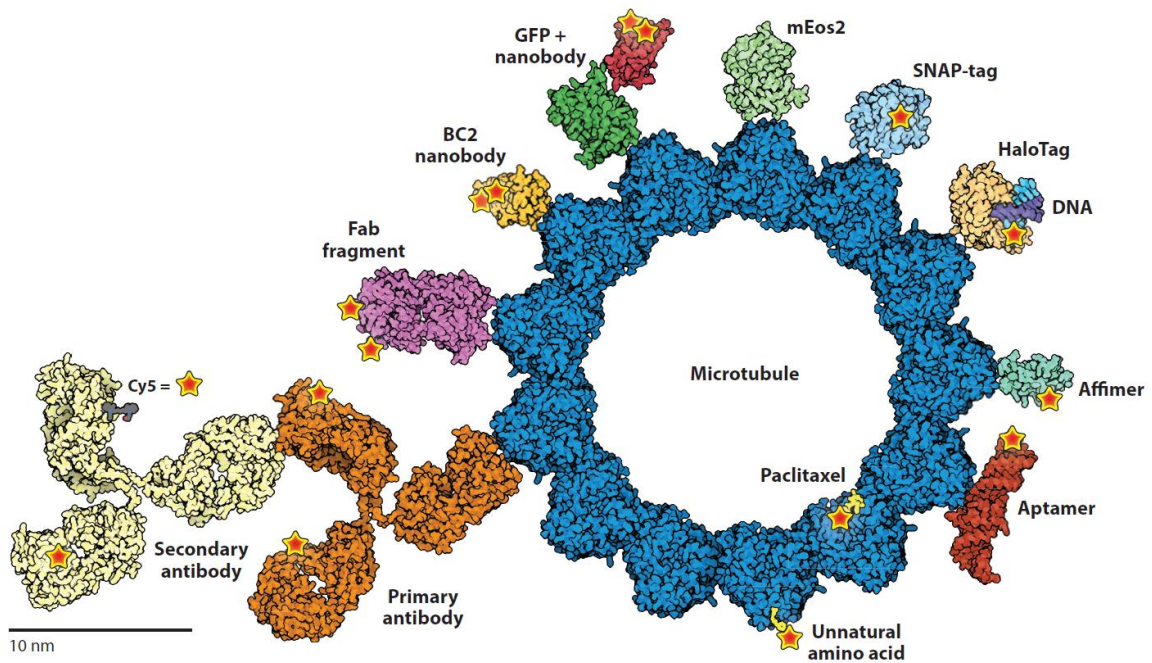
Fig. 5 Sizes of commonly used labeling probes. In this visualization the structure of interest is a microtubule. Binding probes can be transferred to any structure or protein of interest, except for Paclitaxel which stains microtubules specifically. Source: Liu et al., 2022.

2.5.2 Fluorescent labeling of T3SS components for fluorescence microscopy

In theory, all T3SS components could be labeled with a conventional immunofluorescence approach using primary and secondary antibodies. Anyway, this option will not be included within this paragraph, as this labeling is limited to fixed stainings and is not beneficial for super-resolution microscopy because of the linkage error (compare 2.5.1.). Additionally, antibodies against T3SS components are not commercially available and self-produced antibodies are of varying quality, which might result in a highly notable unspecific background staining, preventing especially high-quality SMLM imaging.

T3SS components can be divided into two categories when it comes to fluorescent labeling: First, intrabacterial components that do not get secreted through the T3SS. Second, components that get secreted.

Tagging components of the first category is comparatively straight forward. Depending on the purpose and the type of microscopy that should be performed, genetically encoded fluorophores (e.g. GFP, eYFP) or self-labeling enzymes (e.g. Halo-tag) can be fused to the protein of interest and then visualized (e.g.: eYFP-

YsnN (Prindle et al., 2022); Halo-YscL (Rocha et al., 2018)). If this labeling method does not impair the protein's function, it is highly beneficial for super-resolution microscopy and even allows live-microscopy (Diepold et al., 2017, Prindle et al., 2022, Rocha et al., 2018, Banaz et al., 2019, Landgraf et al., 2012).

In contrast, tagging of T3SS components that get secreted has proven to be challenging in the past. Neither of the approaches mentioned for components that do not need to get translocated through the needle filament can be applied, as both approaches seem to block the T3SS. As mentioned in 2.3.3.1 T3SS components that get translocated need to be unfolded before translocation. Adding a fluorescent label/self-labeling enzyme prevents translocation of the protein as the label seems to be resistant against T3SS-mediated protein unfolding (Radics et al., 2014). Even though the label's size is only 2-4 nm, it is large enough to block the T3SS and thus prevents secretion of the POI.

Other labeling approaches of translocated T3SS components have been shown to be functional but lack the properties for super-resolution and/or live-microscopy. One of the most widely applied labeling strategy is the use of β-lactamase (bla), which cleaves coumarin cephalosporin fluorescin resulting in a fluorescence shift from green to blue in the host cell (Zlokarnik et al., 1998). Using this approach in different *Yersinia* species, among others, immune cell targeting of YopM and YopE was identified (Marketon et al., 2005, Koberle et al., 2009). Additionally, in *Y. enterocolitica* an increased translocation rate was shown for both a YopE deletion mutant and for treatment of host cells with cytotoxic necrotizing factor-Y using YopE-bla (Viboud and Bliska, 2001, Viboud and Bliska, 2005, Viboud et al., 2006, Aili et al., 2006, Aili et al., 2008, Mejia et al., 2008, Wolters et al., 2013, Wolters et al., 2015). Although this labeling approach allows microscopic visualization of translocated effectors in host cells, the fluorescent signals are distributed throughout the host cell and do not deliver more detailed information about the precise protein localization.

Another tag that was used for successful effector protein visualizations is the light, oxygen and voltage-sensing (LOV) domain from *Arabidopsis thaliana*. It binds flavin mononucleotides in the host cell resulting in green fluorescence, has a molecular weight of only 10 kDa, is stable in different environments and matures rapidly (Shu et al., 2011, Buckley et al., 2015). The optimized phiLOV tag allowed visualizations of IpaB from *Shigella,* real-time translocation of Tir from *Escherichia coli* and VirE2

from *Agrobacterium tumefaciens* (Gawthorne et al., 2016, Roushan et al., 2018). It also enabled the quantification of caspase-3 activation by SipA (McIntosh et al., 2017). The major drawback of this tag for super-resolution microscopy is the low fluorescence intensity, especially problematic for low abundant proteins such as the *Yersinia* translocators YopB and YopD (see also chapter 2.3.3.1.).

Using a 4Cys tag (12 aa) in combination with FlAsH (fluorescin based biarsenical dye; 0.7 kDa) was used to label *S. flexneri* effectors IpaB and IpaC intrabacterially before translocation and also SopE and SptP from Salmonella (Enninga et al., 2005, Van Engelenburg and Palmer, 2008). Anyhow, signal quality of these stainings is relatively poor and the dye has a cytotoxic effect on cells (Gaietta et al., 2002).

The concept of fluorophore complementation has been shown to enable T3SS effector visualizations in several publications. It is based on separate expression of an incomplete fluorescent protein and the missing part that restores fluorescence. For example, a GFP molecule consists of 11 β-strands. When using a split-GFP approach, strands 1-10 are expressed separately (e.g. on an expression vector), whilst GFP11 (16 aa) is fused to the protein of interest (Cabantous et al., 2005). Only upon ligation of the 11 strands, GFP is emitting fluorescence. The small size of the GFP11 strand can avoid functional interference of the protein of interest and in addition it is small enough so that effector proteins can still be translocated through the needle complex of the T3SS (Waldo et al., 1999). Successful application of this kind of T3SS effector labeling has been demonstrated with *Salmonella* effectors PipB2, SteA and SteC (Van Engelenburg and Palmer, 2010), as well as *Salmonella* effectors SseF, SseG and SlrP in a live imaging study (Young et al., 2017). Furthermore, using a split-GFP approach, localizations of effector proteins IncA, CT005, CT867 and CTP868 was shown in HeLa cells infected with *Chlamydia trachomatis* (Wang et al., 2018). Split-GFP approaches have also been proven successfully in plant pathology studies of *Arabidopsis* infected with *Pseudomonas syringae* (Park et al., 2017, Lee et al., 2018) and in researches studying type 4 secretion system effectors (Li et al., 2014, Yang et al., 2017, Batan et al., 2018, Kulzer et al., 2013). Despite the wide functionality of the split–labeling approach as well as the usability for live-cell microscopy, the genetically encoded fluorophores lack properties needed for (live-) super-resolution microscopy, as they are often not bright enough, do not show on-/off-switching behavior or are prone to bleaching. Also, for given reasons, this labeling approach lacks a certain flexibility concerning

the choice of different fluorophores with differing properties that might be needed, when using variable microscopy techniques.

The lacking flexibility and absence of properties needed for super-resolution microscopy of the labeling approaches mentioned before can be solved by the use of nanobodies. Nanobodies are antibody fragments consisting of a single, monomeric variable domain of a conventional antibody and can be found in camelid species, e.g. llamas and alpacas (Hamers-Casterman et al., 1993) and also in sharks (Greenberg et al., 1995). Nanobodies (15 kDa) are ten times smaller than IgG antibodies (150 kDa) and can be labeled with fluorophores allowing the use for fluorescence microscopy (Rothbauer et al., 2006). Unfortunately, only very few nanobodies against specific proteins are commercially available. The introduction of the recently introduced epitope tags Spot-tag and ALFA-tag circumvent this issue, as the small epitopes can be fused to any protein of interest, enabling fluorescence microscopy studies with the use of nanobodies in any biological system that can be genetically modified (Virant et al., 2018, Gotzke et al., 2019). These tags are only up to 15 amino acids long and are thus likely to not interfere with the function of the protein of interest and in addition can be translocated through the T3SS needle complex when studying T3SS effector proteins. This labeling approach should be beneficial for super-resolution microscopy (compare 2.5.1.) and also allow live-microscopy as long as the epitope tag is accessible for the nanobody in the experimental set up. In addition, nanobodies with different fluorophores, whose properties allow different kinds of super-resolution microscopy are commercially available. Both systems have been shown to work successfully for microscopic studies in eukaryotic cells (Virant et al., 2018, Gotzke et al., 2019), but due to the novelty of this approach there are so far no studies in bacteria. Rudolph and colleagues showed for the first time the use of the ALFA-tag system in bacteria (Rudolph et al., 2022). Parts of this publication were established within the framework of this present thesis.

3 Aims

Many gram-negative bacteria harbor a T3SS that enables the translocation of bacterial effector proteins into the host cell cytoplasm (Wagner et al., 2018). Previous studies have provided molecular-resolution blueprints of T3SS needle complexes (e.g. the basal body (Yip et al., 2005) or the sorting platform (Berger et al., 2021)) and provided functional and also microscopical analyses of injectisome components and their dynamics (Diepold et al., 2017, Rocha et al., 2018). A not very well understood part of the injectisome is the translocon, forming a translocation pore in the host cell membrane to allow for effector translocation (Rosqvist et al., 1995). When needle complexes are isolated from pure bacterial cultures, they do not contain translocons, which are only formed upon host cell contact. To better understand bacterial pathogenicity, it is crucial to elucidate the processes that allow translocation of effector proteins. The few data available about T3SS translocons are either not based on the Yersinia translocons (Salmonella translocon: (Park et al., 2018, Romano et al., 2016) or show limitations to understand translocon dynamics (Nauth et al., 2018). Both Nauth and colleagues and Park and colleagues managed to visualize translocons during cell infection with STED microscopy or Cryo-electron tomography, respectively (Nauth et al., 2018, Park et al., 2018). Also, both approaches used fixed samples and thus did not provide any data concerning translocon dynamics in living bacteria. In addition, the use of primary and secondary antibodies for immunofluorescence by Nauth and colleagues results in a large offset distance of e.g. 15-25 nm between the fluorophore and the protein of interest (Liu et al., 2022), which is detrimental for e.g. MINFLUX nanoscopy achieving localization precisions in the low nanometer range. In general, fluorescent proteins or self-labeling enzymes are well suited for live cell imaging and imaging of structures with a low offset distance, but it has been shown that these tags affect effector translocation as they prevent the required protein unfolding for translocation (Akeda and Galan, 2005, Radics et al., 2014). To overcome these issues and gain new information about the translocon in *Yersinia enterocolitica* the following aims are center of this work:

- identification of a tag suitable and beneficial for both live-cell microscopy and different nanoscopy techniques (STED, STORM and MINFLUX) to visualize T3SS components with a specific focus on the translocator proteins

- visualization of the translocon during cell infection with the highest possible resolution to estimate size, dimensions and organization of the translocon
- providing further insights into translocon dynamics during cell infection by employing live cell (super-resolution) imaging

4 Results

4.1 Super-resolution microscopy of T3SS components

Within the framework of this thesis and the thesis of Dr. Maren Rudolph, a tag to successfully visualize the translocon component YopD under physiological conditions was found. Details about the generation and the analysis of functionality of this strain are published (Carsten et al., 2022, Rudolph et al., 2022). In brief, an ALFA-tag (compare chapter 2.5.1.) was inserted between amino acids 194 and 195 of the endogenous YopD translocator protein. Insertion of the ALFA-tag at this position kept the functionality of the protein and the resulting strain WA-314 YopD-ALFA. Additionally, it allowed live-cell microscopy as the insertion site of YopD faces the extracellular side once YopD is inserted into the host cell plasma membrane (Fig. 6). This fact allows the nanobody to bind the ALFA-tag without prior permeabilization. It was shown successfully that adding the nanobody to the cell culture medium during bacterial infection allows the live visualization of the pore formation and dynamics during the infection process (Rudolph et al., 2022).
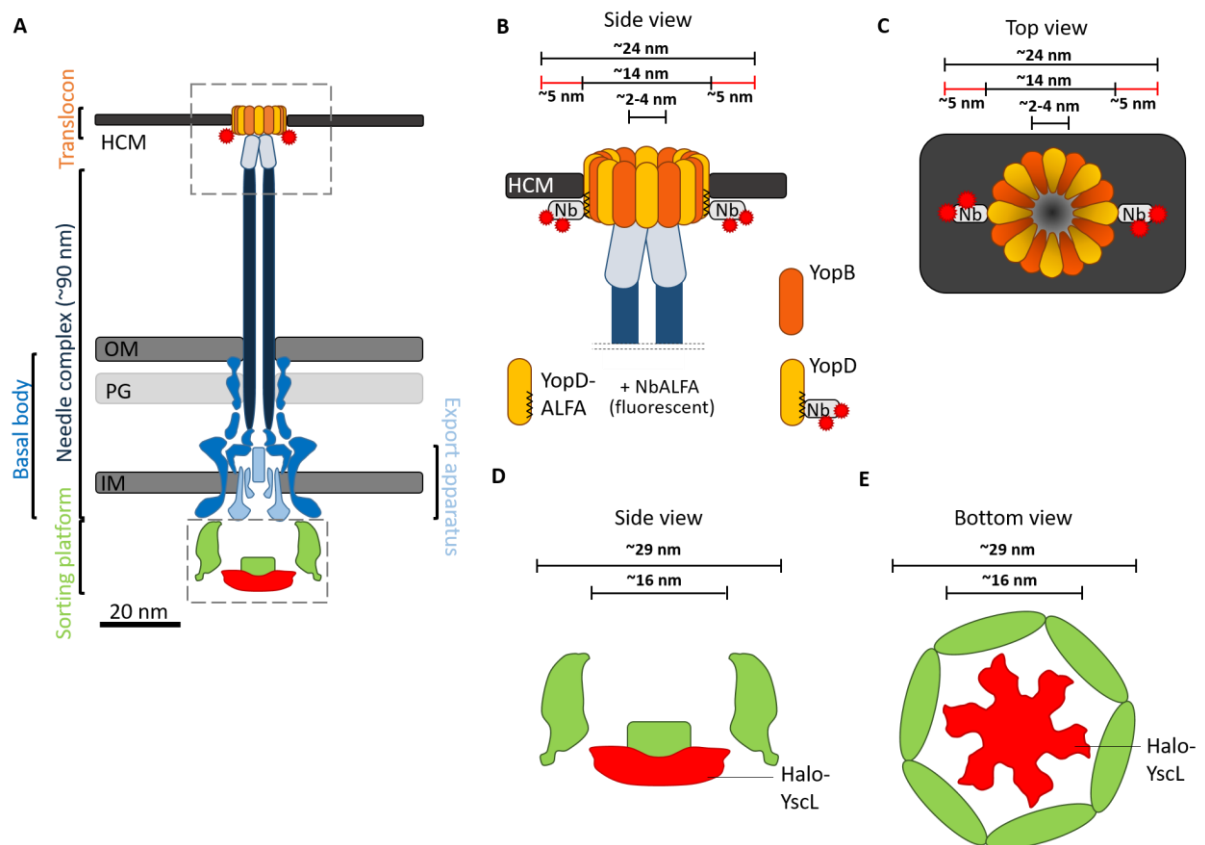
Fig. 6 Schematic representations of YopD-ALFA bound extracellularly to fluorescent NbALFA within the pore complex. Adapted from: Carsten et al., 2022.

(A) Schematic representation of Y. enterocolitica T3SS. HCM: host cell membrane; OM: outer membrane; PG: peptidoglycan layer; IM: inner membrane. Boxed areas indicate components that were enlarged in (B, C) and (D, E).

(B, C) Enlarged schematic representations of YopD-ALFA bound extracellularly to fluorescent NbALFA within the pore complex. Nb: fluorescent NbALFA. Dimension of the *Y. enterocolitica* pore complex was derived from the dimension of the *S.* Typhimurium pore complex (Park et al., 2018). Putative number and organization of YopD and YopB proteins in the *Y. enterocolitica* pore complex were derived from the number and organization of PopD and PopB in the *P. aeruginosa* pore complex (Romano et al., 2016). Length of the fluorescent nanobody is about 5 nm (Gotzke et al., 2019). (B): side view; (C): top view.

(D, E) Schematic representation of Halo-YscL in the sorting platform. Sorting platform dimensions were derived from Berger et al., 2021. (D): side view; (E): bottom view.

4.1.1 YopD-ALFA colocalizes with YopB during cell infection using STED microscopy

Previously it was shown that the strain WA-314 YopD-ALFA allows to visualize the translocator protein YopD using fluorescently labeled nanobodies directed against the ALFA-tag. In parallel, YopD and YopB could still be stained with anti-YopD and anti-YopB antibodies respectively and, as expected, the signals co-localized (Rudolph et al., 2022). In addition, it was shown that the other translocator protein YopB could be found as an interacting protein of YopD-ALFA performing a YopD-ALFA pulldown from infected cell lysates (Carsten et al., 2022). To provide further evidence that YopD-ALFA and YopB co-localize under infection conditions, STED microscopy staining both YopD-ALFA and YopB with an anti-ALFA nanobody and an anti-YopB antibody respectively was performed. Also using STED microscopy and reaching single translocon resolutions, YopD-ALFA stained with a nanobody and YopB stained with an antibody still mostly co-localized.
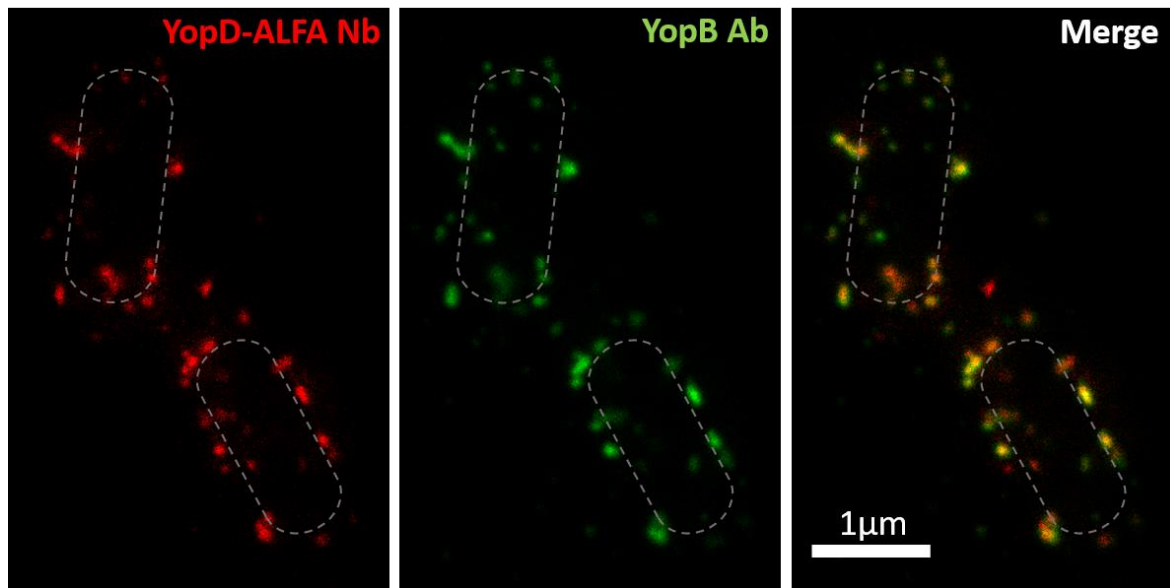
Fig. 7 YopB and YopD-ALFA colocalize during cell infection, shown by STED microscopy. Hela cells expressing Rac1Q61L were infected with WA-314 YopD-ALFA (multiplicity of infection 10) for 1 h and stained with α-YopB (Alexa Fluor 594+, shown in green) and NbALFA-Abberior STAR 635P (shown in green). Adapted from: Carsten et al., 2022.

4.1.2 2D- and 3D-STED allow clear distinction between intrabacterial and translocon-associated YopD-ALFA

As described previously, the use of differential permeabilization allows for selective staining of YopD-ALFA in different cellular compartments (Rudolph et al., 2022). In brief, the use of digitonin allows to stain all translocon-associated YopD-ALFA independent if bacteria are still in a cellular pre-phagosome or already in a closed phagosome vacuole. Digitonin does not permeabilize bacterial membranes and thus staining of intrabacterial YopD-ALFA is prevented. The intrabacterial YopD-ALFA can be stained using a Triton permeabilization after the translocon-associated YopD-ALFA proteins were stained with the α-ALFA nanobody. Using this approach and imaging the bacteria with STED microscopy, allows to clearly distinguish between intrabacterial and translocon-associated YopD-ALFA. It can be seen in Fig. 8 that 2D-STED microscopy shows a rather blurry, non-structured signal for intrabacterial YopD-ALFA (shown in green). 3D-STED on the other hand not only shows the two distinct YopD-ALFA pools, but also provides further localization information about the intrabacterial YopD-ALFA. An accumulation of YopD-ALFA signal in the periphery of the bacteria is clearly visible.
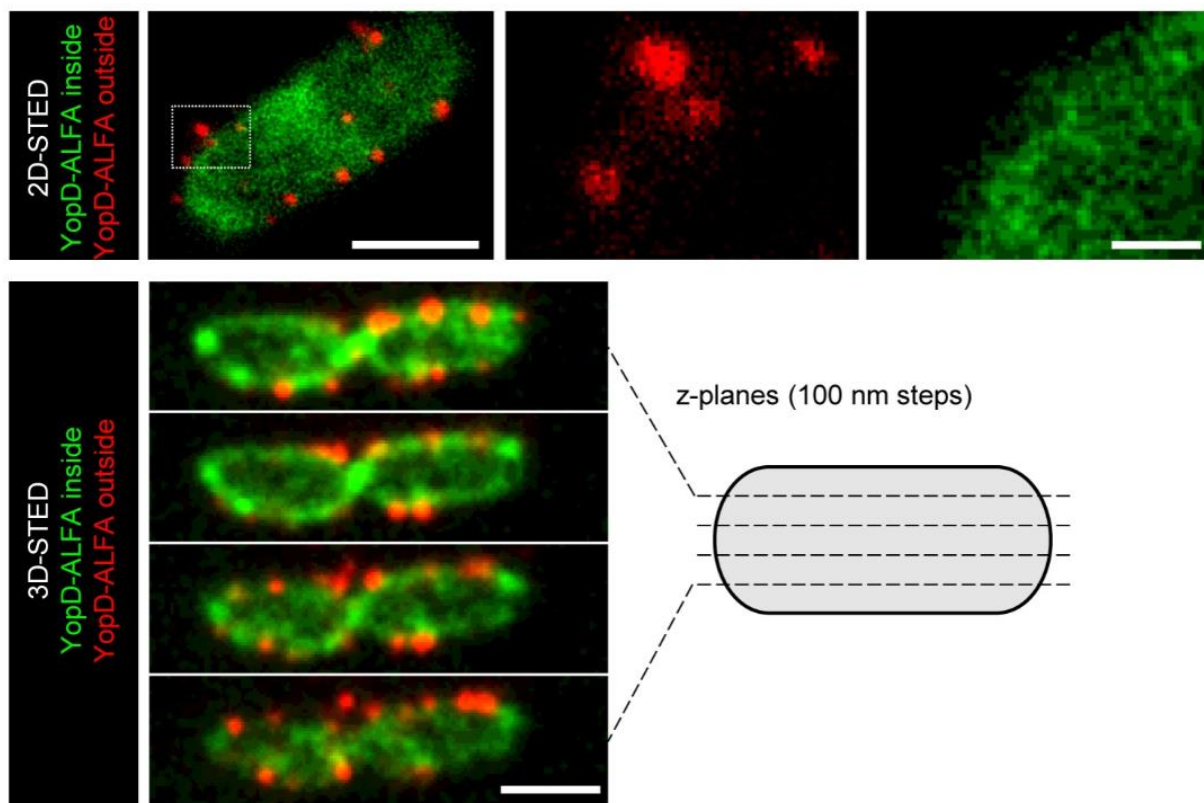
Fig. 8 2D and 3D-STED imaging of intrabacterial and translocon-associated YopD-ALFA. Rac1Q61L expressing HeLa cells were infected with WA-314 YopD-ALFA at an MOI of 10 for 1 h, fixed and stained with NbALFA-635 (shown in red) with prior permeabilization of host cell membranes using digitonin to stain translocon associated YopD-ALFA. Bacterial membranes were permeabilized with Triton and the intrabacterial pool of YopD-ALFA was stained with NbALFA-580 (shown in green). The boxed region in the left of the image is depicted as enlargements in separate channels at the side. Scale bars: 1 µm (2D-STED overview and 3D STED) and 200 nm (2D-STED enlargements). Source: Rudolph et al., 2022.

4.1.3 Comparison of YopD-ALFA stainings between STED, STORM and MINFLUX nanoscopy

As shown by Nauth and colleagues, the resolution of diffraction-limited confocal microscopy is not sufficient to resolve single translocons (Nauth et al., 2018). To assess the number and localization of single translocons of the T3SS during cell infection the use of super-resolution microscopy is necessary. Nauth and colleagues used a conventional immunofluorescence approach with primary and secondary antibodies (Nauth et al., 2018). As this approach does not allow for live-microscopy

and is not beneficial for super-resolution microscopy due to the big offset between fluorophore and protein of interest, the nanobody stain of YopD-ALFA was compared using STED, STORM and MINFLUX microscopy. This way it was assessed, if the nanobody staining approach of a translocator protein is in general useable for super-resolution microscopy and to also get a better impression how MINFLUX microscopy might advance in terms of resolution and localization precision compared to the more established super resolution methods STED and STORM. For each microscopy approach a nanobody coupled to an appropriate dye was used. The photostable dye Abberior Star 635P was used for STED microscopy, while AlexaFluor 647 known for its on-/off-switching properties was used for STORM and MINFLUX microscopy.

In all performed microscopy methods the improvement in resolution and localization precision using super-resolution microscopy became apparent. In Fig. 9 the diffraction limited microscopy method signals (confocal for STED and MINFLUX, epifluorescence for STORM) are shown in red, while the super-resolution microscopy signals are depicted in green. As can be seen, the large red fluorescent signals, that sometimes appear circular, sometimes rather elliptical or "smeared" can be resolved into smaller, circular signals using super-resolution microscopy (green).

To clarify the improvement between diffraction limited and super resolution microscopy, single YopD-ALFA clusters (dashed boxed areas in Figs. 9 A i, iv, vii) were magnified and the full width at half maximum (FWHM) was determined (dashed lines in Figs. 9 A ii, v, viii indicate where the FWHM was measured). Measuring the FWHM is a way to determine the resolution in a present microscopy picture (Demmerle et al., 2015). The FWHM of the diffraction limited microscopy methods shows values around 250 and 300 nm. In comparison, STED and STORM microscopy achieve a 5 to 6 fold lower FWHM of around 50 nm (Figs. 9 A iii, vi). These numbers are based on the exemplary measurement shown in Fig. 9. The values might vary depending on the signal that is measured. On the other hand, MINFLUX signals (Fig. 9 A vii) are visibly smaller than STED and STORM signals. Measuring the FWHM confirms this first impression: The FWHM is in the range of around 25 nm. In addition, looking at single clusters in the MINFLUX image, the signals appear to be not necessarily circular anymore, but show different shapes.

Often two or three small clusters can be seen in close proximity (Fig. 9 A viii; Fig. 11). This observation is further described in chapter 4.1.5.

To further clarify the improvement of MINFLUX microscopy compared to STED and STORM microscopy in relation to the performed YopD-ALFA staining, translocon models showing a complete YopD-ALFA nanobody labeling are superimposed over the signals from each super-resolution microscopy method (Fig. 9 B). For STED and STORM microscopy signals, the translocon model would fit inside the signals several times, here it is put in the center for visualization purposes (Figs. 9 B i, ii). The recorded MINFLUX signal fits well to the size of the provided translocon model. As the model covers the majority of the MINFLUX signal, two versions are shown in Fig. 9 B iii: on top the MINFLUX signal without model, below the signal with the superimposed model.
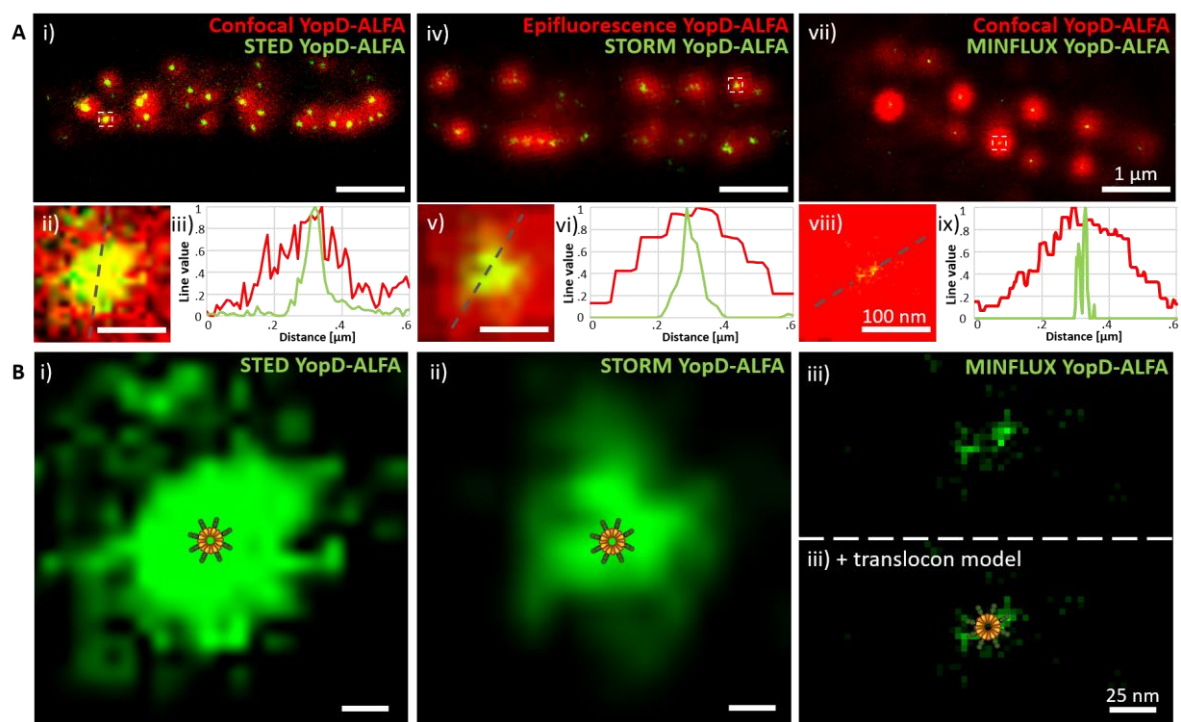
Fig. 9 Super-resolution microscopy of *Y. enterocolitica* translocon protein YopD-ALFA. Adapted from: Carsten et al., 2022.

(A) Comparison of STED-, STORM- and MINFLUX super-resolution microscopy of YopD-ALFA.

Hela cells expressing Rac1Q61L were infected with WA-314 YopD-ALFA (multiplicity of infection 10) for 1 h and stained with NbALFA-Abberior STAR 635P or NbALFA-Alexa Fluor 647. (i, iv, vii): YopD-ALFA fluorescence signals recorded using STED-, STORM- and MINFLUX microscopy and corecorded with confocal or

epifluorescence microscopy as indicated. Scale bar: 1 μm. (ii, v, viii): 10-fold magnifications of boxed areas in i, iv, vii. Scale bar: 100 nm. (iii, vi, ix): Plot profiles for super-resolution nanoscopy (green lines) or confocal/epifluorescence microscopy (red lines) along dashed lines in ii, v and viii. Fluorescence intensity/number of localizations is displayed in arbitrary units and was normalized to the maximal value of each individual imaging method.

(B) Comparison of enlarged super-resolution nanoscopy (STED, STORM, MINFLUX) pore signals with superimposed pore complex models assuming a complete nanobody labeling. In iii, upper part, the MINFLUX signal is shown alone and in the lower part the MINFLUX signal is overlaid by the translocon model. Scale bar: 25 nm.

4.1.4 MINFLUX translocon clusters fit to the models translocon size

Because single signal clusters varied in size and it's hard to draw conclusions about the size of the *Yersinia* translocon based on individual clusters, several MINFLUX signal clusters representing translocon complexes were measured and averaged. In more detail, it was performed as depicted in the inset of Fig. 10 (left side): single MINFLUX translocon clusters were identified, the largest lateral extent of the signal was determined and a plot profile line was drawn. In total 26 translocons of different bacteria were measured, averaged, plotted and the FWHM was determined (Fig. 10, plot profile) to be 28 nm. Assuming a translocon model as depicted in Figs. 9 B, C the translocon itself has a diameter of 14 nm, as shown from Park and colleagues in *Salmonella* (Park et al., 2018). As a nanobody staining is performed, an offset distance of up to 5 nm between the protein and the fluorophore has to be assumed. As shown in Figs. 9 B, C this would result in an effective diameter of 24 nm that would be observed in MINFLUX imaging. Considering the localization precision of ~ 5 nm in these MINFLUX measurements (Suppl. Fig. 1), the averaged FWHM of 28 nm fits very well to the expected model of the translocon.
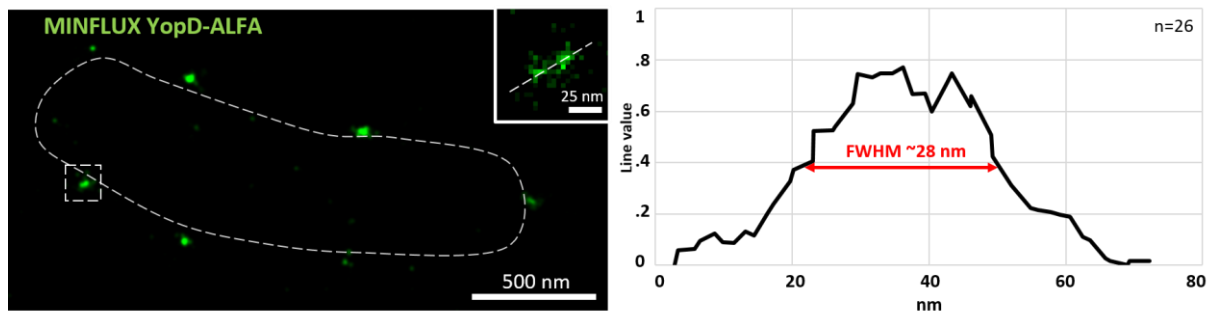
Fig. 10 MINFLUX nanoscopy of ALFA-tagged YopD in a bacterial cell. Hela cells expressing Rac1Q61L were infected with WA-314 YopD-ALFA (multiplicity of infection 10) for 1 h and stained with NbALFA-Alexa Fluor 647. A Gaussian blur with σ=2 was added to the bacterial overview figure for better visibility of single pore signals. Scale bar: 500 nm. Inset (scale bar: 25 nm) shows a magnification of the dashed boxed area. The dashed line across the single pore indicates the position where FWHM was measured.

Line profile represents mean FWHM values of single pores (moving average with a period of 2; mean of 26 pores; Methods). Fluorescence intensity is displayed in arbitrary units and was normalized to the maximal intensity of each individual image. Adapted from: Carsten et al., 2022.

4.1.5 MINFLUX enables visualizations of the translocon protein YopD-ALFA down to the single molecular level

As already mentioned in chapter 4.1.3., when looking at clusters from MINFLUX microscopy that resemble single translocons, the signals do not appear circular as in STED- and STORM- microscopy, but there are often two to three subclusters within in a single translocon cluster visible (Fig. 11, top row). Superimposing these translocon clusters consisting of several smaller subclusters with the translocon model introduced in Figs. 6 and 9 assuming different incomplete labelings of YopD-ALFA with NbALFA it becomes clear how well the MINFLUX signal clusters resemble the expected size of a translocon. The incomplete labelings are just putative, but in general, immunofluorescence labelings are never 100 % efficient.

Generally, these MINFLUX recordings were performed in 2D mode. This means that a very high resolution and localization precision is achieved in *x* and *y*, but only a confocal resolution in the *z* axis of around 600 nm. This means, that the single translocon clusters by MINFLUX microscopy could actually show translocons in

different angles. Due to this fact, translocon models with putative incomplete nanobody labelings are depicted in different spatial orientations. The orientations of the actual T3SS translocon are not necessarily in this orientation, as these are just interpretations based on the signals obtained from MINFLUX microscopy. Still, these images prove that using a combination of a nanobody labeling and MINFLUX microscopy not only can resolve single translocons, but also resolve single molecules of the translocons themselves.
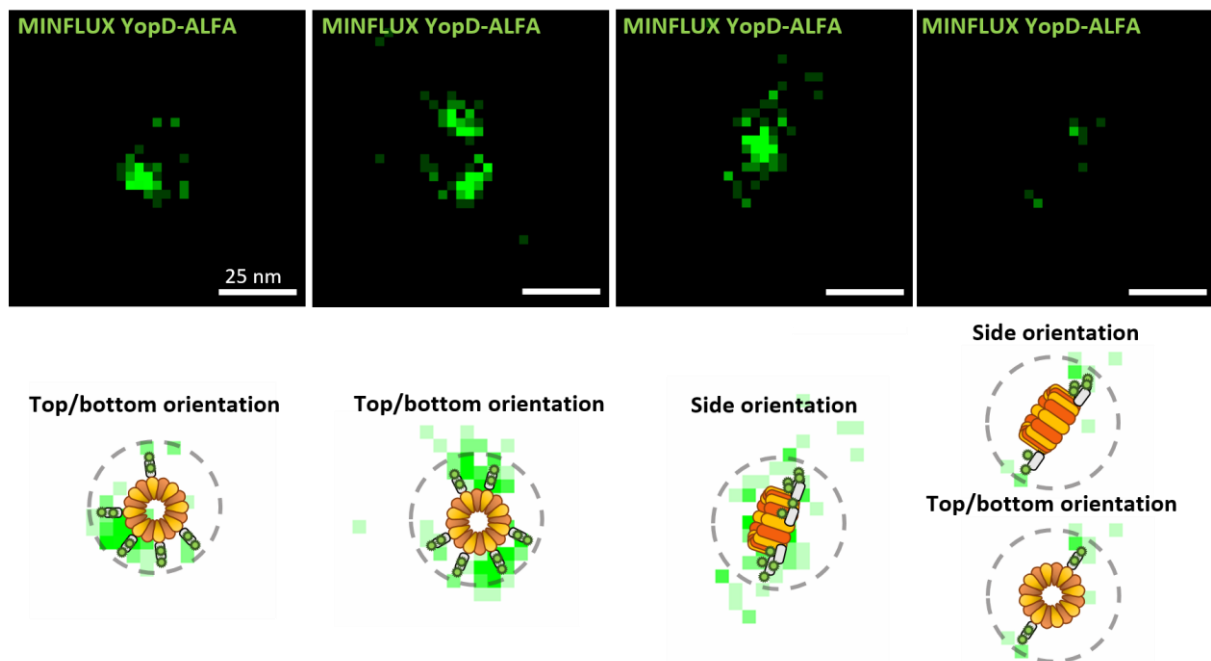
Fig. 11 MINFLUX nanoscopy of ALFA-tagged YopD in single pores.

(Top row): MINFLUX nanoscopy showing YopD-ALFA fluorescence signals in single pore complexes. Scale bar: 25 nm. (Bottom row): Interpretation of the YopD-ALFA signals in the above figures assuming incomplete labeling of YopD-ALFA with Nb-ALFA and considering putative spatial orientations of the pore complexes. The superimposed dashed circle indicates the average FWHM of 28 nm, measured as depicted in Fig. 10. Scale bar: 25 nm. Adapted from: Carsten et al., 2022.

4.1.6 MINFLUX resolves single sorting platforms at the actual size of the protein complex in comparison to STORM microscopy

As shown in chapters 4.1.3. to 4.1.5. the MINFLUX images of a YopD-ALFA translocon staining match well with the translocon model derived from *Salmonella* and *Pseudomonas*. As the dimensions of the *Y. enterocolitica* translocon are

actually not known and thus it cannot be assured that the recorded signals are reliable and imaging at the actual size of the molecular complexes was performed or they might reflect an artifact, a proper control is crucial. In general, the T3SS is a well-studied molecular machine, with structures of a lot of its components available. Among other things, the structure of the sorting platform in *Yersinia enterocolitica* was elucidated recently (Berger et al., 2021). The schematic model shown in Fig. 6 D, E was made based on this study. As control for the T3SS MINFLUX imaging, the protein YscL was chosen. Assuming a side view, the twelve YscL proteins per sorting platform form a bowl-shaped protein complex with a diameter of 16 nm. From a bottom view the protein complex shows a star/sun shape (compare Fig. 6 D, E). A *Y. enterocolitica* strain expressing a Halo-tagged version of YscL (Halo-YscL) enabled super-resolution microscopy. The offset distance between the protein of interest and the fluorophore bound to the Halo-tag is similar to the one using nanobodies (compare Fig. 5), thus the use of this tag is similarly beneficial for MINFLUX microscopy.

To again compare the resolution power of MINFLUX on a different example in comparison to more established super-resolution microscopy, STORM imaging was performed on the same strain. For both microscopy techniques Halo-YscL was labeled with Alexa Fluor 647.

Comparing the Halo-YscL STORM images to its respective diffraction limited epifluorescence microscopy counterpart the improvement in resolution becomes obvious immediately (Figs. 12 A, B). Enlarging a smaller part of the image (boxed area in Fig 12 B shows that signals in closer proximity can be resolved, which cannot be seen in diffraction limited microscopy methods.

Using MINFLUX microscopy, not only the difference between confocal- and MINFLUX- microscopy can be clearly seen (Figs. 12 E, F), but also the difference between STORM- and MINFLUX- microscopy is visible. Especially when comparing the enlarged portions of the images (boxed areas in Figs. 12 B and F it can be seen that only MINFLUX microscopy provides the resolution power that is needed to actually resolve sorting platforms in very close proximity. This difference can also be quantified, as shown in Fig. 12 D: The FWHM (based on the dashed line depicted in Fig. 12 C obtained in STORM microscopy is around 50 to 60 nm, comparable to the FWHM measured in the YopD-ALFA samples (Fig. 9 B). In comparison, MINFLUX signals show a FWHM (based on the dashed line depicted in Fig. 12 G)

of 15 to 20 nm, which is the range of the actual size of the Halo-YscL complex (diameter: 16 nm). To further ensure that imaging at the actual size of the protein structure was performed, a Halo-YscL model was superimposed over the MINFLUX signals (Figs. 12 G, H). To make comparability between MINFLUX imaging and STORM imaging results easier, this was also done for the STORM signals (Fig. 12 C). The signals obtained with MINFLUX microscopy resemble the actual size of the Halo-YscL protein complex very well (Figs. 12 G, H). In contrary, the Halo-YscL model would fit inside a single STORM signal several times, no conclusions can be drawn about the number and the actual precise localization of this T3SS component. This experiment proves that MINFLUX microscopy and a state-of-the-art labeling approach allows imaging of bacterial structures at the actual size of their structure.
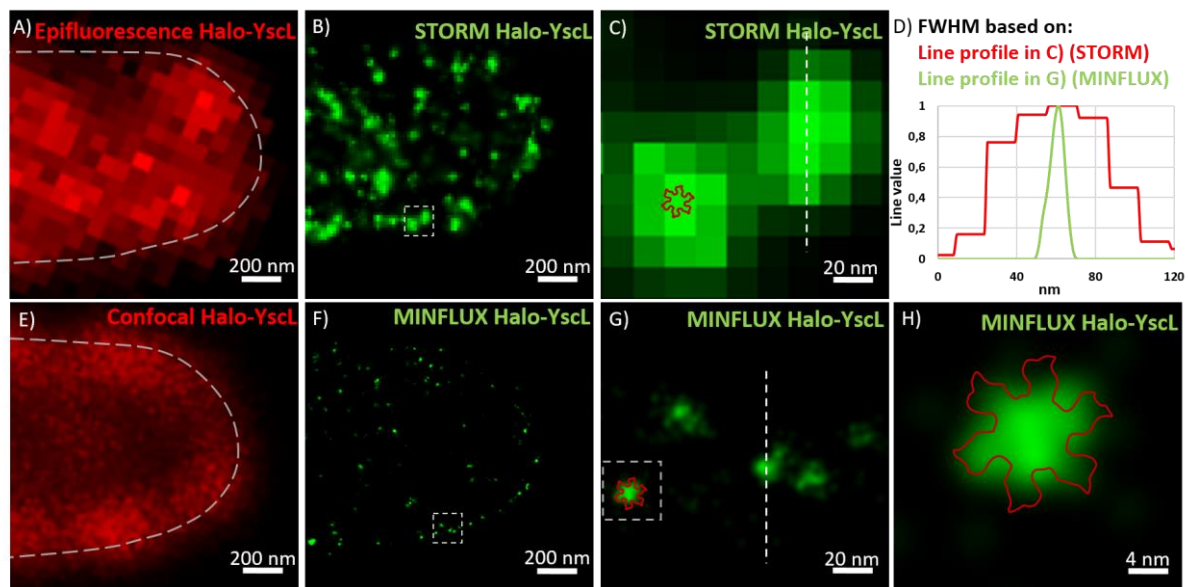
Fig. 12 STORM and MINFLUX microscopy of *Y. enterocolitica* sorting platform protein Halo-YscL.

Y. enterocolitica bacteria expressing Halo-tagged YscL (Halo-YscL) were shifted to calcium-depleted medium at 37 °C for 3 h to activate T3SS secretion and then stained with Alexa Fluor 647-labeled Halo substrate. Adapted from: Carsten et al., 2022.

(A-D) Epifluorescence microscopy (A) and STORM microscopy (B, C) of Halo-YscL. Boxed area in B (Scale bar: 200 nm) is magnified 10-fold in C (Scale bar: 20 nm). (D): Line profiles of YscL signals from C (STORM; red) and G (MINFLUX; green) along indicated dashed lines in C and G. Number of localizations is displayed in

arbitrary units and was normalized to the maximal value of each individual imaging method.

(E-H) Confocal microscopy (E) and MINFLUX microscopy (F, G, H) of Halo-YscL. Boxed area in F) (Scale bar: 200 nm) is magnified 10-fold in G) (Scale bar: 20 nm), Schematic representation depicted in Fig. 6 E was superimposed on STORM- and MINFLUX microscopy images C, G and H.

4.1.7 3D-MINFLUX resolves single sorting platforms in a whole bacterium

The MINFLUX images above show that a combination of state-of-the-art labeling approaches and MINFLUX microscopy enables imaging of biological structures down to their actual molecular size. The results depicted so far are 2D-MINFLUX images, providing a very high resolution and localization precision in *xy*, but a confocal resolution of around 600 nm in *z*. The diameter of *Y. enterocolitica* bacteria is ~ 800 nm. When imaging an 800 nm organism with a *z* resolution of 600 nm an important part of the localization information is missing. For example, in Figure 12 F most of the localizations are in the periphery of the bacterium. But there are also localizations that seem to be in the center of the cell. With the missing information about the precise *z* localization, it cannot be properly judged if the localizations really resemble sorting platforms in the center of the cell or if those are sorting platforms that are also in the periphery, but at the "top" or the "bottom" of this bacterium. As described in 2.4.3., 3D-MINFLUX enables an isotropic localization precision and resolution in the single digit nanometer range. Performing 3D-MINFLUX microscopy with a Halo-YscL staining it becomes clear that the majority of the localizations actually come from sorting platforms that are localized in the periphery of the bacterium. Still, there are some sorting platforms that seem to be cytosolic. Also compare supplemental movies 1 and 2 from Carsten et al., 2022 for a clearer view on single sorting platforms within a whole bacterium.
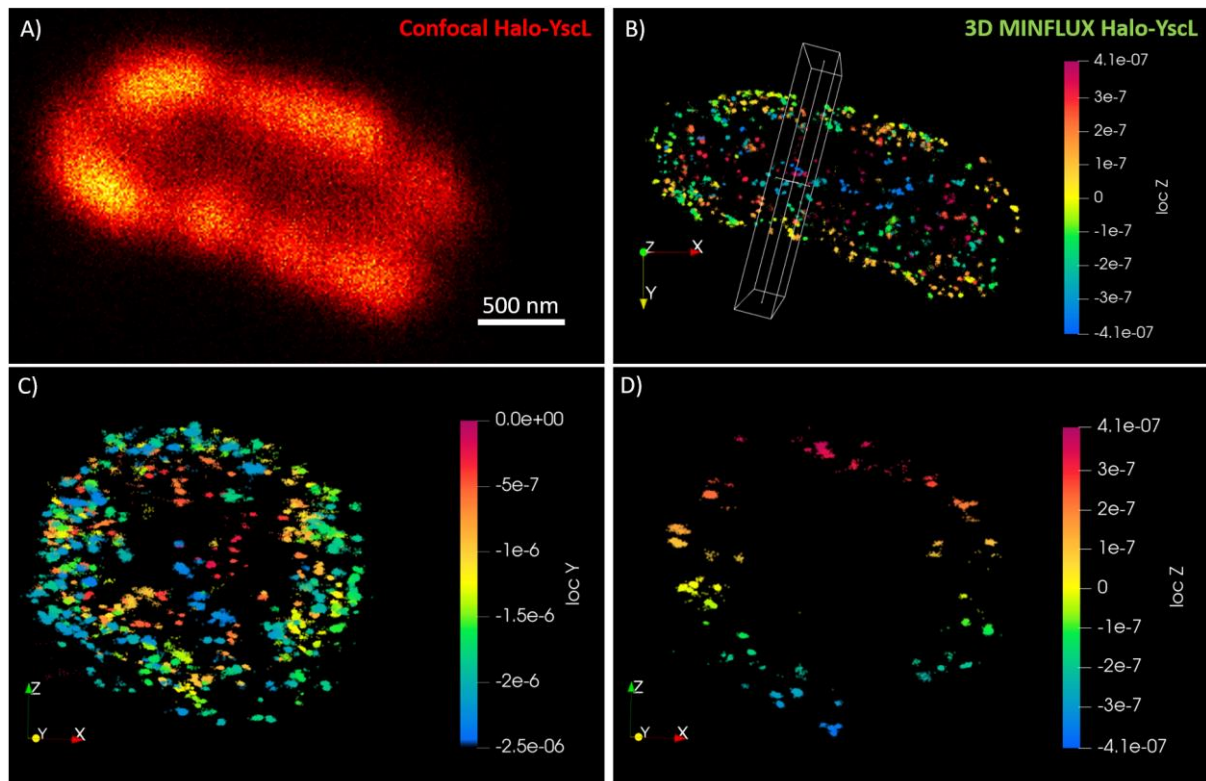
Fig. 13 3D-MINFLUX nanoscopy of Halo-YscL.

Y. enterocolitica expressing Halo-tagged YscL (Halo-YscL) were shifted to calcium-depleted medium at 37 °C for 3 h to activate T3SS secretion and then stained with Alexa Fluor 647-labeled Halo substrate. Axis labeling in m. Adapted from: Carsten et al., 2022.

(A) Confocal image of Halo-YscL in xy view in a whole bacterium.

(B) 3D-MINFLUX image of Halo-YscL in *xy* view in a whole bacterium. The z-axis is color coded. The white boxed area with a depth of 200 nm along the y-axis indicates the section shown in Fig. 13 D.

(C) 3D-MINFLUX image of Halo-YscL in *xz* view of a whole bacterium. The y-axis is color coded.

(D) 3D-MINFLUX image of Halo-YscL in *xz* view of a 200 nm section. The z-axis is color coded. The displayed section is depicted by the white boxed area in Fig. 13 B.

4.1.8 2-color MINFLUX resolves single sorting platforms and translocons during cell infection

To further elucidate T3SS functionality, 2 color imaging is crucial. Only by looking at two T3SS components at the same time, questions about e.g. the ratio or the

distance between different T3SS components within a single bacterium or even in a single T3SS can be answered. As MINFLUX microscopy is a relatively new microscopy approach, 2 color imaging can be difficult with the present available dyes. In general, for 2-color MINFLUX the same MINFLUX excitation laser is used for both dyes, in this case a 640 nm MINFLUX laser. The used dyes SCy5 and CF680 get both excited by this laser, but they have measurable differences in their emission spectra. The fluorescence is split into two spectral fractions by a dichroic laser and then the fractions are counted by two photo-counting detectors. One detector detects photons at a shorter wavelength (< 685 nm), whilst the other one detects photons at a longer (≥ 685 nm) wavelength. Comparing the counts of each fraction enables fluorophores classification (Gwosch et al., 2020).

Here, the Halo-tagged sorting platform protein YscL was stained with SCy5, while the translocon protein YopD was stained using a conventional primary and secondary antibody staining, using CF680 as a dye. These two components are the ones that are the furthest apart in a T3SS (compare Figs. 1 and 6 A), with an approximate distance of 120 nm. These two components would not be resolved in diffraction-limited microscopy approaches. Here, the two components can clearly be resolved, but still the images provided here only depict preliminary results. Briefly, the distances between the two proteins are not always in accordance with the expected 120 nm and furthermore, signals resembling both proteins seem to be present at the same spot. For further details and discussion of potential issues and drawbacks, compare the discussion in chapter 5.3.
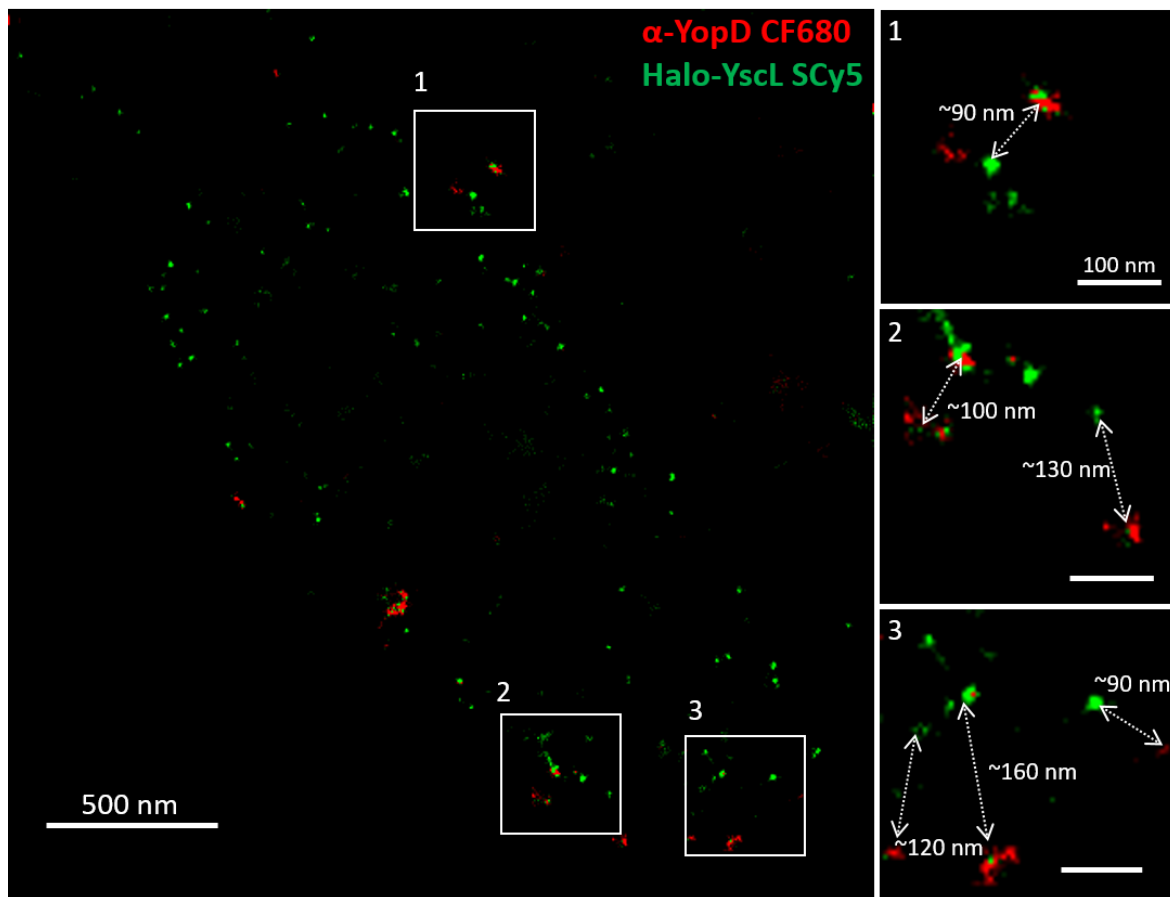
Fig. 14 2-color MINFLUX microscopy of the sorting platform protein YscL and the translocon protein YopD during host cell infection. Hela cells expressing Rac1Q61L were infected with *Y. enterocolitica* strain expressing Halo-YscL (multiplicity of infection 10) for 1 h and stained with Halo-tag substrate SCy5. In addition, YopD was stained using a primary α-YopD antibody and a secondary antibody coupled with CF680. Halo-YscL stained with SCy5 is depicted in green, YopD stained with CF680 is depicted in red. Boxed areas in the overview picture on the left are enlarged on the ride side. Arrows indicate approximate distances between signal clusters resembling the sorting platform protein YscL and the translocon protein YopD.

4.2 Live-STED nanoscopy of YopD-ALFA

The way that the *Y. enterocolitica* strain YopD-ALFA was genetically modified allows live-visualization of T3SS translocon formation during host cell infection (compare chapter 4.1., Fig. 6 and (Rudolph et al., 2022)). This allows to elucidate spatiotemporal dynamics of translocon formation and fate during cell infection. Among other things it was shown that YopD-ALFA was integrated into translocons

around two minutes after uptake of bacteria into a phosphatidylinositol-4,5-biphosphate enriched pre-phagosomal compartment. It remained there for an average time of 27 minutes. Around 14 minutes after translocon formation the phagosomal membrane was damaged, shown by recruitment of GFP-tagged galectin-3. Shortly after, GBP-1 was recruited to phagosomes, accompanied by decrease of translocon signal intensity, which suggested their degradation (Rudolph et al., 2022). All data presented are diffraction limited microscopy data using a confocal or spinning disc microscope. While these microscopy approaches are ideal for visualizing translocons on a single-cell or even single-bacterium level, they cannot operate on a single-translocon level as their resolution is not sufficient to resolve single translocons from each other. Here, Live-STED was established and used to be able to follow single translocon complexes of *Y. enterocolitica* during cell infection.

4.2.1 Live-2D STED enables super-resolved live visualization of translocon protein YopD during cell infection over a long timeframe

Live-2D STED microscopy (right column for each time point) gives a clearly observable advantage in *xy* resolution during live cell imaging in comparison to the diffraction limited confocal live microscopy (left column for each time point). As already observed in fixed STED imaging (compare Fig. 9), large elliptical shaped fluorescence emission signals can be resolved to smaller, more circular clusters, indicating that this method allows observation on a single translocon level, at least in *x* and *y*. In contrast to confocal microscopy, STED microscopy operates by using two lasers (excitation and depletion laser; compare chapter 2.4.1.) and with a smaller pixel size in order to allow a higher resolution. All these factors result in a higher amount of laser light that is brought to the sample and to the fluorophores. Still, it was possible to film a live infection over a long timeframe of approximately two hours without bleaching the fluorophores. In addition, they were still bright enough to observe clearly super-resolved signals (Fig. 15, time point: 01:45:00). In the recording from which excerpts are shown in Fig. 15, 78 time points with 13 images per stack were recorded, resulting in 1.014 STED images over a time frame of 1:57 h. No notable dynamics between single translocons could be observed.
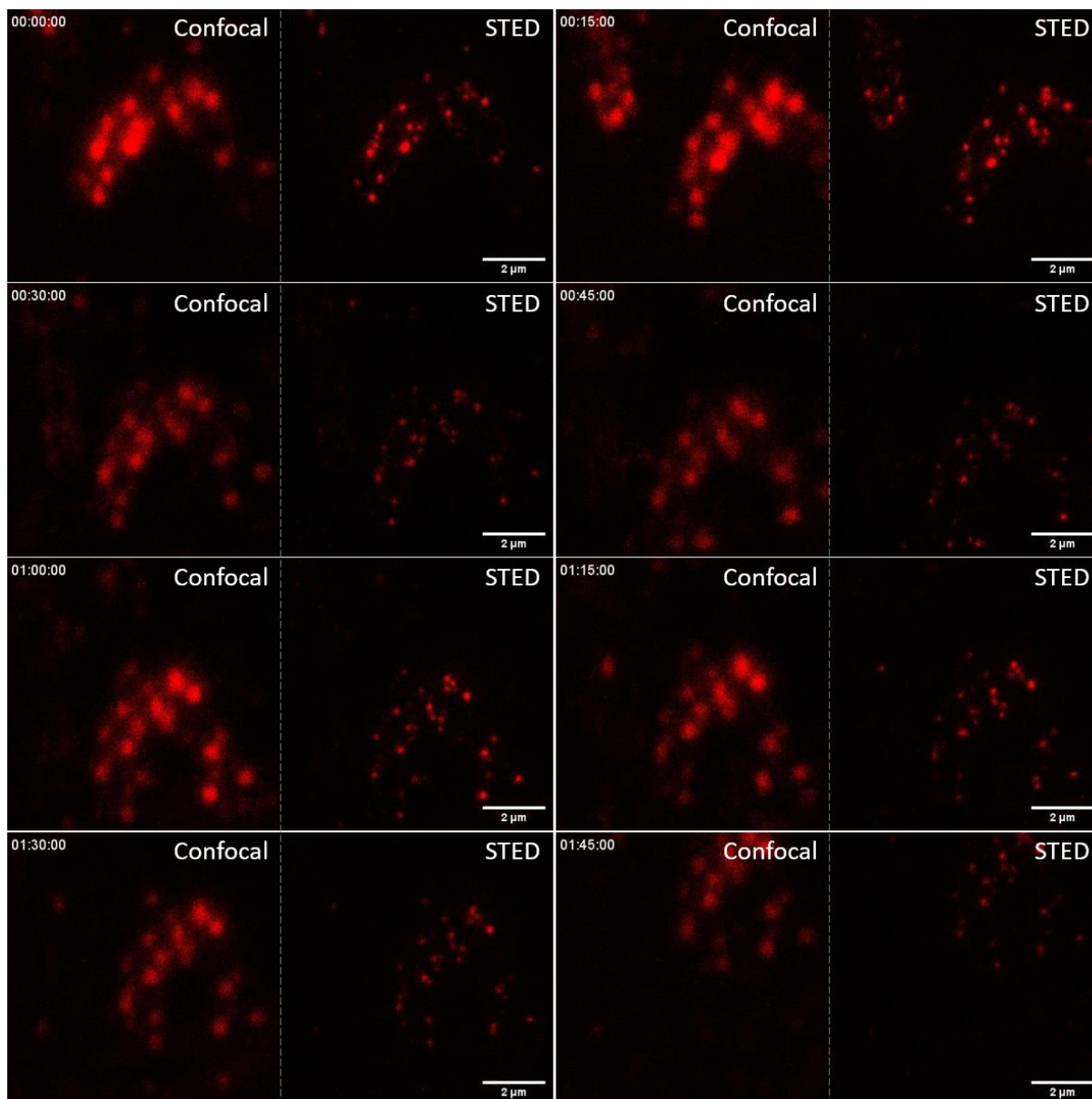
Fig. 15 Live 2D STED microscopy of the translocon protein YopD-ALFA during cell infection. HeLa cells transfected with myc-Rac1Q61L and PLCδ-PH-GFP were infected with WA-314 YopD-ALFA at a multiplicity of infection of 30 and stained with NbALFA-Abberior Star 635P diluted 1:200 in cell culture medium. The PLCδ-PH-GFP channel is not depicted here. Cells were imaged with a STED microscope and one z-stack of 13 slices was taken every 90 seconds with an interval of 300 µm between each slice over a timeframe of one hour and 57 minutes. Stacks for each time point were combined to one image using maximum intensity projection and one projection every 15 min is shown.

4.2.2 Live-3D STED allows super-resolved live visualization of translocon protein YopD during cell infection in all three dimensions

2D-Live STED enables to observe super-resolved YopD-ALFA over a long timeframe. The resolution in *xy* using 2D STED is highly improved, while the resolution in *z* remains at around 600 nm, as in confocal microscopy. As mentioned before, *Y. enterocolitica* has a diameter of around 800 nm. Using microscopy methods that have no improvement of resolution in *z* do not allow to clearly judge if truly single translocons in all three dimensions are imaged. 3D-STED microscopy improves resolution in all three dimensions. Even though a bit of resolution is lost in *xy*, the benefit of resolution in *z* is massive. Using this method to observe YopD-ALFA during a cell infection resolves the rather large "clouds" of fluorescence emission in confocal mode (left column in Fig. 16) to more defined, spherical signals in 3D-STED (right column in Fig. 16). Especially the improvement in *z* is clearly visible, as the elongated signals in *z* in confocal mode get a more spherical shape. In the movie from which excerpts are shown in Fig. 16, 15 time points with 80 images per stack were recorded, resulting in 1.200 STED images over a timeframe of 45 min, without major bleaching of fluorophores. Imaging for longer timeframes resulted in bleaching of fluorophores and prevented from longer Live-3D STED imaging (data not shown). Also here, no notable dynamics between single translocons could be observed.
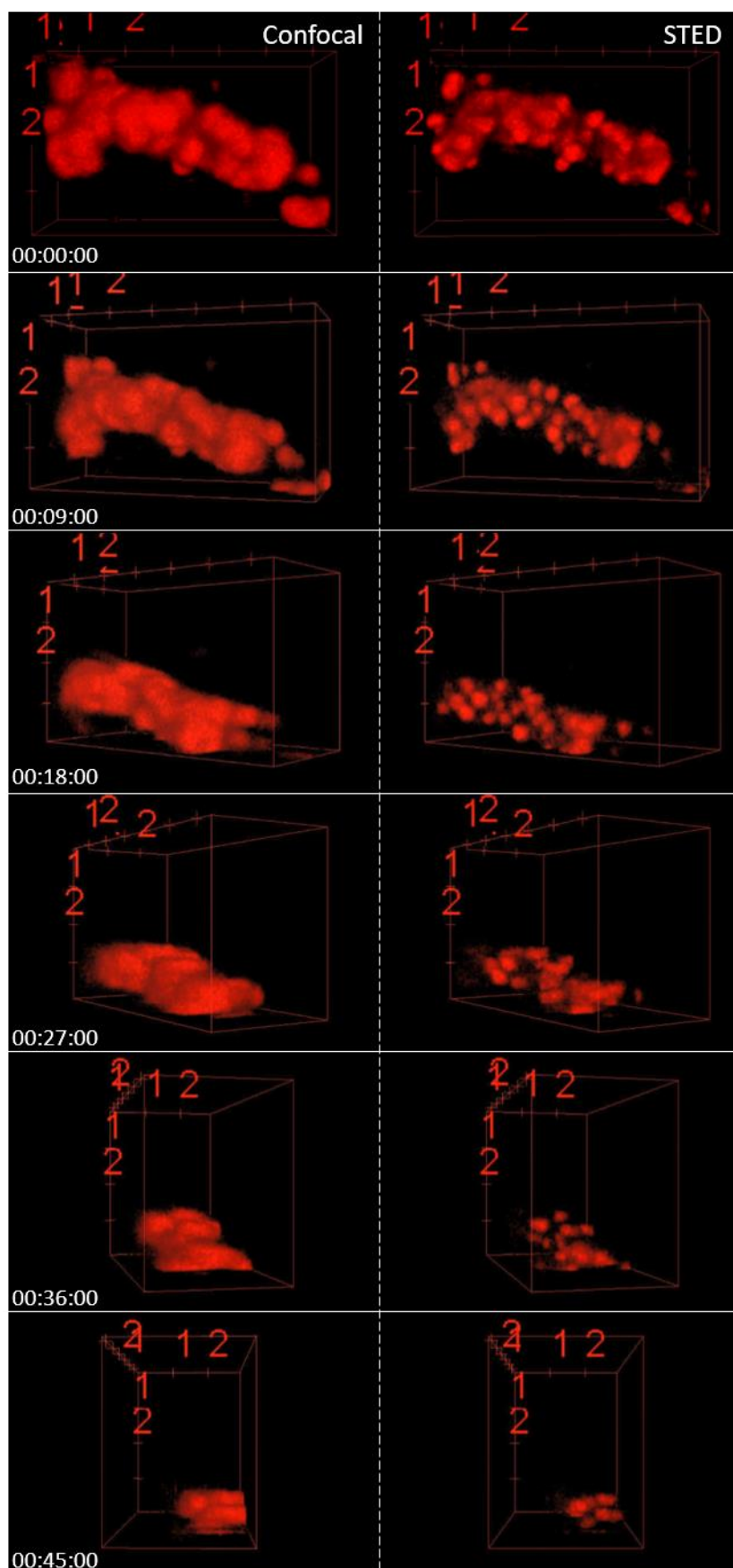
Fig. 16 Live 3D STED microscopy of the translocon protein YopD-ALFA during cell infection. HeLa cells transfected with myc-Rac1Q61L and PLCδ-PH-GFP were

infected with WA-314 YopD-ALFA at an MOI of 30 and stained with NbALFA-Abberior Star 635P diluted 1:200 in cell culture medium. The PLCδ-PH-GFP channel is not depicted here. Cells were imaged with a STED microscope and one z-stack of 80 slices was taken every 3 min with an interval of 50 µm between each slice over a timeframe of 45 min. Stacks for each time point were combined to one image using maximum intensity projection and one projection every 9 min is shown. The 3D reconstruction was made using the Fiji Plugin "3D Viewer".

5 Discussion

The bacterial T3SS is a highly complex macromolecular protein machine crucial for translocation of bacterial effector proteins to manipulate the host cells immune response. Its importance in infection of numerous organisms ranging humans, animals and plants and its abundance in about 25 bacterial species led to extensive research to elucidate the structure, function and dynamics of T3SS components and its effectors (Mota et al., 2005, Cornelis, 2006, Wagner et al., 2018, Diepold and Armitage, 2015, Bergeron and Marlovits, 2022). Despite of these major efforts to fully understand the T3SS and its function, there are still a lot of questions that remain elusive. One reason for that are technical and methodological limitations that prevent researchers to answer certain research questions. While the structure and localization of the majority of T3SS components are known due to cryo-EM/ET based studies (Bergeron and Marlovits, 2022), it is still a challenge to investigate the T3SS and its effectors under physiological conditions, due to its complex structure and different, specific biological environments. Fluorescence microscopy is an ideal tool to observe biological processes under physiological conditions, but so far limitations of resolution and also protein labeling methods prevented to gain further insights into T3SS mediated infection processes. Labeling effector proteins with conventional fluorophores such as GFP results in a clogged secretion system as the translocated effectors need to be unfolded for secretion and translocation. GFP is resistant to T3SS mediated unfolding due to its high thermostability (Radics et al., 2014). Additionally, the complexity of the T3SS makes it difficult to tag proteins at suitable positions as protein function is easily disrupted. Nevertheless, for observation of specific T3SS proteins under a fluorescence microscope, labeling is essential. Conventional labeling approaches using primary and secondary antibodies not only make it impossible to use live cell microscopy, but in addition are not beneficial for super-resolution and especially MINFLUX microscopy, due to the offset distance between fluorophore and protein of interest. For live- and super-resolution microscopy an epitope tagged mutant allowing visualization of the so far mostly understudied translocon was established within the framework of this thesis and was applied to different super-resolution microscopy approaches.

5.1 The ALFA-tag allows the super-resolved visualization of the translocon component YopD and is highly beneficial for MINFLUX microscopy

Tagging the translocator protein YopD with the ALFA-tag allows to label this protein by using a fluorescently labeled nanobody. Because of the properties of the nanobody and the ALFA-tag this approach can be used for multiple research questions. The nanobody's high affinity to the ALFA-tag allows to perform live-cell microscopy without the need of washing steps to avoid unspecific binding of the nanobody to cellular or bacterial proteins (Figs. 15 and 16; (Rudolph et al., 2022)). This is also a crucial factor for all SMLM approaches such as STORM and MINFLUX. As these methods display the number of localized blinking events of fluorophores and not intensities it is important that an extensive unspecific staining is avoided. Otherwise, the structures of interest cannot be clearly distinguished from an unwanted background staining anymore. One of the major benefits for super-resolution microscopy is the small size of the ALFA-tag and its nanobody. As shown in Figs. 9-11 this not only allows to visualize single translocons at the expected size and to get an actual idea about the so far unknown dimensions of the *Yersinia* translocon, but also it presumably allows to visualize single YopD-ALFA proteins within a translocon. It has been proven previously that the reduction of the displacement between protein of interest and fluorophore not only makes a theoretical difference but can also be measured in super-resolution microscopy methods, in this case STORM microscopy (Ries et al., 2012). The nanobody's small size has another benefit that widens the field of applications for this tagging approach. In contrast to the larger conventional antibodies, nanobodies can stain intrabacterial proteins using comparatively mild permeabilization with 0.1 % Triton X-100 (Fig. 8). Theoretically it is possible to stain intrabacterial proteins using antibodies, but this requires harsher permeabilization methods using 2 % SDS (Nauth et al., 2018). In our hands, this complicates the staining process, as the use of 2 % SDS often leads to the fact that most bacteria are washed away from the coverslip.

Furthermore, nanobodies can be purchased or labeled in the lab with all fluorescent dyes commercially available. This gives researchers the absolute necessary flexibility of dyes when using different microscopy approaches, in contrast to the use

of genetically encoded fluorophores. As shown in Figs. 9 and 14, depending on the microscopy method and its modalities (e.g. single-color, multi-color) that are used, different dye combinations are of need. To always clone a new genetically modified bacterial strain with e.g. a different genetically encoded fluorophore would result in exceeding amounts of work.

In summary, the use of nanobodies is close to be the perfect match when performing advanced microscopy, like MINFLUX or live super-resolution microscopy.

5.2 MINFLUX microscopy in combination with a state-of-the-art labeling approach allows imaging of bacterial structures down to their actual size

One goal of this work was to gain further information about the *Yersinia* T3SS translocon. To achieve this, a state-of-the-art labeling approach using fluorescently labeled nanobodies in combination with the highest resolving fluorescent microscopy method to date called MINFLUX was used. The difference in localization and precision of a YopD-ALFA translocon staining becomes obvious in direct comparison of the more established STED and STORM microscopy and MINFLUX microscopy (Fig. 9). Looking at single translocons in closer detail the irregular shape of the signals become obvious, which contrasts with the signals from STED- and STORM-microscopy. As shown in Fig. 11 these signals correspond well to putative translocon models in different orientations with possible incomplete labelings. Because these images were taken in 2D mode, the orientation of the translocons cannot be further elucidated in these images. The resolution in z using 2D-MINFLUX is the same as in confocal microscopy, so ~ 600 nm. At the time these experiments were performed, 3D-MINFLUX was still not available in commercially available microscopes. As mentioned before, the incomplete labelings assumed for different translocons are just interpretations. Due to the fact that immunofluorescence labelings are usually not 100 % efficient, this is not an unlikely interpretation. Especially keeping in mind that for these labelings rather low concentrations of nanobodies were used (1:1,500) to avoid unspecific background staining.

For some of the signals it can convincingly be claimed that single YopD-ALFA proteins from translocons can be visualized. For other subclusters within a translocon cluster recorded by MINFLUX, it seems like several YopD-ALFA proteins are merged into a larger signal. In theory MINFLUX microscopy should also be able to resolve those single proteins in very close proximity, when reaching localization

precisions of 1 nm. These rather extreme values are mostly not reached in "real-life" biological samples, but in already long time established proof-of-principle samples like nuclear pore complexes or DNA origamis. The localization precision reached around 5 nm in these samples (Suppl. Fig. 1). Assuming the potential close proximity of fluorophores, 5 nm would be enough so that single localizations blur into a larger signal-cluster. Another factor that might play into this, is the fact that fluorophores in a closer proximity than 10 nm may show collective behavior, which can result in a compromise of their independent on-/off-switching (Schmidt et al., 2021). In addition, for 2 color MINFLUX microscopy, further development of specialized MINFLUX dyes will improve imaging in the next years (Gwosch et al., 2022).

Despite these factors that need to be accounted for when doing MINFLUX image analysis, it has been shown in this work, that MINFLUX microscopy in combination with state-of-the-art labeling approaches enables visualization of T3SS components down to their actual molecular size. Fig. 12 shows that the signals obtained from a Halo-YscL staining precisely resemble the actual molecular size of this protein complex (Berger et al., 2021). A single sorting platform consists of twelve YscL proteins in total. If all these proteins would have been clearly resolved in this experiment, one sorting platform cluster should consist of twelve subsignals visible in MINFLUX, assuming a complete labeling. In the Figs. 12 and 13 rather homogenous signals at the size of a single sorting platform are visible. Also here, the same explanations as for the irregular YopD-ALFA signals are to be mentioned. The dyes are very likely in a closer proximity to each other than 10 nm, so here as well the independent on-/off-switching capabilities might be compromised (Schmidt et al., 2021). Additionally, these images were recorded on a very early version of a MINFLUX microscope, which might not have the resolving power the further developed MINFLUX microscopes have today. Still, it is important to mention, that it is possible to visualize protein complexes at their actual size in situ using fluorescent microscopy, which has not been possible before and is a major breakthrough, not only, but specifically for microbiological research.

5.3 Multi-color MINFLUX microscopy shows T3SS components in relation to each other during cell infection

Theoretically multi-color MINFLUX microscopy is the perfect tool to visualize multiple components of a complex, tightly packed protein machinery such as the T3SS. As shown in Fig. 14 this approach generally works, visualizing both the translocon protein YopD and the intrabacterial sorting platform protein YscL in parallel. The enlarged areas provide examples in which the distance between these two components is within the expected range of around 120 nm. Looking at these examples in more detail, several inconsistencies to the expectations appear. First of all, the measured distances between the two T3SS components range between 90 and 160 nm. This range of distances might reflect to a certain level biological variations of T3SS length control. The exact mechanism of T3SS needle length control is controversial (Cornelis, 2006). Several publications suggest a molecular ruler (Kubori et al., 2000, Wagner et al., 2010, Bergeron et al., 2016), but also needle length regulation by a precise timing of substrate switching is claimed (Nariya et al., 2016). Between species, the length of assembled T3SS needles varies between 45 and 80 nm (Kubori et al., 1998, Radics et al., 2014, Park et al., 2018, Lombardi et al., 2019, Tamano et al., 2000, Pastor et al., 2005) Especially the shorter distances than the expected 120 nm can be explained by the fact that here, 2D-MINFLUX microscopy was performed. The maximal distance between YopD and YscL would thus only be reflected in the images when the T3SS would be perfectly in plane. Any angular deviation would result in a shorter distance between YopD and YscL in the image. This issue could now be resolved by using 3D-MINFLUX microscopy, which was not possible at the time this image was taken. Another option to explain the variations in distances between YopD and YscL is, that the arrows in Fig. 14 do not actually indicate translocons and sorting platforms that belong to one T3SS. It is possible that some of the Halo-YscL protein complexes were not stained at all, thus they are not visible and as a consequence a translocon was assigned to a "wrong" Halo-YscL signal.

Another reason why this image only reflects a preliminary result, is that in some cases, both fluorescent signals are visible at the same position (e.g. Fig. 14, enlarged areas 1 and 2). This could also be explained by the fact that 2D-MINFLUX was used and the T3SS has a perpendicular orientation to the coverslip. This would result in signals from two different colors at the same *xy* position. In theory, a cross-

reaction/binding between the dyes themselves Halo-SCy5 and 2nd antibody CF680 is imaginable, but there are no publications to date that actually proof that concern. A likely option for the fact that fluorescent signals from the two dyes are visible at the same localization, is that the spectral unmixing did not work 100 % properly. Generally, 2 color-MINFLUX is achieved by using two dyes (here: SCy5 and CF680) that get excited by the same laser. The fluorescent signal is then split up onto two different detectors and can be spectrally unmixed after imaging (described in more detail in chapter 4.1.8. (Schmidt et al., 2021)). It might be possible that some of the signal actually belonging to one dye was assigned to the other dye.

Comparing the number of sorting platform signals present in Fig. 14 to the ones present in Figs. 12 and 13, it seems that the bacterium in Fig. 14 has fewer sorting platforms. Also, this might be due to biological variations but also be accounted to the imaging modalities. In MINFLUX microscopy a buffer to support the on-/off-switching properties of the dyes is used. For one color imaging the optimization of this buffer is straight forward as the buffer needs to be adapted to only one dye and thus can have an optimal composition for that dye. Using two different dyes such as SCy5 and CF680 results in the use of a buffer that is a compromise for both dyes. In comparison to SCy5, CF680 needs higher amounts of MEA (cysteamine) to be switched off, so the amount of MEA (cysteamine) in the buffer needs to be increased. As a drawback, SCy5 is also forced into its off-state. SCy5 needs a lower amount of MEA (cysteamine) to be switched off, so increasing the amount of MEA (cysteamine) in the buffer can result in a higher fraction of SCy5 that is always in its off-state and does not switch on at all. This would result in dyes and in this case sorting platforms, that will not be detected at all by the MINFLUX system.

The dyes SCy5 and CF680 are to this point the best choices for 2 color-MINFLUX microscopy, but that does not mean that they are ideal for this purpose, as they were not specifically designed to be MINFLUX dyes. Also here, in future years more dyes specifically for MINFLUX microscopy will be developed and will further improve MINFLUX imaging (Gwosch et al., 2022).

5.4 Following infection processes using Live-STED microscopy

Live microscopy is an essential tool to follow dynamics of infection processes. It has been shown recently that the innovative labeling approach using an ALFA-tag and fluorescently labeled nanobodies allows live microscopy of the translocon protein

YopD (Rudolph et al., 2022). Using this approach dynamics of pore formation and degradation in combination with different cellular e.g. immune-markers can be performed and set into relation with each other. To gain more detailed insights into single translocons during a live infection process live STED-microscopy is a useful tool. The results depicted in Figs. 15 and 16 show images of proof-of-principle experiments that generally use the same experimental approach as shown by Rudolph and colleagues (Rudolph et al., 2022). A major concern was that infections could maybe not be visualized over a long time period due to higher laser intensities in STED microscopy that might lead to bleaching of fluorophores quickly. Not only is the pixel size in STED microscopy decreased to achieve higher resolutions, but also two lasers are used in STED microscopy, one excitation and one depletion laser. In comparison to fixed microscopy, the samples cannot be embedded into a mounting medium that includes anti-fading reagents. Contrary to these concerns, a large number of STED images (~1200 images) can be taken before major bleaching effects start to appear, as proven in Figs. 15 and 16. This allows imaging of infections over a long time period as shown in Fig. 15 or of shorter time periods, but with 3D-STED, potentially providing further insights into single translocons during an infection. As shown recently, YopD-ALFA signal intensity also decreases and/or disappears after some time (Rudolph et al., 2022). The fact that a decrease or disappearance of the YopD-ALFA signal cannot be seen in the Live-STED experiments shown here might have two different reasons. On the one hand, in the experiments of Rudolph and colleagues, Galectin3-GFP, which has been used as marker for host cell membrane damage was transfected into the Hela cells (Paz et al., 2010). Theoretically this component could be the reason for translocon degradation. As Galectin3-GFP was not used in the Live-STED experiments, translocons would not be degraded if this was the case. Galectin3 generally participates in multiple ways in the innate immune response against invading pathogens (Diaz-Alvarez and Ortega, 2017).

5.5 Outlook

The previously described innovative labeling approaches and the recent developments in super-resolution microscopy offer a lot of options for future research questions. Using the ALFA-tag to visualize the translocon during a cell infection using live- and super-resolution microscopy gave new insights into

infection processes (Carsten et al., 2022, Rudolph et al., 2022). In recent experiments, stainings of translocated effectors such as YopQ and YopE were achieved (data not shown). This labeling system can likely be adapted to all translocated effectors, as the ALFA-tag itself is small enough to not disrupt protein functions. The live-visualization of the pore formation by YopD-ALFA stainings was only possible as the ALFA-tag can be accessed by the nanobody from the extracellular space (compare Fig. 6). This is not possible for translocated effectors as they pass from the bacterium through the T3SS into the cell and no part of the protein can be accessed from the extracellular space at any time. Thus, until now only fixed samples that are permeabilized prior to nanobody staining can be used for translocated effector visualizations using this kind of labeling approach. There are recent publications that provide information on how to deliver nanobodies or even antibodies into living cells via photoporation or also transfection reagents, e.g. PULSin (Liu et al., 2020, Hebbrecht et al., 2020, Weill et al., 2008). Using a combination of *Yersinia* strains expressing ALFA-tagged effector proteins and a nanobody transfection should enable a live visualization of translocated proteins and analyses concerning dynamics of effectors during different infection stages. Another approach to visualize translocated, ALFA-tagged proteins could be to express the nanobody that is fluorescently labeled with a genetically encoded fluorophore (e.g. mScarlet) on a plasmid. This plasmid could be transfected into the host cells. This approach was shown to work in proof-of-principle experiments, but in our biological system, the background of the highly expressed labeled nanobody was too strong to clearly visualize translocated effector proteins (data not shown) (Gotzke et al., 2019).

As already shown in chapter 4.1.8. multi-color MINFLUX microscopy is possible but needs improvement. A way to improve multi-color MINFLUX imaging from the sample preparation side would be to use two tags in parallel that have a low offset distance between the protein of interest and the fluorophore. Visualizing both an intrabacterial T3SS component and a translocated effector a combination of self-labeling enzyme and ALFA-tag could be used, respectively. Depending on the T3SS component that should be visualized, also a combination of two different nanobodies could be useful. In addition to a nanobody binding the ALFA-tag, a second nanobody binding to another peptide tag, the Spot-tag, could be used. The Spot-tag itself has a similar size to the ALFA-tag and generally works in a similar way (Virant et al.,

2018). Experiments in our lab have also shown that YopD can also be visualized in the same way using a Spot-tag inserted into YopD at the same position as the ALFA-tag (data not shown). It is imaginable that a mutant that allows for parallel staining of both translocon forming proteins YopD and YopB with nanobodies could further elucidate the dynamics and the composition of the *Yersinia* T3SS translocon.

An additional option to obtain more detailed information specifically about the T3SS translocon could be single-particle averaging. In this present study, single translocons with different potential orientations and staining patterns were shown. To get a more detailed picture of an average translocon it would be helpful to record a large amount of translocons stained with nanobodies using 3D-MINFLUX microscopy and to average the obtained data using single particle averaging, as it is often performed in cryo electron- or STORM microcopy (Doerr, 2016, Sieben et al., 2018).

MINFLUX single particle tracking would be the perfect tool to gain further insights about dynamics of T3SS components, e.g. the intrabacterial sorting platform. The diffusion coefficients of different sorting platform components have already been obtained by single particle tracking of STORM/PALM microscopy (Rocha et al., 2018, Prindle et al., 2022). As MINFLUX allows a higher temporal and spatial resolution in single particle tracking it could be interesting to find out if the results can be confirmed or to also measure diffusions of other T3SS components, e.g. chaperones.

Last, but not least, the combination of nanobodies that can access the cytosol of permeabilized bacteria and/or cell permeant dyes for self-labeling enzymes and MINFLUX microscopy enables for the first time to properly visualize and analyze intrabacterial T3SS components. First experiments in which YopD-ALFA was stained intrabacterially already showed that these proteins are not only present in an "unlocalized" cytosolic state, but seem to accumulate in the periphery of the bacteria during infection (Fig. 8). This could indicate that proteins are translated where they are needed, so in this case in close proximity to T3SSs. Further experiments using mutants for multiple visualizations of T3SS components, effectors, DNA and RNA could help understand the intrabacterial processes during different stages of infection.

Additionally, questions that seem to be very basic and elemental are not yet answered due to technical limitations in the past, which are now overcome. For

example, it is not exactly known how many T3SS there are present per bacterium in different bacterial species. Furthermore, relations between different T3SS components during different stages of infection could be assessed. So far it is unknown how many sorting platforms there are per T3SS or how many of the T3SSs actually form a translocon, resulting in a fully functional and actually infecting T3SS.

6 Material and methods

6.1 Materials

6.1.1 Devices

Table 1 Devices

Device	Product, Manufacturer
Accu-Jet	Accu-jet pro, Brand, Wertheim, Germany
Agarose gel electrophoresis	Agarose gel chamber: Roth, Karlsruhe, Germany
Blotting chamber	OWL HEP-1, Thermo Fisher Scientific, Waltham, USA
Cell counting chamber	Neubauer-Zellzählkammer, Hartenstein, Würzburg, Germany
Cell incubator	CB Series, Binder, Tuttlingen, Germany
Centrifuges	Sorvall RC-5B, Thermo Fisher Scientific, Waltham, USA
	5417R and 5810R, Eppendorf, Hamburg, Germany
	Biofuge pico, Heraeus Instruments, Hanau, Germany
	Sigma 3-18K, Sigma-Aldrich, St. Louis, Missouri, USA
	Sarstedt MC 6 Centrifuge, Nümbrecht, Germany
	Strip rotor MC 6 – 0.2 ml, 2x 8f, Sarstedt, Nümbrecht, Germany
Clean bench	Hera Safe, Thermo Fisher Scientific, Waltham, USA
Developer for X-ray films	Curix 60, Agfa, Morstel, Belgium
Electroporator	Gene Pulser II electroporator with Puls controller Plus, Biorad
Electrophoresis	Mini-Protean II, Biorad, Munich, Germany
Film cassette	Hartenstein, Würzburg, Germany
Freezer	-20 °C: comfort, Liebherr-International AG, Bulle, Switzerland
	-80 °C: HERA freezer, Heraeus, Kendro Laboratory, Hanau, Germany
Freezing containers	Cryo freezing containers, Nalgene Scientific, Rockford, USA
Incubator shaker	Certomat BS-1, Sartorius, Göttingen, Germany
Magnetic stirrer	RCT-Basic, IKA-Labortechnik, Staufen, Germany
NanoDrop® ND-1000	PeqLab, Erlangen, Germany
pH meter	Seven easy, Mettler-Toledo, Giessen, Germany
Photometer	Ultrosepc 3000 pro, Amersham/GE Healthcare Europe, Munich, Germany
Pipettes	2, 10, 100, 200, 1000 µl, Research Plus, Eppendorf, Hamburg, Germany
Power supply unit	Power Pac 2000, BioRad, Munich, Germany
Refrigerator	4-8 °C, Liebherr Premium, Liebherr-International AG, Bulle, Switzerland
SDS-PAGE electrophoresis cell	SDS-PAGE: Mini-Protean II Biorad, Munich, Germany
Scanner	CanoScan 4400F, Canon, Amsterdam, Netherlands

Thermoblock	DRI-Block DB3, Techne, Bibby Scientific Limited, Staffordshire, USA
Thermocycler	Thermocycler peqStar, PeqLab, Erlangen, Germany
Transilluminator	Vilber Lourmat, ETX, Eberhardzell, Germany
UV-Transillumnator and detector	ChemiDocXRS, Biorad, Hercules, California, USA
Vortex	REAX Topo, Heidolph Instruments, Scwabach, Germany
Water bath	GFL Typ 1013, GFL, Burgwedel, Germany
Weighing scales	440-47N, Kern, Balingen-Frommern, Germany
Western blot imaging system	Cytica ImageQuant 800

6.1.2 Microscopes

Table 2 Technical data for the confocal Laser-Scanning-microscope Leica TCS SP8 X

Components	Product, manufacturer
Microscope	Leica DMi8, Leica, Wetzlar, Germany
Objectives	63x HC PL APO Oil CS2; NA: 1.40; WD (mm): 0.14
Detectors	2x HyD, 2x PMT, 1x Trans-PMT
Laser lines	White light laser, pulsed (WLL): 470-670; Diode: 405
Filters for fluorescence	Filtersystem (em.-color, dye): excitation | beamsplitter | emission L5 ET (green; AF488, GFP): BP 480/40 | FP 505 | em. BP 527/30 A (blue; DAPI): BP 340-380 | FP | LP 425 I 3 (green; AF488, GFP): BP 450-490 | FP | LP 515 N 2.1 (red; AF568, mCherry): BP 515-560 | FP |LP 590
UV-lamp	EL 6000 120 W (LQHXP 120 LEJ)
Halogen lamp	100 W, 12 V
Further features	Piezo Focus drive: SuperZ Galvo type H
Software	Leica LAS X SP8

Table 3 Technical data for the confocal Laser-Scanning-microscope Leica TCS SP5

Components	Product, manufacturer
Microscope	Leica DMI 6000, Leica, Wetzlar, Germany
Objectives	63x HCX PL APO Lbd. Bl. Oil; NA: 1.4-0.60; WD (mm): 0.11
Detectors	3x HyD, 1x PMT, 1x Trans-PMT
Laser lines	Diode: 405; Multi-Ar: 458/476/488/496/514; DPSS: 561; HeNe: 633
Filters for fluorescence	Filtersystem (em.-color, dye): excitation | beamsplitter | emission L5 ET (green; AF488, GFP): BP 480/40 | FP 505 | em. BP 527/30

A (blue; DAPI):
BP 340-380 | FP | LP 425
I 3 (green; AF488, GFP):
BP 450-490 | FP | LP 515
N 2.1 (red; AF568, mCherry):
BP 515-560 | FP |LP 590

UV-lamp	EL 6000 120 W (LQHXP 120 LEJ)
Halogen lamp	100 W, 12 V
Spectral separation	AOBS® + spectral detectors
Tandem-Scanner	Variable: 512x512 @ 5 fps; max. 8192x8192 px; max. 2800 lines/s; 1x-32x zoom
	Resonant: 512x512 @25 fps; max. 1024x1024 px; max. 16.000 lines/s; 1.7x-32x zoom
Further features	Piezo Focus drive: SuperZ Galvo type H
Software	Leica LAS AF

Table 4 Technical data for the superresolution microscope Olympus-Abbelight SMLM

Components	Product, manufacturer
Microscope	Olympus IX-81, Evident Europe GmbH, Hamburg, Germany
Objectives	100x UPlan Apo HR TIRF Oil, NA: 1.50, WD (mm): 0.11 (CS: 0.13-0.19 @ 37 °C), pixel size in image (µm): 0.116
	150x U Apo N TIRF Oil, NA: 1.45, WD (mm): 0.07 (CS: 0.13-0.19), pixel sizw in image (µm): 0.078
Cameras	Hamamatsu ORCA Flash 4.0 V2, Gain: 0.5 e$^-$/ADU
Laser lines	Solid-state: 405 nm (100 mW); 488 nm (200 mW); 561 nm (100 mW); 640 nm (140 mW)
Acquisition software	OlympusCell Sense V1.14, Abbelight Neo
Analysis software	Abbelight Neo
TIRF light path	Motorized, for 405/488/561/640 nm excitable fluorophores
3D SMLM extension	Abbelight SAFe 180 with astigmatism lens
Hardware focus	ZSC2
Actively damped optical table	Newport

Table 5 Technical data for the superresolution microscope Abberior STED

Components	Product, manufacturer
Microscope	Nikon Ti-E with perfect focus system, Nikon Europe B.V., Amstelveen, Netherlands
Objectives	60x P-Apo Oil, NA: 1.40, WD (mm): 0.13
Detectors	4x APD, 1xCCD camera (The Imaging Source DMK 33G274)
Laser lines	Excitation lines (nm): Pulsed & continuous wave: 518/640; Pulsed (nm): 405/488/561

	STED laser lines (nm): 595/775
Pinhole size	Variable
Gated STED	Resolution <30x30 nm in XY
Detection channels	GFP 495/25; YFP 545/25; Red1 615/20; Red2 685/70
Filters for epifluorescence	Filtersystem (em.-color, dye): excitation DAPI: 405 nm FITC, Star488: 470 nm CY3: 590 nm CY5, Star635P: 635 nm
UV-VIS illlumination	LED
Halogen lamp	100 W
CO2 controller	Okolab
Temperature controller	Okolab
Software	Abberior Imspector
Easy 3D	Spatial light modulators for 3D STED @ 595 & 775 nm and resolution <100x100x100 nm in XYZ
RESCue STED	For bleaching reduction
DyMIN STED	Light dose management for super-resolution live-imaging
MINFIELD STED	Light dose management for higher contrast and resolution
Motorized XY stage	M-687 PILine (Physik Instrumente)
Piezo focus drive	P-736 PInano (Physik Instrumente, 220 μm travel range)
Quad-scanner	512x512 @ 5 fps; max. 16.000x16.000 px
FLIM/FCS/FCCS	Becker&Hickl SPC150 TCSPC board
Actively damped optical table	Thorlabs

Table 6 Technical data for the superresolution microscope Abberior MINFLUX

Components	Product, manufacturer
Microscope	Olympus IX83, Evident Europe GmbH, Hamburg, Germany
Objectives	100x UPlanXApo; NA: 1.45; WD (mm): 0.13
Detectors	4xAPD, 1xPMT
Laser lines	Excitation (nm): Pulsed & continuous wave: 640; Pulsed: 561; Continuous wave: 405, 488 MINFLUX laser lines (nm): 640
Pinhole size	Variable
2D/3D MINFLUX	Localization precision 1-3 nm in XY (2D mode) and in Z (3D mode)
Detection channels (nm)	GFP: 500-550; Cy3: 545/25; Cy5 (near): 650-685; Cy5 (far): 685-720
Filters for epifluorescence	Filtersystem (em.-color, dye): Quad-band, EX | BS | EM (nm) DAPI: 387/11 | 410 | 440/40 FITC, Star488: 485/20 | 504 | 521/21 CY3: 559.5/25 | 582 | 607/34 FLUX-640, AlexaFluor647: 649.5/13 | 669 | 700/45

UV-VIS illumination	CoolLED pE-4000, 16 LEDs for excitation in the range 365-770 nm
Halogen lamp	100 W, standard housing
MINFLUX 3D	Electronically deformable mirrors for 3D MINFLUX @ 640 nm and localization precision 1-3 nm in XYZ
Alignment	Motorized auto-alignment of all lasers and pinhole
Motozized XY stage	Olympus
XYZ stabilization	Physic Instruments PI Nano XYZ, active sample stabilization with nm precision along all 3 dimensions; 975 nm laser (Cobalt), CCD Camera (The Imaging Source)
Scanners	QUADscan beam scanner; ultra fast beam scanner for MINFLUX imaging
Actively damped optical table	Thorlabs
Software	Abberior Imspector

6.1.3 Disposables

Table 7 Disposables

Item	Company
Bottle-top sterile filter units	Steritop Filter Units 0.22 µm, Merck Millipore, Darmstadt, Germany
Cell culture dishes	100 mm, Sarstedt, Nümbrecht, Germany
Coverslips	12mm, No. 1.5H for high resolution, Marienfeld GmbH, Lauda-Königshafen, Germany
	18 mm, No. 1.5H, Marienfeld GmbH, Lauda-Königshafen, Germany
Cryo tubes	1.6 ml, Sarstedt, Nümbrecht, Germany
Disposable inoculation loop	10 µl, Sarstedt, Nümbrecht, Germany
Electroporation cuvettes with 1 mm elctrode gap	PeqLab Biotechnologie GmbH, Erlangen, Germany
Glass pasteur pipettes	230 mm, Heinz Herenz Medizinalbedarf, Hamburg, Germany
Multi-well-plates	6-/24-well, Sarstedt, Nümbrecht, Germany
Object slides	76x26 mm, Karl Hecht, Sondheim, Germany
Parafilm	M Bemis, Pechiney Plastic Packaging, Neenah, USA
Pipette tips	Sterile filter tips, Biosphere 10, 200, 1.000 µl, Sarstedt, Nümbrecht, Germany
PVDF-membrane	Immobilion-P, 0.45 µm pore size, Mollipore, Billerica, USA
Reaction tubes	Sterile 15 ml/50 ml, Sarstedt, Nümbrecht, Germany
	0.2 ml, Biozym Scientific, Hessisch Odendorf, Germany
	0.5 ml; 1.5 ml; 2 ml, Sarstedt, Nümbrecht, Germany
Scalpel	Sterile, B. Braun, Melsungen, Germany

Serological Pipettes	Sterile 2, 5, 10, 25 ml, Sarstedt, Nümbrecht, Germany
Syringe filters	SFCA 0.2 µm, Thermo Scientific/Nalgene, Rockford, Illionois, USA
Whatman paper	190 g/m², BioRad, Munich, Germany
X-Ray film	Super RX, Fuji Medical X-Ray films, Fujifilm, Tokyo, Japan

Table 8 Kits, enzymes, reagents

Kits, enzymes, reagents	Manufacturer
16% paraformaldehyde	Electron Microscopy Science, Hatfield, USA
µ-Slide 8 well (80826)	Ibidi, Gräfelfing, Germany
Catalase from bovine liver	Sigma-Aldrich, St. Louis, USA
Digitonin	Sigma-Aldrich, St. Louis, USA
Glass Bottom Microwell Dishes	MatTek Corporation, Ashland, Massachusetts, USA
Glucose Oxidase from *Aspergillus niger*	Sigma-Aldrich, St. Louis, USA
Gold nanorods	Nanopartz Inc., Loveland, USA
Mercaptoethylamine (Cysteamine)	Sigma-Aldrich, St. Louis, USA
NucleoBond® Xtra Maxi EF	Macherey-Nagel, Düren, Germany
NucleoSpin® Gel and PCR Clean-up	Macherey-Nagel, Düren, Germany
PageRuler Prestained Protein Ladder	Thermo Fisher Scientific, Waltham, USA
Phosphate buffered saline	Sigma-Aldrich, St. Louis, Missouri, USA
Plasmid miniprep kit I (C-Line)	PeqLab, Erlangen, Germany
ProLong Glass	Thermo Fisher Scientific, Waltham, USA
Smart kit for STORM	Abbelight, Cachan, France
SuperSignal West Femto/Pico detection	Thermo Fisher Scientific, Waltham, USA
Trypsin 0.05 %, 0.53 mM EDTA x 4Na with phenol red	Invitrogen, Life Technologies, USA
TurboFect Transfection Reagent	Thermo Fisher Scientific, Waltham, USA
twinsil	Picodent, Wipperfürth, Germany

6.1.4 Buffers and reagents

Chemicals were obtained from Amersham/GE Healthcare, Munich (Germany), BD Biosciences, Heidelberg (Germany), Biozyme, Oldendorf (Germany), Dianova, Hamburg (Germany), Fermentas, St. Leon-Rot (Germany), Invitrogen/Life Technologies, Carlsbad (USA), Merck, Darmstadt (Germany), PAA, Pasching (Austria), PromoCell, Heildelberg (Germany), Roth, Karlsruhe (Germany) and

Sigma-Aldrich, St. Louis (USA): Buffers were autoclaved for 20 min at 121 °C and 1.4 bar or sterile filtered.

Table 9 Buffer compositions

Buffers	Concentration	Components
Digitonin permeabiliztaion buffer for immunofluorescence	0.009 % (w/v)	Digitonin in 1x PBS
Triton permeabilization buffer for immunofluorescence	0.1 % (v/v) 0.005 % (v/v)	Triton X-100 in 1x PBS
<u>SDS-PAGE/Western Blot</u>		
4x Laemmli (sample buffer for SDS-PAGE)	240 mM 8 % (w/v) 40 % (w/v) 5 % (v/v) 0.04 % (w/v)	Tris pH 6.8 SDS Glycerol β-mercaptoethanol Bromphenol blue
Resolving buffer	1.5 M 0.1 % (w/v)	Tris-HCl pH 8.8 SDS
Stacking buffer	0.5 M 0.1 % (w/v)	Tris-HCl pH 6.8 SDS
SDS-PAGE running buffer	25 mM 190 mM 0.1 % (w/v)	Tris Glycine SDS
Transfer buffer	150 mM 25 mM 20 % (v/v)	Tris Glycine Methanol
TBS-T	1x 0.1 % (v/v)	TBS Tween20

6.1.5 Antibodies

The antibodies used for immunofluorescence stainings were diluted in 3 % BSA (in 1x PBS). The antibodies used for Western Blots were diluted in 5% milk powder in 1x TBS-T or PBS-T.

Table 10 Primary antibodies

Antigen	Species	Dilution (IF)	Dilution (WB)	Origin
Actin (monoclonal)	Mouse	-	1:10,000	Millipore, Schwalbach, Germany
Calnexin (polyclonal)	Rabbit	-	1:2,000	Enzo, Lörrach, Germany
YopB (1-168)	Rat	1:50	1:1,000	Serum

YopD (150-287)	Rabbit	1:50	1:1,000	Serum

Table 11 Secondary antibodies

Name/Conjugation	Dilution in 3 % BSA	Manufacturer
AlexaFluor Plus 594	1:200	Invitrogen, Life Technologies, USA
CF680	1:400	Biotium Inc., USA
Donkey anti-rabbit IgG HRP	WB: 1:50,000	GE Healthcare
Goat anti-rat IgG HRP	WB: 1:50,000	GE Healthcare

6.1.6 Nanobodies, dyes and labeling substrates

Table 12 Nanobodies, dyes and labeling substrates

Name	Target	Conjugation	Dilution	Origin
Nanobodies				
FluoTag-X2 anti-ALFA	ALFA-tag	Abberior® Star 580, 635P AlexaFluor 647 SulfoCy5 HRP	IF: Confocal: 1:300 STED: 1:150 STORM: 1:1,500 MINFLUX: 1:1,500 WB: 1:40,000	NanoTag Biotechnologies, Göttingen, Germany
Labeling substrates				
HaloTag AlexaFluor 647	Halo-tag	AlexaFluor 647	IF: Confocal: 1 µM STORM: 0.25 µM MINFLUX: 0.25 µM	Promega, Madison, Wisconsin, USA
Dyes				
Phalloidin	F-Actin	AlexaFluor 488, 568, 647	IF: 1:200	Invitrogen, Carlsbad, USA
300 nM DAPI	DNA	405	IF: 1:5,000	Invitrogen, Carlsbad, USA

6.1.7 Growth media and additives

Media were autoclaved for 20 min at 121 °C and 1.4 bar. Supplements, that could not be autoclaved were sterile filtered.

Table 13 Growth media for the cultivation of bacteria

Medium	Concentration	Component
LB (Lysogeny broth)-Medium, pH 7.5	10 g/l	Tryptone
	5 g/l	Yeast extract
(Roth, Karlsruhe, Germany)	10 g/l	NaCl
LB (Lysogeny broth)-Agar, pH 7.0	10 g/l	Tryptone
(Roth, Karlsruhe, Germany)	5 g/l	Yeast extract
	10 g/l	NaCl
	15 g/l	Agar

Table 14 Antibiotics and additives for the cultivation and selection of bacteria

Additive	Dissolved in	Concentration	Manufacturer
Nalidixic acid	1 M NaOH	100 µg/ml	Sigma-Aldrich, St. Louis, USA
Kanamycin	ddH$_2$O	50 µg/ml	Sigma-Aldrich, St. Louis, USA
Diaminopimelic acid	ddH$_2$O	8 mg/ml	Sigma-Aldrich, St. Louis, USA
Arsenite	ddH$_2$O	19.5 mg/ml	Sigma-Aldrich, St. Louis, USA
EGTA	ddH$_2$O	0.5 M	Sigma-Aldrich, St. Louis, USA
Magnesiumchloride	ddH$_2$O	1 M	Merck, Darmstadt, Germany
D-(+)-Glucose	ddH$_2$O	20 %	Merck, Darmstadt, Germany

Table 15 Growth media for the cultivation of eukaryotic cells

Medium	Concentration	Additive	Manufacturer
Dulbecco's Modified Eagle Medium (DMEM)			Gibco, Carlsbad, California, USA
	10 % (v/v)	Fetal calf serum	Gibco, Carlsbad, California, USA

6.1.8 Plasmids

Table 16 Expression plasmids

Plasmid	Vector		Origin
Myc-Rac1Q61L	pRK5-myc, active Rac1	constituviely	Pontus Aspenström, Uppsala, Sweden (Aspenstrom et al., 2004)
PLCδ1-PH-GFP	pEGFP-N1, membrane marker, PI84,5)P2 indicator; Kan^R	plasma	Aepfelbacher lab (Rudolph et al., 2022)

6.1.9 *Yersinia* strains and eukaryotic cells

Table 17 *Yersinia enterocolitica* strains

Strain	Features	Reference
WA-314	Wild type strain carrying the virulence plasmid pYV; serogroup O8; kanamycin resistance cassette (Kan^R)	(Heesemann and Laufs, 1983, Oellerich et al., 2007)
WA-314 YopD-ALFA	Wild type strain carrying the virulence plasmid pYV (Kan^R) with ALFA-tag inserted between amino acid 194 and 195	(Rudolph et al., 2022)
E40ΔHOPEMT Halo-YscL	Deletion mutant lacking effector proteins YopH,O,P,E,M,T; arsenite resistance cassette (Ars^R)	(Diepold et al., 2017)

Table 18 Eukaryotic cells

Name	Features	Origin
HeLa	Human cervical carcinoma cell line	ACC# 57, DSMZ-Deutsche Sammlung von Mikroorganismen und Zellkulturen GmbH, Brunswick, Germany

Table 19 Software

Software	Manufacturer
FijiVersion 1.53t/ImageJ	Bethesda, USA
Abberior Imspector	Abberior Instruments GmbH, Göttingen, Germany
Abbelight Neo	Abbelight, Cachan, France
Paraview	Sandia National Laboratories, Kitware, Los Alamos National Laboratory

6.2. Methods

6.2.1 Cell culture

All cell culture experiments were performed at clean benches under sterile condition.

6.2.1.1 Cultivation of eukaryotic cells

HeLa cells were cultivated in DMEM (Dulbecco's Modified Eagle Medium, Gibco, USA) supplemented with 10 % (v/v) FCS (Gibco, USA) in a humidified incubator at 37 °C and 5 % CO_2. The cells were passaged when becoming confluent. For this, the growth medium was removed and cells growing in 10 cm dishes were washed

with 3 ml sterile 1x PBS and 1 ml 0.05 % Trypsin was added for 5 min at 37 °C to detach cells from the dish. The cells were resuspended in pre-warmed DMEM+FCS to stop the enzymatic activity of the trypsin and their density was determined using a counting chamber. The suspension was diluted either for further cultivation in 10 cm dishes or for seeding on coverslips (approximately $6x10^4$ cells /cm²) or in live imaging dishes for microscopy experiments (approximately $2-3x10^4$ cells/cm² for 8-well ibidi chamber slide or $3x10^5$ cells/cm² for MATTEK dishes).

6.2.1.2 Cryoconservation and reactivation of eukaryotic cell lines

For cryoconservation, HeLa cells were resuspended in 1.5 ml FCS with 10 % (v/v) DMSO preventing the formation of crystals damaging the cells. The suspension was transferred to a cryo-tube which was placed in an isopropanol filled cryocontainer (Nalgene Scientific, USA). The container was frozen overnight at -80 °C and the tubes transferred to liquid nitrogen storage containers afterwards.

For reactivation, HeLa cells were thawed and immediately resuspended in pre-warmed cell culture medium. The cells were resuspended in 10 ml cell culture medium and transferred to a cell culture dish for further cultivation. The medium was renewed once the majority of cells attached. After one round of splitting and recultivating the HeLa cells, they were used for further experiments.

6.2.1.3 Transfection of HeLa cells

HeLa cells were transfected using Turbofect (Thermo Fisher Scientific, USA) as a transfection reagent. For each 24-well 0.25 µg DNA for myc-Rac1Q61L or 0.5-1 µg for other plasmids was diluted in 100 µl Opti-MEM (Gibco, USA) and mixed with 2 µl Turbofect. After vortexing and 20 min incubation at room temperature, the solution was added to the coverslips before adding Hela cells on top and incubated at 37 °C and 5 % CO_2 for approximately 16 h. At least 2 h before infection the medium was replaced to prevent the transfection reagent interfering with infection or affecting immunofluorescence staining.

6.2.2 Microbiological methods

6.2.2.1 Cultivation and strain maintenance of Yersinia enterocolitica

The *Yersinia enterocolitica* strains used in this study were cultivated from frozen stocks at 27 °C for 24-48 hours on Lysogeny broth (LB) plates containing the specific antibiotics and could be stored at 4 °C for up to 4 weeks. Liquid bacteria culture in the exponential growth phase were mixed in equal proportions with 40 % glycerol in LB medium and frozen at -80 °C for long term storage. For experiments, bacteria were inoculated from LB plates in 2.5 ml LB medium in test tubes with suitable antibiotics added and were grown overnight at 27 °C in a shaker incubator at 180 rpm.

6.2.2.2 Secretion conditions (*released proteins* assay)

In vitro secretion of Yop effectors can be achieved by Ca^{2+} depletion of the culture medium at 37 °C (Heesemann et al., 1986). For activation of the T3SS, *Yersinia* precultures were diluted 1:20 in fresh LB medium and cultivated for 1.5 h shaking at 37 °C. By adding 15 nM $MgCl_2$, 5 nM EGTA and 0.2 % glucose to the medium and incubating the cultures at 37 °C for three hours, secretion of Yop effectors was induced. Secreted proteins were separated from the bacteria by centrifugation (10 min, 5,000 x *g*, 4 °C).

Immunofluorescence stainings of Yop secretion active bacteria are further described in chapter 6.2.5.1.

For biochemical investigations of the secreted Yops, 10 % TCA (trichloroacetic acid) was added to the supernatant after centrifugation and sterile filtration. Precipitation of bacterial proteins was performed at -20 °C overnight. Precipitates were centrifuged (20,000 x *g*, 4 °C, 1 h) and washed with ice-cold acetone (10,000 x *g*, 4 °C, 10 mins). The protein pellet was dried and resuspended in Laemmli buffer. Due to the previous treatment and through remainings of acetone, a change in pH and a resulting color shift could appear. This could be corrected by adding crystalline Tris-Base. The samples were then incubated at 95 °C for 5 minutes and stored a -20 °C.

6.2.2.3 *Yersinia* infection

For infection experiments, *Yersinia* overnight cultures were diluted 1:20 in fresh LB medium with added suitable antibiotics and grown at 37 °C for 1.5 h in a shaker

incubator (180 rpm) to induce expression of the virulence plasmid. Then, bacteria were pelleted by centrifugation (10 min, 5000 x g, 4 °C) and the pellet was resuspended in 1 ml ice-cold 1x PBS. The OD_{600} was set to 3.6 and depending on the experiment and its needed multiplicity of infection (MOI) further adjusted to a lower OD_{600} (0.36 or 0.72). The number of bacteria used for infection was adjusted depending on the area of the culture dish seeded with cells and MOI intended for the experiment. The cell culture dishes were spun down (1 min, 200 x g, RT) to synchronize the beginning of infection before being placed into the 37 °C incubator with 5 % CO_2. The duration of infection varied between experiments, mostly between 40 to 120 mins. The infected cells were washed once with 1x PBS to remove unattached bacteria. Afterwards the cells were wither fixed with 4 % PFA in PBS for immunofluorescence staining (see chapter 6.2.5.1.) or further processed for live-cell imaging (see chapter 6.2.5.2.).

6.2.2.4 Preparation of chemically competent bacteria

To introduce plasmids into *E. coli* Top10 for cloning or plasmid production, bacteria were made chemically competent.

Bacteria were grown overnight at 37 °C. The overnight culture was diluted 1:100 in 100 ml LB medium and grown until OD_{600} of 0.6-0.8. Bacteria were pelleted by centrifugation (10 min, 5000 x g, 4 °C), the supernatant was removed and bacteria were resuspended in 100 ml ice-cold 50 mM $CaCl_2$. The suspension was incubated for 10 min at 4 °C before further centrifugation (10 min, 5000 x g, 4 °C). The resulting pellet was resuspended in 50 ml ice-cold 50 mM $CaCl_2$ and incubated on ice for at least 1.5 h. After centrifugation (8 min, 5000 x g, 4 °C) bacteria were resuspended in 4 ml ice-cold $CaCl_2$ with 15 % glycerol. Aliquots of 50-100 µl were flash frozen in liquid nitrogen and stored at -80 °C.

6.2.2.5 Transformation of chemically competent bacteria

For plasmid transformation, the aliquots were thawed on ice and incubated with approximately 1 µg DNA for 20 min. The tubes were placed at 42 °C for 45 sec and then left on ice for 2 min. Then, 500 µl of LB medium was added and bacteria were incubated at 37 °C for 1.5 h in a shaker incubator. Afterwards the bacterial suspension was plated on LB plates containing the appropriate antibiotics.

6.2.3 Molecular biology methods

6.2.3.1 Isolation of plasmid DNA

Plasmid isolations were performed using the Plasmid miniprep kit I (C-Line, Peqlab, Germany) according to the protocol supplied by the manufacturer. Larger amounts of DNA were acquired using the NucleoBond® Xtra Maxi EF kit (Macherey-Nagel, Germany) according to the protocol supplied by the manufacturer. All DNA was stored at -20 °C.

6.2.3.2 Determination of DNA concentration

To determine the concentration of dsDNA in solution, the absorption at 260 nm was measured using the NanoDrop® ND-1000 spectrophotometer with the ND-1000 V 3.1.0 software (PeqLab, Germany). Following the manufacturer's instructions, the samples were measured against a blank (ddH$_2$O or elution buffer from plasmid isolation kits mentioned in 6.2.3.1). By looking at the ratio of absorption OD$_{260}$/OD$_{280}$ the solution was tested for contamination with protein or phenol. Values between 1.8 and 2 show the lowest level of contaminants.

6.2.4 Proteinbiochemical methods

6.2.4.1 Affinity purification of antisera for immunofluorescence stainings

The primary antibodies against YopB and YopD used in this study were produced and tested for their specificity by Franziska Huschka (Huschka, 2017). The sera were affinity purified as described previously (Huschka, 2017).

For detection of YopB and YopD using immunofluorescence microscopy, a further purification step was necessary. Secreted protein of *Y. enterocolitica* strain WA-314 (compare chapter 6.2.2.2.) were transferred to an PVDF membrane via Western Blot. The membrane was incubated in coomassie staining solution, the corresponding protein bands (YopB 43 kDa; YopD 33 kDa) were cut from the membrane and destained with Methanol for further purification. After washing thrice with PBS-T (PBS + 0.1 % Tween20), unspecific binding sites were blocked using 5 % (w/v) milk powder in PBS-T. Afterwards, the membrane pieces were washed with PBS-T again and cut into little stripes. Those were incubated rotating in diluted antiserum (1:3 in PBS) overnight at 4 °C. Membrane stripes were washed thrice using PBS-T and the diluted antisera were sterile filtrated and stored at –20 °C for

further purifications. The membrane fragments were immediately neutralized in 5.5 µl 1 M Tris-Base. BSA (final concentration > 3 %) and glycerin (50 % in antibody solution) were added for stabilizing the antibody solutions at cryo conditions.

6.2.4.2 SDS-polyacrylamide gel electrophoresis

The separation of proteins by their molecular weight via denaturating SDS-polyacrylamide gel electrophoresis (SDS-PAGE) is an analytic procedure developed by Laemmli (Laemmli, 1970).

Laemmli buffer is added to the proteins before denaturating them at 95 °C for 5 min. Disulfid-bridges are reduced by β-mercaptoethanol. Sodiumdodecylsulfate (SDS) denaturates and covers the proteins with a strong negative charge, so that the proteins can be separated by their molecular weight in an electrical field towards the anode. The negatively charged proteins are separated by a gel consisting of two parts, a 4 % stacking gel (Tris-HCl pH 6.8) and a 10-15 % resolving gel (Tris-HCl pH 8.8). The composition of the two components of these gels is given in table 20 below. A prestained molecular weight marker was used as standard. First, the gel was run at 80 V for 30 min to allow the proteins to focus at the edge of the resolving gel. A current of 150 V was used for separation of the proteins within in the resolving gel.

Table 20 Composition of a 10 % acrylamide SDS-PAGE mini gel

Component	4 % stacking gel	10 % resolving gel
ddH$_2$O	1.55 ml	4.2 ml
Stacking buffer pH 6.8	625 µl	
Resolving buffer pH 8.8		625 µl
Acrylamide 30 %	3.3 ml	325 µl
APS (10 mg/ml)	50 µl	12.5 µl
TEMED	5 µl	2.5 µl

6.2.4.3 Western blot analysis

Transferring the gel electrophoretic separated proteins onto a PVDF membrane (Immobilion-P, Millipore) was achieved with a semidry-proteinblot-system. The PVDF-membranes were activated in methanol. For the transfer, the membrane was put onto the gel at its anode-site. All components of the protein blot were soaked in transfer buffer. Membrane and gel were enclosed by three layers of Whatman filter paper. The transfer of the proteins took place at constant electric current (125 mA/cm²) for 75 min. The immunodetection of specific proteins was achieved using

epitope specific antibodies (Table 10). The membrane was blocked in 5 % milkpowder in PBS-T for at least 30 min on room temperature. The antibodies were also diluted in 5 % milkpowder in PBS-T. The membrane was incubated with the primary antibody overnight at 4 °C. After washing thrice with PBS-T, the membrane was incubated with the secondary antibody coupled to HRP (horseradish peroxidase). Membranes were washed thrice in PBS-T, incubated with chemiluminescence reagent (Supersignal West Femto, Pierce Chemical) for 5 min and developed.

6.2.5 Microscopy

6.2.5.1 Immunofluorescence staining

Immunofluorescence stainings were performed as described in Carsten et al., 2022. HeLa cells seeded on coverslips were infected with *Yersinia* as described in section 6.2.2.3. After infection for the required time the cells were washed with 1x PBS and fixed with 4% formaldehyde (prepared from PFA; Electron Microscopy Science, Hatfield, USA) in PBS for 5 - 10 min and then treated with digitonin solution (90 µg mL^{-1} in PBS) to allow fluorescently labeled NbALFA access translocon-associated but not intrabacterial YopD-ALFA. Bacteria grown under *in-vitro* Yop secretion conditions (compare chapter 6.2.2.2.) were fixed with 4 % formaldehyde in PBS for 5-10 min and then treated with 0.005 % Triton X-100 in PBS to allow the fluorescently labeled Halo-tag substrate to access the intrabacterial Halo-YscL proteins. Unspecific binding sites were blocked with 3% bovine serum albumin (BSA, w/v) in PBS for at least 45 min.

Depending on the microscopy method samples were then incubated with different dilutions of fluorescently labeled FluoTag®-X2 anti-ALFA nanobody in 3 % BSA/PBS (STED: 1:200 dilution for 16 h, NbALFA coupled to Abberior Star 635P; STORM and MINFLUX: 1:1500 dilution for 1 to 2 h, NbALFA coupled to Alexa Fluor 647) or HaloTag® Fluorescent Ligand (Promega, Walldorf, Germany) coupled to Alexa Fluor 647 (STORM and MINFLUX: 0.25 µM for 16 h) (Invitrogen, Rockford, USA). Samples incubated with primary rabbit anti-YopB antibody (STED: 1:50 for 1 h) were washed three times with PBS and then incubated with a 1:200 dilution of anti-rat secondary antibody coupled to Alexa Fluor Plus 594 for at least 2 h. In case of staining intrabacterial YopD-ALFA, bacteria were permeabilized with 0.1 % Triton X-100 for 15 min. Staining of intrabacterial YopD-ALFA was performed with a 1:200

dilution of NbALFA coupled to Abberior Star 580 in 3 % BSA/PBS + 0.05% Triton X-100 over-night. After staining with the respective fluorescent labels, samples were washed multiple times with PBS. All PBS used for immunofluorescence staining was bought from Sigma-Aldrich (USA) and contained $MgCl_2$ and $CaCl_2$ and all antibodies and their dilutions can be found in Table 9 and Table 10.

6.2.5.2 Nanobody staining for Live-STED nanoscopy

HeLa cells (transfected with PLCδ1-PH-GFP) seeded on either 8-well ibidi chamber slides or MatTek 35 mm dishes were placed into the environmental chamber (conditions: 37 °C; 5 % CO_2) of the Abberior STED microscope. *Yersinia* infection and nanobody staining were performed in parallel at the microscope by replacing the DMEM medium in the imaging dish with fresh, pre-warmed DMEM containing *Yersinia* with an MOI of 20-40 and NbALFA coupled to Abberior® Star 635P (dilution: 1:150). When PLCδ1-PH-GFP showed formation of pre-vacuoles the Live-STED imaging was started in these positions, as described in 6.2.5.5.

6.2.5.3 Confocal microscopy

The microscopy samples were observed either using the laser scanning microscope Leica TCS SP8 with a 63x oil immersion objective (NA 1.4) and the LAS X SP8 software (Leica Microsystems, Germany) or the laser scanning microscope Leica TCS SP5 with a 63x oil immersion objective (NA 1.4) and the LAS AF software (Leica Microsystems, Germany).

6.2.5.4 STORM nanoscopy

STORM nanoscopy and corresponding epifluorescence microscopy were carried out as described in Carsten et al., 2022 using a Abbelight SAFe 180 setup based on an Olympus IX-81 microscopy body and employed for excitation and detection of the fluorescence signal a 100x UPlan Apo HR TIRF oil immersion objective with a pixel size of 78 nm. A solid-state 640 nm laser was used for excitation (10% laser intensity for epifluorescence imaging; 70% laser intensity for STORM imaging). The detected fluorescence signal was recorded by a Hamamatsu ORCA Flash 4.0 V2 camera. 10,000 frames at 50 ms exposure time were acquired for reconstruction of

the STORM image. Resulting coordinate tables and images were processed using Abbelight SAFe NEO software.

6.2.5.5 (Live-) STED nanoscopy

STED nanoscopy and corresponding confocal microscopy were carried out as described in Carsten et al., 2022 in line sequential mode using an Abberior Instruments Expert Line STED microscope based on a Nikon Ti-E microscopy body and employed for excitation and detection of the fluorescence signal a 60x Plan APO 1.4 oil immersion objective. A pulsed 640 nm laser was used for excitation and a pulsed near-infrared laser (775 nm) was used for STED. The detected fluorescence signal was directed through a variable sized pinhole (1 Airy unit at 640 nm) and detected by avalanche photo diodes (APDs) with appropriate filter settings for Cy5 (615 - 755 nm). Images were recorded with a dwell time between 0.5 and 1 μs and between 50 to 100 line accumulations. The pixel size was set to be 10 nm for 2D-STED, the voxel size was set to be 40x40x50 nm for 3D-STED. For live-STED imaging the images were recorded with a dwell time between 0.5 and 1 μs and between 6 to 12 line accumulations. The pixel size was set to be 20 nm for 2D-Live-STED, the voxel size was set to be 50x50x50 nm for 3D-Live-STED. The acquisitions were carried out in time gating mode i.e. with a time gating delay of 750 ps and a width of 8 ns. 2D-STED images were acquired with a 2D-STED donut, 3D-STED images were acquired with a 3D-STED donut.

6.2.5.6 MINFLUX nanoscopy

MINFLUX nanoscopy, corresponding confocal microscopy and image rendering were carried out using an Abberior MINFLUX setup (previously described in Schmidt et al., 2021 based on an Olympus IX83 microscopy body equipped with a 100x NA 1.4 oil immersion objective.

6.2.5.7 Determination of the FWHM of single translocon fluorescence signals

The determination of the FWHM of single translocon clusters was performed as described in Carsten et al., 2022. Single translocon clusters were identified, the largest lateral extent of the MINFLUX signal was determined and a plot profile line was drawn (representatively shown in Fig. 9A viii). 26 single translocons of different

bacteria were measured, averaged and plotted and the FWHM was determined (Fig. 10)

7 Literature

ABBE, E. 1873. Beiträge zur Theorie des Mikroskops und der mikroskopischen Wahrnehmung. *Archiv für Mikroskopische Anatomie***,** 413-468.

ACHTMAN, M., ZURTH, K., MORELLI, G., TORREA, G., GUIYOULE, A. & CARNIEL, E. 1999. Yersinia pestis, the cause of plague, is a recently emerged clone of Yersinia pseudotuberculosis. *Proc Natl Acad Sci U S A,* 96**,** 14043-8.

ADEOLU, M., ALNAJAR, S., NAUSHAD, S. & R, S. G. 2016. Genome-based phylogeny and taxonomy of the 'Enterobacteriales': proposal for Enterobacterales ord. nov. divided into the families Enterobacteriaceae, Erwiniaceae fam. nov., Pectobacteriaceae fam. nov., Yersiniaceae fam. nov., Hafniaceae fam. nov., Morganellaceae fam. nov., and Budviciaceae fam. nov. *Int J Syst Evol Microbiol,* 66**,** 5575-5599.

AEPFELBACHER, M. 2004. Modulation of Rho GTPases by type III secretion system translocated effectors of Yersinia. *Rev Physiol Biochem Pharmacol,* 152**,** 65-77.

AEPFELBACHER, M., TRASAK, C. & RUCKDESCHEL, K. 2007. Effector functions of pathogenic Yersinia species. *Thromb Haemost,* 98**,** 521-9.

AGRAIN, C., SORG, I., PAROZ, C. & CORNELIS, G. R. 2005. Secretion of YscP from Yersinia enterocolitica is essential to control the length of the injectisome needle but not to change the type III secretion substrate specificity. *Mol Microbiol,* 57**,** 1415-27.

AILI, M., ISAKSSON, E. L., CARLSSON, S. E., WOLF-WATZ, H., ROSQVIST, R. & FRANCIS, M. S. 2008. Regulation of Yersinia Yop-effector delivery by translocated YopE. *Int J Med Microbiol,* 298**,** 183-92.

AILI, M., ISAKSSON, E. L., HALLBERG, B., WOLF-WATZ, H. & ROSQVIST, R. 2006. Functional analysis of the YopE GTPase-activating protein (GAP) activity of Yersinia pseudotuberculosis. *Cell Microbiol,* 8**,** 1020-33.

AKEDA, Y. & GALAN, J. E. 2005. Chaperone release and unfolding of substrates in type III secretion. *Nature,* 437**,** 911-5.

ALEKSIC, S. & BOCKEMUHL, J. 1984. Proposed revision of the Wauters et al. antigenic scheme for serotyping of Yersinia enterocolitica. *J Clin Microbiol,* 20**,** 99-102.

ALLAOUI, A., SCHULTE, R. & CORNELIS, G. R. 1995. Mutational analysis of the Yersinia enterocolitica virC operon: characterization of yscE, F, G, I, J, K required for Yop secretion and yscH encoding YopR. *Mol Microbiol,* 18**,** 343-55.

AMER, A. A., GURUNG, J. M., COSTA, T. R., RUUTH, K., ZAVIALOV, A. V., FORSBERG, A. & FRANCIS, M. S. 2016. YopN and TyeA Hydrophobic Contacts Required for Regulating Ysc-Yop Type III Secretion Activity by Yersinia pseudotuberculosis. *Front Cell Infect Microbiol,* 6**,** 66.

ANDRADES VALTUENA, A., MITTNIK, A., KEY, F. M., HAAK, W., ALLMAE, R., BELINSKIJ, A., DAUBARAS, M., FELDMAN, M., JANKAUSKAS, R., JANKOVIC, I., MASSY, K., NOVAK, M., PFRENGLE, S., REINHOLD, S., SLAUS, M., SPYROU, M. A., SZECSENYI-NAGY, A., TORV, M., HANSEN, S., BOS, K. I., STOCKHAMMER, P. W., HERBIG, A. & KRAUSE, J. 2017. The Stone Age Plague and Its Persistence in Eurasia. *Curr Biol,* 27**,** 3683-3691 e8.

ASPENSTROM, P., FRANSSON, A. & SARAS, J. 2004. Rho GTPases have diverse effects on the organization of the actin filament system. *Biochem J,* 377**,** 327-37.

ATKINSON, S. & WILLIAMS, P. 2016. Yersinia virulence factors - a sophisticated arsenal for combating host defences. *F1000Res,* 5.

AUTENRIETH, I. B. & FIRSCHING, R. 1996. Penetration of M cells and destruction of Peyer's patches by Yersinia enterocolitica: an ultrastructural and histological study. *J Med Microbiol,* 44**,** 285-94.

BALZAROTTI, F., EILERS, Y., GWOSCH, K. C., GYNNA, A. H., WESTPHAL, V., STEFANI, F. D., ELF, J. & HELL, S. W. 2017. Nanometer resolution imaging and tracking of fluorescent molecules with minimal photon fluxes. *Science,* 355**,** 606-612.

BANAZ, N., MAKELA, J. & UPHOFF, S. 2019. Choosing the right label for single-molecule tracking in live bacteria: side-by-side comparison of photoactivatable fluorescent protein and Halo tag dyes. *J Phys D Appl Phys,* 52**,** 064002.

BARASOAIN, I., DIAZ, J. F. & ANDREU, J. M. 2010. Fluorescent taxoid probes for microtubule research. *Methods Cell Biol,* 95**,** 353-72.

BARBIERI, J. T., RIESE, M. J. & AKTORIES, K. 2002. Bacterial toxins that modify the actin cytoskeleton. *Annu Rev Cell Dev Biol,* 18**,** 315-44.

BARLAG, B., BEUTEL, O., JANNING, D., CZARNIAK, F., RICHTER, C. P., KOMMNICK, C., GOSER, V., KURRE, R., FABIANI, F., ERHARDT, M., PIEHLER, J. & HENSEL, M. 2016. Single molecule super-resolution imaging of proteins in living Salmonella enterica using self-labelling enzymes. *Sci Rep,* 6**,** 31601.

BATAN, D., BRASELMANN, E., MINSON, M., NGUYEN, D. M. T., COSSART, P. & PALMER, A. E. 2018. A Multicolor Split-Fluorescent Protein Approach to Visualize Listeria Protein Secretion in Infection. *Biophys J,* 115**,** 251-262.

BELIU, G., KURZ, A. J., KUHLEMANN, A. C., BEHRINGER-PLIESS, L., MEUB, M., WOLF, N., SEIBEL, J., SHI, Z. D., SCHNERMANN, M., GRIMM, J. B., LAVIS, L. D., DOOSE, S. & SAUER, M. 2019. Bioorthogonal labeling with tetrazine-dyes for super-resolution microscopy. *Commun Biol,* 2**,** 261.

BENT, Z. W., POOREY, K., BRAZEL, D. M., LABAUVE, A. E., SINHA, A., CURTIS, D. J., HOUSE, S. E., TEW, K. E., HAMBLIN, R. Y., WILLIAMS, K. P., BRANDA, S. S., YOUNG, G. M. & MEAGHER, R. J. 2015. Transcriptomic Analysis of Yersinia enterocolitica Biovar 1B Infecting Murine Macrophages Reveals New Mechanisms of Extracellular and Intracellular Survival. *Infect Immun,* 83**,** 2672-85.

BERGER, C., RAVELLI, R. B. G., LOPEZ-IGLESIAS, C., KUDRYASHEV, M., DIEPOLD, A. & PETERS, P. J. 2021. Structure of the Yersinia injectisome in intracellular host cell phagosomes revealed by cryo FIB electron tomography. *J Struct Biol,* 213**,** 107701.

BERGERON, J. R. C., FERNANDEZ, L., WASNEY, G. A., VUCKOVIC, M., REFFUVEILLE, F., HANCOCK, R. E. W. & STRYNADKA, N. C. J. 2016. The Structure of a Type 3 Secretion System (T3SS) Ruler Protein Suggests a Molecular Mechanism for Needle Length Sensing. *J Biol Chem,* 291**,** 1676-1691.

BERGERON, J. R. C. & MARLOVITS, T. C. 2022. Cryo-EM of the injectisome and type III secretion systems. *Curr Opin Struct Biol,* 75**,** 102403.

BETZIG, E., PATTERSON, G. H., SOUGRAT, R., LINDWASSER, O. W., OLENYCH, S., BONIFACINO, J. S., DAVIDSON, M. W., LIPPINCOTT-

SCHWARTZ, J. & HESS, H. F. 2006. Imaging intracellular fluorescent proteins at nanometer resolution. *Science,* 313**,** 1642-5.

BHAGAT, N. & VIRDI, J. S. 2009. Molecular and biochemical characterization of urease and survival of Yersinia enterocolitica biovar 1A in acidic pH in vitro. *BMC Microbiol,* 9**,** 262.

BLAYLOCK, B., RIORDAN, K. E., MISSIAKAS, D. M. & SCHNEEWIND, O. 2006. Characterization of the Yersinia enterocolitica type III secretion ATPase YscN and its regulator, YscL. *J Bacteriol,* 188**,** 3525-34.

BLISKA, J. B., WANG, X., VIBOUD, G. I. & BRODSKY, I. E. 2013. Modulation of innate immune responses by Yersinia type III secretion system translocators and effectors. *Cell Microbiol,* 15**,** 1622-31.

BLOCKER, A., GOUNON, P., LARQUET, E., NIEBUHR, K., CABIAUX, V., PARSOT, C. & SANSONETTI, P. 1999. The tripartite type III secreton of Shigella flexneri inserts IpaB and IpaC into host membranes. *J Cell Biol,* 147**,** 683-93.

BLOCKER, A., JOUIHRI, N., LARQUET, E., GOUNON, P., EBEL, F., PARSOT, C., SANSONETTI, P. & ALLAOUI, A. 2001. Structure and composition of the Shigella flexneri "needle complex", a part of its type III secreton. *Mol Microbiol,* 39**,** 652-63.

BONARDI, S., PARIS, A., BASSI, L., SALMI, F., BACCI, C., RIBOLDI, E., BONI, E., D'INCAU, M., TAGLIABUE, S. & BRINDANI, F. 2010. Detection, semiquantitative enumeration, and antimicrobial susceptibility of Yersinia enterocolitica in pork and chicken meats in Italy. *J Food Prot,* 73**,** 1785-92.

BOTTONE, E. J. 1997. Yersinia enterocolitica: the charisma continues. *Clin Microbiol Rev,* 10**,** 257-76.

BOTTONE, E. J. 1999. Yersinia enterocolitica: overview and epidemiologic correlates. *Microbes Infect,* 1**,** 323-33.

BRODSKY, I. E., PALM, N. W., SADANAND, S., RYNDAK, M. B., SUTTERWALA, F. S., FLAVELL, R. A., BLISKA, J. B. & MEDZHITOV, R. 2010. A Yersinia effector protein promotes virulence by preventing inflammasome recognition of the type III secretion system. *Cell Host Microbe,* 7**,** 376-87.

BROZ, P., MUELLER, C. A., MULLER, S. A., PHILIPPSEN, A., SORG, I., ENGEL, A. & CORNELIS, G. R. 2007. Function and molecular architecture of the Yersinia injectisome tip complex. *Mol Microbiol,* 65**,** 1311-20.

BRUBAKER, R. R. 2003. Interleukin-10 and inhibition of innate immunity to Yersiniae: roles of Yops and LcrV (V antigen). *Infect Immun,* 71**,** 3673-81.

BUCKLEY, A. M., PETERSEN, J., ROE, A. J., DOUCE, G. R. & CHRISTIE, J. M. 2015. LOV-based reporters for fluorescence imaging. *Curr Opin Chem Biol,* 27**,** 39-45.

BUTAN, C., LARA-TEJERO, M., LI, W., LIU, J. & GALAN, J. E. 2019. High-resolution view of the type III secretion export apparatus in situ reveals membrane remodeling and a secretion pathway. *Proc Natl Acad Sci U S A,* 116**,** 24786-24795.

BUTKEVICH, A. N., WEBER, M., CERECEDA DELGADO, A. R., OSTERSEHLT, L. M., D'ESTE, E. & HELL, S. W. 2021. Photoactivatable Fluorescent Dyes with Hydrophilic Caging Groups and Their Use in Multicolor Nanoscopy. *J Am Chem Soc,* 143**,** 18388-18393.

CABANTOUS, S., TERWILLIGER, T. C. & WALDO, G. S. 2005. Protein tagging and detection with engineered self-assembling fragments of green fluorescent protein. *Nat Biotechnol,* 23**,** 102-7.

CARSTEN, A., RUDOLPH, M., WEIHS, T., SCHMIDT, R., JANSEN, I., WURM, C. A., DIEPOLD, A., FAILLA, A. V., WOLTERS, M. & AEPFELBACHER, M. 2022. MINFLUX imaging of a bacterial molecular machine at nanometer resolution. *Methods Appl Fluoresc,* 11.

CHAUHAN, N., WROBEL, A., SKURNIK, M. & LEO, J. C. 2016. Yersinia adhesins: An arsenal for infection. *Proteomics Clin Appl,* 10**,** 949-963.

CHIU, S. W. & LEAKE, M. C. 2011. Functioning nanomachines seen in real-time in living bacteria using single-molecule and super-resolution fluorescence imaging. *Int J Mol Sci,* 12**,** 2518-42.

CORDES, F. S., KOMORIYA, K., LARQUET, E., YANG, S., EGELMAN, E. H., BLOCKER, A. & LEA, S. M. 2003. Helical structure of the needle of the type III secretion system of Shigella flexneri. *J Biol Chem,* 278**,** 17103-7.

CORNELIS, G. R. 2002. The Yersinia Ysc-Yop 'type III' weaponry. *Nat Rev Mol Cell Biol,* 3**,** 742-52.

CORNELIS, G. R. 2006. The type III secretion injectisome. *Nat Rev Microbiol,* 4**,** 811-25.

CORNELIS, G. R., BOLAND, A., BOYD, A. P., GEUIJEN, C., IRIARTE, M., NEYT, C., SORY, M. P. & STAINIER, I. 1998. The virulence plasmid of Yersinia, an antihost genome. *Microbiol Mol Biol Rev,* 62**,** 1315-52.

CORNELIS, G. R. & VAN GIJSEGEM, F. 2000. Assembly and function of type III secretory systems. *Annu Rev Microbiol,* 54**,** 735-74.

CORNELIS, G. R. & WOLF-WATZ, H. 1997. The Yersinia Yop virulon: a bacterial system for subverting eukaryotic cells. *Mol Microbiol,* 23**,** 861-7.

COSTA, T. R., FELISBERTO-RODRIGUES, C., MEIR, A., PREVOST, M. S., REDZEJ, A., TROKTER, M. & WAKSMAN, G. 2015. Secretion systems in Gram-negative bacteria: structural and mechanistic insights. *Nat Rev Microbiol,* 13**,** 343-59.

DAY, J. B. & PLANO, G. V. 1998. A complex composed of SycN and YscB functions as a specific chaperone for YopN in Yersinia pestis. *Mol Microbiol,* 30**,** 777-88.

DE KONING-WARD, T. F., WARD, A. C., HARTLAND, E. L. & ROBINS-BROWNE, R. M. 1995. The urease complex gene of Yersinia enterocolitica and its role in virulence. *Contrib Microbiol Immunol,* 13**,** 262-3.

DEMMERLE, J., WEGEL, E., SCHERMELLEH, L. & DOBBIE, I. M. 2015. Assessing resolution in super-resolution imaging. *Methods,* 88**,** 3-10.

DENG, W., MARSHALL, N. C., ROWLAND, J. L., MCCOY, J. M., WORRALL, L. J., SANTOS, A. S., STRYNADKA, N. C. J. & FINLAY, B. B. 2017. Assembly, structure, function and regulation of type III secretion systems. *Nat Rev Microbiol,* 15**,** 323-337.

DERTINGER, T., COLYER, R., IYER, G., WEISS, S. & ENDERLEIN, J. 2009. Fast, background-free, 3D super-resolution optical fluctuation imaging (SOFI). *Proc Natl Acad Sci U S A,* 106**,** 22287-92.

DEUSCHLE, E., KELLER, B., SIEGFRIED, A., MANNCKE, B., SPAETH, T., KOBERLE, M., DRECHSLER-HAKE, D., REBER, J., BOTTCHER, R. T., AUTENRIETH, S. E., AUTENRIETH, I. B., BOHN, E. & SCHUTZ, M. 2016. Role of beta1 integrins and bacterial adhesins for Yop injection into leukocytes in Yersinia enterocolitica systemic mouse infection. *Int J Med Microbiol,* 306**,** 77-88.

DEWOODY, R. S., MERRITT, P. M. & MARKETON, M. M. 2013. Regulation of the Yersinia type III secretion system: traffic control. *Front Cell Infect Microbiol,* 3**,** 4.

DEY, S., CHAKRAVARTY, A., GUHA BISWAS, P. & DE GUZMAN, R. N. 2019. The type III secretion system needle, tip, and translocon. *Protein Sci,* 28**,** 1582-1593.

DIAZ-ALVAREZ, L. & ORTEGA, E. 2017. The Many Roles of Galectin-3, a Multifaceted Molecule, in Innate Immune Responses against Pathogens. *Mediators Inflamm,* 2017**,** 9247574.

DIEPOLD, A., AMSTUTZ, M., ABEL, S., SORG, I., JENAL, U. & CORNELIS, G. R. 2010. Deciphering the assembly of the Yersinia type III secretion injectisome. *EMBO J,* 29**,** 1928-40.

DIEPOLD, A. & ARMITAGE, J. P. 2015. Type III secretion systems: the bacterial flagellum and the injectisome. *Philos Trans R Soc Lond B Biol Sci,* 370.

DIEPOLD, A., KUDRYASHEV, M., DELALEZ, N. J., BERRY, R. M. & ARMITAGE, J. P. 2015. Composition, formation, and regulation of the cytosolic c-ring, a dynamic component of the type III secretion injectisome. *PLoS Biol,* 13**,** e1002039.

DIEPOLD, A., SEZGIN, E., HUSEYIN, M., MORTIMER, T., EGGELING, C. & ARMITAGE, J. P. 2017. A dynamic and adaptive network of cytosolic interactions governs protein export by the T3SS injectisome. *Nat Commun,* 8**,** 15940.

DOERR, A. 2016. Single-particle cryo-electron microscopy. *Nat Methods,* 13**,** 23.

DRUMMOND, N., MURPHY, B. P., RINGWOOD, T., PRENTICE, M. B., BUCKLEY, J. F. & FANNING, S. 2012. Yersinia enterocolitica: a brief review of the issues relating to the zoonotic pathogen, public health challenges, and the pork production chain. *Foodborne Pathog Dis,* 9**,** 179-89.

ENNINGA, J., MOUNIER, J., SANSONETTI, P. & TRAN VAN NHIEU, G. 2005. Secretion of type III effectors into host cells in real time. *Nat Methods,* 2**,** 959-65.

EUROPEAN CENTRE FOR DISEASE PREVENTION AND CONTROL 2022. Yersiniosis. In: ECDC. Annual epidemiological report for 2021. Stockholm: ECDC; 2022. [Online im Internet.] URL: https://www.ecdc.europa.eu/en/publications-data/yersiniosis-annual-epidemiological-report-2021 [State: 20.01.2023, 11:43].

FERRACCI, F., SCHUBOT, F. D., WAUGH, D. S. & PLANO, G. V. 2005. Selection and characterization of Yersinia pestis YopN mutants that constitutively block Yop secretion. *Mol Microbiol,* 57**,** 970-87.

FILLOUX, A. 2022. Bacterial protein secretion systems: Game of types. *Microbiology (Reading),* 168.

FOOD AND DRUG ADMINISTRATION 2012. *Bad Bug Book, Foodborne Pathogenic Microorganisms and Natural Toxins. Second Edition. 2012. [Online im Internet.] URL: https://www.fda.gov/files/food/published/Bad-Bug-Book-2nd-Edition-%28PDF%29.pdf [State: 20.01.2023, 11:52].*

FORSBERG, A., VIITANEN, A. M., SKURNIK, M. & WOLF-WATZ, H. 1991. The surface-located YopN protein is involved in calcium signal transduction in Yersinia pseudotuberculosis. *Mol Microbiol,* 5**,** 977-86.

FOULTIER, B., TROISFONTAINES, P., VERTOMMEN, D., MARENNE, M. N., RIDER, M., PARSOT, C. & CORNELIS, G. R. 2003. Identification of substrates and chaperone from the Yersinia enterocolitica 1B Ysa type III secretion system. *Infect Immun,* 71**,** 242-53.

FREDRIKSSON-AHOMAA, M. 2007. Yersinia enterocolitica and Yersinia pseudotuberculosis. *Foodborne Diseases,* 98**,** 79-113.

FREDRIKSSON-AHOMAA, M., STOLLE, A. & KORKEALA, H. 2006. Molecular epidemiology of Yersinia enterocolitica infections. *FEMS Immunol Med Microbiol,* 47**,** 315-29.

FRUH, S. M., MATTI, U., SPYCHER, P. R., RUBINI, M., LICKERT, S., SCHLICHTHAERLE, T., JUNGMANN, R., VOGEL, V., RIES, J. & SCHOEN, I. 2021. Site-Specifically-Labeled Antibodies for Super-Resolution Microscopy Reveal In Situ Linkage Errors. *ACS Nano,* 15**,** 12161-12170.

GAIETTA, G., DEERINCK, T. J., ADAMS, S. R., BOUWER, J., TOUR, O., LAIRD, D. W., SOSINSKY, G. E., TSIEN, R. Y. & ELLISMAN, M. H. 2002. Multicolor and electron microscopic imaging of connexin trafficking. *Science,* 296**,** 503-7.

GALINDO, C. L., ROSENZWEIG, J. A., KIRTLEY, M. L. & CHOPRA, A. K. 2011. Pathogenesis of Y. enterocolitica and Y. pseudotuberculosis in Human Yersiniosis. *J Pathog,* 2011**,** 182051.

GARCIA, J. T., FERRACCI, F., JACKSON, M. W., JOSEPH, S. S., PATTIS, I., PLANO, L. R., FISCHER, W. & PLANO, G. V. 2006. Measurement of effector protein injection by type III and type IV secretion systems by using a 13-residue phosphorylatable glycogen synthase kinase tag. *Infect Immun,* 74**,** 5645-57.

GAUS, K., HENTSCHKE, M., CZYMMECK, N., NOVIKOVA, L., TRULZSCH, K., VALENTIN-WEIGAND, P., AEPFELBACHER, M. & RUCKDESCHEL, K. 2011. Destabilization of YopE by the ubiquitin-proteasome pathway fine-tunes Yop delivery into host cells and facilitates systemic spread of Yersinia enterocolitica in host lymphoid tissue. *Infect Immun,* 79**,** 1166-75.

GAUTIER, A., JUILLERAT, A., HEINIS, C., CORREA, I. R., JR., KINDERMANN, M., BEAUFILS, F. & JOHNSSON, K. 2008. An engineered protein tag for multiprotein labeling in living cells. *Chem Biol,* 15**,** 128-36.

GAWTHORNE, J. A., AUDRY, L., MCQUITTY, C., DEAN, P., CHRISTIE, J. M., ENNINGA, J. & ROE, A. J. 2016. Visualizing the Translocation and Localization of Bacterial Type III Effector Proteins by Using a Genetically Encoded Reporter System. *Appl Environ Microbiol,* 82**,** 2700-2708.

GERASIMAITE, R. T., BUCEVICIUS, J., KISZKA, K. A., SCHNORRENBERG, S., KOSTIUK, G., KOENEN, T. & LUKINAVICIUS, G. 2021. Blinking Fluorescent Probes for Tubulin Nanoscopy in Living and Fixed Cells. *ACS Chem Biol,* 16**,** 2130-2136.

GOTZKE, H., KILISCH, M., MARTINEZ-CARRANZA, M., SOGRATE-IDRISSI, S., RAJAVEL, A., SCHLICHTHAERLE, T., ENGELS, N., JUNGMANN, R., STENMARK, P., OPAZO, F. & FREY, S. 2019. The ALFA-tag is a highly versatile tool for nanobody-based bioscience applications. *Nat Commun,* 10**,** 4403.

GRABNER, C. P., JANSEN, I., NEEF, J., WEIHS, T., SCHMIDT, R., RIEDEL, D., WURM, C. A. & MOSER, T. 2022. Resolving the molecular architecture of the photoreceptor active zone with 3D-MINFLUX. *Sci Adv,* 8**,** eabl7560.

GREEN, E. R. & MECSAS, J. 2016. Bacterial Secretion Systems: An Overview. *Microbiol Spectr,* 4.

GREENBERG, A. S., AVILA, D., HUGHES, M., HUGHES, A., MCKINNEY, E. C. & FLAJNIK, M. F. 1995. A new antigen receptor gene family that undergoes rearrangement and extensive somatic diversification in sharks. *Nature,* 374**,** 168-73.

GROSDENT, N., MARIDONNEAU-PARINI, I., SORY, M. P. & CORNELIS, G. R. 2002. Role of Yops and adhesins in resistance of Yersinia enterocolitica to phagocytosis. *Infect Immun,* 70**,** 4165-76.

GROSSMAN, A. S., MAUER, T. J., FOREST, K. T. & GOODRICH-BLAIR, H. 2021. A Widespread Bacterial Secretion System with Diverse Substrates. *mBio,* 12**,** e0195621.

GRUTZKAU, A., HANSKI, C., HAHN, H. & RIECKEN, E. O. 1990. Involvement of M cells in the bacterial invasion of Peyer's patches: a common mechanism shared by Yersinia enterocolitica and other enteroinvasive bacteria. *Gut,* 31**,** 1011-5.

GUERRA, J. M. 1995. Super-resolution through illumination by diffraction-born evanescent waves. *Appl. Phys. Lett.,* 66.

GUO, E. Z. & GALAN, J. E. 2021. Cryo-EM structure of the needle filament tip complex of the Salmonella type III secretion injectisome. *Proc Natl Acad Sci U S A,* 118.

GURRY, J. F. 1974. Acute terminal ileitis and Yersinia infection. *Br Med J,* 2**,** 264-6.

GWOSCH, K. C., BALZAROTTI, F., PAPE, J. K., HOESS, P., ELLENBERG, J., RIES, J., MATTI, U., SCHMIDT, R., SAHL, S. J. & HELL, S. W. 2022. Reply to: Assessment of 3D MINFLUX data for quantitative structural biology in cells. *Nat Methods*.

GWOSCH, K. C., PAPE, J. K., BALZAROTTI, F., HOESS, P., ELLENBERG, J., RIES, J. & HELL, S. W. 2020. MINFLUX nanoscopy delivers 3D multicolor nanometer resolution in cells. *Nat Methods,* 17**,** 217-224.

HABENSTEIN, B., EL MAMMERI, N., TOLCHARD, J., LAMON, G., TAWANI, A., BERBON, M. & LOQUET, A. 2020. Structures of Type III Secretion System Needle Filaments. *Curr Top Microbiol Immunol,* 427**,** 109-131.

HAKANSSON, S., SCHESSER, K., PERSSON, C., GALYOV, E. E., ROSQVIST, R., HOMBLE, F. & WOLF-WATZ, H. 1996. The YopB protein of Yersinia pseudotuberculosis is essential for the translocation of Yop effector proteins across the target cell plasma membrane and displays a contact-dependent membrane disrupting activity. *EMBO J,* 15**,** 5812-23.

HAMERS-CASTERMAN, C., ATARHOUCH, T., MUYLDERMANS, S., ROBINSON, G., HAMERS, C., SONGA, E. B., BENDAHMAN, N. & HAMERS, R. 1993. Naturally occurring antibodies devoid of light chains. *Nature,* 363**,** 446-8.

HEBBRECHT, T., LIU, J., ZWAENEPOEL, O., BODDIN, G., VAN LEENE, C., DECOENE, K., MADDER, A., BRAECKMANS, K. & GETTEMANS, J. 2020. Nanobody click chemistry for convenient site-specific fluorescent labelling, single step immunocytochemistry and delivery into living cells by photoporation and live cell imaging. *N Biotechnol,* 59**,** 33-43.

HEESEMANN, J., GROSS, U., SCHMIDT, N. & LAUFS, R. 1986. Immunochemical analysis of plasmid-encoded proteins released by enteropathogenic Yersinia sp. grown in calcium-deficient media. *Infect Immun,* 54**,** 561-7.

HEESEMANN, J. & LAUFS, R. 1983. Construction of a mobilizable Yersinia enterocolitica virulence plasmid. *J Bacteriol,* 155**,** 761-7.

HELL, S. W. & WICHMANN, J. 1994. Breaking the diffraction resolution limit by stimulated emission: stimulated-emission-depletion fluorescence microscopy. *Opt Lett,* 19**,** 780-2.

HOICZYK, E. & BLOBEL, G. 2001. Polymerization of a single protein of the pathogen Yersinia enterocolitica into needles punctures eukaryotic cells. *Proc Natl Acad Sci U S A,* 98**,** 4669-74.

HOLMSTROM, A., PETTERSON, J., ROSQVIST, R., HAKANSSON, S., TAFAZOLI, F., FALLMAN, M., MAGNUSSON, K. E., WOLF-WATZ, H. & FORSBERG, A. 1997. YopK of Yersinia pseudotuberculosis controls translocation of Yop effectors across the eukaryotic cell membrane. *Mol Microbiol,* 24**,** 73-91.

HU, J., WORRALL, L. J., HONG, C., VUCKOVIC, M., ATKINSON, C. E., CAVENEY, N., YU, Z. & STRYNADKA, N. C. J. 2018. Cryo-EM analysis of the T3S injectisome reveals the structure of the needle and open secretin. *Nat Commun,* 9**,** 3840.

HUANG, B., BATES, M. & ZHUANG, X. 2009. Super-resolution fluorescence microscopy. *Annu Rev Biochem,* 78**,** 993-1016.

HUANG, B., WANG, W., BATES, M. & ZHUANG, X. 2008. Three-dimensional super-resolution imaging by stochastic optical reconstruction microscopy. *Science,* 319**,** 810-3.

HUSCHKA, F. 2017. *Visualisierung des Typ III Translokator-Komplexes von Yersinia enterocolitica während der Witszellinfektion. Dissertation. Universität Hamburg.*

IRIARTE, M., SORY, M. P., BOLAND, A., BOYD, A. P., MILLS, S. D., LAMBERMONT, I. & CORNELIS, G. R. 1998. TyeA, a protein involved in control of Yop release and in translocation of Yersinia Yop effectors. *EMBO J,* 17**,** 1907-18.

ISAKSSON, E. L., AILI, M., FAHLGREN, A., CARLSSON, S. E., ROSQVIST, R. & WOLF-WATZ, H. 2009. The membrane localization domain is required for intracellular localization and autoregulation of YopE in Yersinia pseudotuberculosis. *Infect Immun,* 77**,** 4740-9.

JALAVA, K., HAKKINEN, M., VALKONEN, M., NAKARI, U. M., PALO, T., HALLANVUO, S., OLLGREN, J., SIITONEN, A. & NUORTI, J. P. 2006. An outbreak of gastrointestinal illness and erythema nodosum from grated carrots contaminated with Yersinia pseudotuberculosis. *J Infect Dis,* 194**,** 1209-16.

JEPSON, M. A. & CLARK, M. A. 1998. Studying M cells and their role in infection. *Trends Microbiol,* 6**,** 359-65.

JONES, T. F., BUCKINGHAM, S. C., BOPP, C. A., RIBOT, E. & SCHAFFNER, W. 2003. From pig to pacifier: chitterling-associated yersiniosis outbreak among black infants. *Emerg Infect Dis,* 9**,** 1007-9.

JOSEPH, S. S. & PLANO, G. V. 2013. The SycN/YscB chaperone-binding domain of YopN is required for the calcium-dependent regulation of Yop secretion by Yersinia pestis. *Front Cell Infect Microbiol,* 3**,** 1.

JOURNET, L., AGRAIN, C., BROZ, P. & CORNELIS, G. R. 2003. The needle length of bacterial injectisomes is determined by a molecular ruler. *Science,* 302**,** 1757-60.

KEPPLER, A., GENDREIZIG, S., GRONEMEYER, T., PICK, H., VOGEL, H. & JOHNSSON, K. 2003. A general method for the covalent labeling of fusion proteins with small molecules in vivo. *Nat Biotechnol,* 21**,** 86-9.

KIMBROUGH, T. G. & MILLER, S. I. 2000. Contribution of Salmonella typhimurium type III secretion components to needle complex formation. *Proc Natl Acad Sci U S A,* 97**,** 11008-13.

KIRJAVAINEN, V., JARVA, H., BIEDZKA-SAREK, M., BLOM, A. M., SKURNIK, M. & MERI, S. 2008. Yersinia enterocolitica serum resistance proteins YadA and ail bind the complement regulator C4b-binding protein. *PLoS Pathog,* 4**,** e1000140.

KITASATO, S. 1894. THE BACILLUS OF BUBONIC PLAGUE. *The Lancet,* 144**,** 428-430.

KLAR, T. A. & HELL, S. W. 1999. Subdiffraction resolution in far-field fluorescence microscopy. *Opt Lett,* 24**,** 954-6.

KLEIN, T., LOSCHBERGER, A., PROPPERT, S., WOLTER, S., VAN DE LINDE, S. & SAUER, M. 2011. Live-cell dSTORM with SNAP-tag fusion proteins. *Nat Methods,* 8**,** 7-9.

KOBERLE, M., KLEIN-GUNTHER, A., SCHUTZ, M., FRITZ, M., BERCHTOLD, S., TOLOSA, E., AUTENRIETH, I. B. & BOHN, E. 2009. Yersinia enterocolitica targets cells of the innate and adaptive immune system by injection of Yops in a mouse infection model. *PLoS Pathog,* 5**,** e1000551.

KOSTER, M., BITTER, W., DE COCK, H., ALLAOUI, A., CORNELIS, G. R. & TOMMASSEN, J. 1997. The outer membrane component, YscC, of the Yop secretion machinery of Yersinia enterocolitica forms a ring-shaped multimeric complex. *Mol Microbiol,* 26**,** 789-97.

KUBORI, T., MATSUSHIMA, Y., NAKAMURA, D., URALIL, J., LARA-TEJERO, M., SUKHAN, A., GALAN, J. E. & AIZAWA, S. I. 1998. Supramolecular structure of the Salmonella typhimurium type III protein secretion system. *Science,* 280**,** 602-5.

KUBORI, T., SUKHAN, A., AIZAWA, S. I. & GALAN, J. E. 2000. Molecular characterization and assembly of the needle complex of the Salmonella typhimurium type III protein secretion system. *Proc Natl Acad Sci U S A,* 97**,** 10225-30.

KUDRYASHEV, M., DIEPOLD, A., AMSTUTZ, M., ARMITAGE, J. P., STAHLBERG, H. & CORNELIS, G. R. 2015. Yersinia enterocolitica type III secretion injectisomes form regularly spaced clusters, which incorporate new machines upon activation. *Mol Microbiol,* 95**,** 875-84.

KUHLEN, L., ABRUSCI, P., JOHNSON, S., GAULT, J., DEME, J., CAESAR, J., DIETSCHE, T., MEBRHATU, M. T., GANIEF, T., MACEK, B., WAGNER, S., ROBINSON, C. V. & LEA, S. M. 2018. Structure of the core of the type III secretion system export apparatus. *Nat Struct Mol Biol,* 25**,** 583-590.

KULZER, S., PETERSEN, W., BASER, A., MANDEL, K. & PRZYBORSKI, J. M. 2013. Use of self-assembling GFP to determine protein topology and compartmentalisation in the Plasmodium falciparum-infected erythrocyte. *Mol Biochem Parasitol,* 187**,** 87-90.

LAEMMLI, U. K. 1970. Cleavage of structural proteins during the assembly of the head of bacteriophage T4. *Nature,* 227**,** 680-5.

LANDGRAF, D., OKUMUS, B., CHIEN, P., BAKER, T. A. & PAULSSON, J. 2012. Segregation of molecules at cell division reveals native protein localization. *Nat Methods,* 9**,** 480-2.

LARA-TEJERO, M., KATO, J., WAGNER, S., LIU, X. & GALAN, J. E. 2011. A sorting platform determines the order of protein secretion in bacterial type III systems. *Science,* 331**,** 1188-91.

LEE, H. Y., LEE, S. E., WOO, J., CHOI, D. & PARK, E. 2018. Split Green Fluorescent Protein System to Visualize Effectors Delivered from Bacteria During Infection. *J Vis Exp.*

LEE, L. A., GERBER, A. R., LONSWAY, D. R., SMITH, J. D., CARTER, G. P., PUHR, N. D., PARRISH, C. M., SIKES, R. K., FINTON, R. J. & TAUXE, R. V. 1990. Yersinia enterocolitica O:3 infections in infants and children, associated with the household preparation of chitterlings. *N Engl J Med,* 322**,** 984-7.

LEE, V. T., ANDERSON, D. M. & SCHNEEWIND, O. 1998. Targeting of Yersinia Yop proteins into the cytosol of HeLa cells: one-step translocation of YopE across bacterial and eukaryotic membranes is dependent on SycE chaperone. *Mol Microbiol,* 28**,** 593-601.

LI, X., YANG, Q., TU, H., LIM, Z. & PAN, S. Q. 2014. Direct visualization of Agrobacterium-delivered VirE2 in recipient cells. *Plant J,* 77**,** 487-95.

LIPPINCOTT-SCHWARTZ, J. & PATTERSON, G. H. 2009. Photoactivatable fluorescent proteins for diffraction-limited and super-resolution imaging. *Trends Cell Biol,* 19**,** 555-65.

LIU, J., HEBBRECHT, T., BRANS, T., PARTHOENS, E., LIPPENS, S., LI, C., DE KEERSMAECKER, H., DE VOS, W. H., DE SMEDT, S. C., BOUKHERROUB, R., GETTEMANS, J., XIONG, R. & BRAECKMANS, K. 2020. Long-term live-cell microscopy with labeled nanobodies delivered by laser-induced photoporation. *Nano Res,* 13**,** 485-495.

LIU, S., HOESS, P. & RIES, J. 2022. Super-Resolution Microscopy for Structural Cell Biology. *Annu Rev Biophys,* 51**,** 301-326.

LOMBARDI, C., TOLCHARD, J., BOUILLOT, S., SIGNOR, L., GEBUS, C., LIEBL, D., FENEL, D., TEULON, J. M., BROCK, J., HABENSTEIN, B., PELLEQUER, J. L., FAUDRY, E., LOQUET, A., ATTREE, I., DESSEN, A. & JOB, V. 2019. Structural and Functional Characterization of the Type Three Secretion System (T3SS) Needle of Pseudomonas aeruginosa. *Front Microbiol,* 10**,** 573.

LOS, G. V., ENCELL, L. P., MCDOUGALL, M. G., HARTZELL, D. D., KARASSINA, N., ZIMPRICH, C., WOOD, M. G., LEARISH, R., OHANA, R. F., URH, M., SIMPSON, D., MENDEZ, J., ZIMMERMAN, K., OTTO, P., VIDUGIRIS, G., ZHU, J., DARZINS, A., KLAUBERT, D. H., BULLEIT, R. F. & WOOD, K. V. 2008. HaloTag: a novel protein labeling technology for cell imaging and protein analysis. *ACS Chem Biol,* 3**,** 373-82.

LYNCH, M., PAINTER, J., WOODRUFF, R., BRADEN, C., CENTERS FOR DISEASE, C. & PREVENTION 2006. Surveillance for foodborne-disease outbreaks--United States, 1998-2002. *MMWR Surveill Summ,* 55**,** 1-42.

MANTLE, M. & HUSAR, S. D. 1993. Adhesion of Yersinia enterocolitica to purified rabbit and human intestinal mucin. *Infect Immun,* 61**,** 2340-6.

MARKETON, M. M., DEPAOLO, R. W., DEBORD, K. L., JABRI, B. & SCHNEEWIND, O. 2005. Plague bacteria target immune cells during infection. *Science,* 309**,** 1739-41.

MARLOVITS, T. C., KUBORI, T., LARA-TEJERO, M., THOMAS, D., UNGER, V. M. & GALAN, J. E. 2006. Assembly of the inner rod determines needle length in the type III secretion injectisome. *Nature,* 441**,** 637-40.

MARLOVITS, T. C., KUBORI, T., SUKHAN, A., THOMAS, D. R., GALAN, J. E. & UNGER, V. M. 2004. Structural insights into the assembly of the type III secretion needle complex. *Science,* 306**,** 1040-2.

MARLOVITS, T. C. & STEBBINS, C. E. 2010. Type III secretion systems shape up as they ship out. *Curr Opin Microbiol,* 13**,** 47-52.

MCINTOSH, A., MEIKLE, L. M., ORMSBY, M. J., MCCORMICK, B. A., CHRISTIE, J. M., BREWER, J. M., ROBERTS, M. & WALL, D. M. 2017. SipA Activation of Caspase-3 Is a Decisive Mediator of Host Cell Survival at Early Stages of Salmonella enterica Serovar Typhimurium Infection. *Infect Immun,* 85.

MCNALLY, A., THOMSON, N. R., REUTER, S. & WREN, B. W. 2016. 'Add, stir and reduce': Yersinia spp. as model bacteria for pathogen evolution. *Nat Rev Microbiol,* 14**,** 177-90.

MEJIA, E., BLISKA, J. B. & VIBOUD, G. I. 2008. Yersinia controls type III effector delivery into host cells by modulating Rho activity. *PLoS Pathog,* 4**,** e3.

MIHAILA, T. S., BATE, C., OSTERSEHLT, L. M., PAPE, J. K., KELLER-FINDEISEN, J., SAHL, S. J. & HELL, S. W. 2022. Enhanced incorporation of subnanometer tags into cellular proteins for fluorescence nanoscopy via optimized genetic code expansion. *Proc Natl Acad Sci U S A,* 119**,** e2201861119.

MILETIC, S., FAHRENKAMP, D., GOESSWEINER-MOHR, N., WALD, J., PANTEL, M., VESPER, O., KOTOV, V. & MARLOVITS, T. C. 2021. Substrate-engaged type III secretion system structures reveal gating mechanism for unfolded protein translocation. *Nat Commun,* 12**,** 1546.

MILETIC, S., GOESSWEINER-MOHR, N. & MARLOVITS, T. C. 2020. The Structure of the Type III Secretion System Needle Complex. *Curr Top Microbiol Immunol,* 427**,** 67-90.

MILLER, V. L. & FALKOW, S. 1988. Evidence for two genetic loci in Yersinia enterocolitica that can promote invasion of epithelial cells. *Infect Immun,* 56**,** 1242-8.

MILLER, V. L., FARMER, J. J., 3RD, HILL, W. E. & FALKOW, S. 1989. The ail locus is found uniquely in Yersinia enterocolitica serotypes commonly associated with disease. *Infect Immun,* 57**,** 121-31.

MOTA, L. J., SORG, I. & CORNELIS, G. R. 2005. Type III secretion: the bacteria-eukaryotic cell express. *FEMS Microbiol Lett,* 252**,** 1-10.

MUELLER, C. A., BROZ, P. & CORNELIS, G. R. 2008. The type III secretion system tip complex and translocon. *Mol Microbiol,* 68**,** 1085-95.

MUELLER, C. A., BROZ, P., MULLER, S. A., RINGLER, P., ERNE-BRAND, F., SORG, I., KUHN, M., ENGEL, A. & CORNELIS, G. R. 2005. The V-antigen of Yersinia forms a distinct structure at the tip of injectisome needles. *Science,* 310**,** 674-6.

MUHLENKAMP, M., OBERHETTINGER, P., LEO, J. C., LINKE, D. & SCHUTZ, M. S. 2015. Yersinia adhesin A (YadA)--beauty & beast. *Int J Med Microbiol,* 305**,** 252-8.

NARIYA, M. K., ISRAELI, J., SHI, J. J. & DEEDS, E. J. 2016. Mathematical Model for Length Control by the Timing of Substrate Switching in the Type III Secretion System. *PLoS Comput Biol,* 12**,** e1004851.

NAUTH, T., HUSCHKA, F., SCHWEIZER, M., BOSSE, J. B., DIEPOLD, A., FAILLA, A. V., STEFFEN, A., STRADAL, T. E. B., WOLTERS, M. & AEPFELBACHER, M. 2018. Visualization of translocons in Yersinia type III protein secretion machines during host cell infection. *PLoS Pathog,* 14**,** e1007527.

NEYT, C. & CORNELIS, G. R. 1999. Insertion of a Yop translocation pore into the macrophage plasma membrane by Yersinia enterocolitica: requirement for translocators YopB and YopD, but not LcrG. *Mol Microbiol,* 33**,** 971-81.

NORDFELTH, R. & WOLF-WATZ, H. 2001. YopB of Yersinia enterocolitica is essential for YopE translocation. *Infect Immun,* 69**,** 3516-8.

NOTTI, R. Q., BHATTACHARYA, S., LILIC, M. & STEBBINS, C. E. 2015. A common assembly module in injectisome and flagellar type III secretion sorting platforms. *Nat Commun,* 6**,** 7125.

OELLERICH, M. F., JACOBI, C. A., FREUND, S., NIEDUNG, K., BACH, A., HEESEMANN, J. & TRULZSCH, K. 2007. Yersinia enterocolitica infection of mice reveals clonal invasion and abscess formation. *Infect Immun,* 75**,** 3802-11.

OSTERSEHLT, L. M., JANS, D. C., WITTEK, A., KELLER-FINDEISEN, J., INAMDAR, K., SAHL, S. J., HELL, S. W. & JAKOBS, S. 2022. DNA-PAINT MINFLUX nanoscopy. *Nat Methods,* 19**,** 1072-1075.

PAI, C. H. & MORS, V. 1978. Production of enterotoxin by Yersinia enterocolitica. *Infect Immun,* 19**,** 908-11.

PAPE, J. K., STEPHAN, T., BALZAROTTI, F., BUCHNER, R., LANGE, F., RIEDEL, D., JAKOBS, S. & HELL, S. W. 2020. Multicolor 3D MINFLUX nanoscopy of mitochondrial MICOS proteins. *Proc Natl Acad Sci U S A,* 117**,** 20607-20614.

PARK, D., LARA-TEJERO, M., WAXHAM, M. N., LI, W., HU, B., GALAN, J. E. & LIU, J. 2018. Visualization of the type III secretion mediated Salmonella-host cell interface using cryo-electron tomography. *Elife,* 7.

PARK, E., LEE, H. Y., WOO, J., CHOI, D. & DINESH-KUMAR, S. P. 2017. Spatiotemporal Monitoring of Pseudomonas syringae Effectors via Type III Secretion Using Split Fluorescent Protein Fragments. *Plant Cell,* 29**,** 1571-1584.

PARTE, A. C., SARDA CARBASSE, J., MEIER-KOLTHOFF, J. P., REIMER, L. C. & GOKER, M. 2020. List of Prokaryotic names with Standing in Nomenclature (LPSN) moves to the DSMZ. *Int J Syst Evol Microbiol,* 70**,** 5607-5612.

PASTOR, A., CHABERT, J., LOUWAGIE, M., GARIN, J. & ATTREE, I. 2005. PscF is a major component of the Pseudomonas aeruginosa type III secretion needle. *FEMS Microbiol Lett,* 253**,** 95-101.

PAZ, I., SACHSE, M., DUPONT, N., MOUNIER, J., CEDERFUR, C., ENNINGA, J., LEFFLER, H., POIRIER, F., PREVOST, M. C., LAFONT, F. & SANSONETTI, P. 2010. Galectin-3, a marker for vacuole lysis by invasive pathogens. *Cell Microbiol,* 12**,** 530-44.

PEPE, J. C. & MILLER, V. L. 1993. Yersinia enterocolitica invasin: a primary role in the initiation of infection. *Proc Natl Acad Sci U S A,* 90**,** 6473-7.

PEPE, J. C., WACHTEL, M. R., WAGAR, E. & MILLER, V. L. 1995. Pathogenesis of defined invasion mutants of Yersinia enterocolitica in a BALB/c mouse model of infection. *Infect Immun,* 63**,** 4837-48.

PERRY, R. D. & FETHERSTON, J. D. 2011. Yersiniabactin iron uptake: mechanisms and role in Yersinia pestis pathogenesis. *Microbes Infect,* 13**,** 808-17.

PHA, K. & NAVARRO, L. 2016. Yersinia type III effectors perturb host innate immune responses. *World J Biol Chem,* 7**,** 1-13.

PIENKOSS, S., JAVADI, S., CHAOPRASID, P., HOLLER, M., ROSSMANITH, J., DERSCH, P. & NARBERHAUS, F. 2022. RNA Thermometer-coordinated Assembly of the Yersinia Injectisome. *J Mol Biol,* 434**,** 167667.

PIENKOSS, S., JAVADI, S., CHAOPRASID, P., NOLTE, T., TWITTENHOFF, C., DERSCH, P. & NARBERHAUS, F. 2021. The gatekeeper of Yersinia type III secretion is under RNA thermometer control. *PLoS Pathog,* 17**,** e1009650.

PIERSON, D. E. & FALKOW, S. 1993. The ail gene of Yersinia enterocolitica has a role in the ability of the organism to survive serum killing. *Infect Immun,* 61**,** 1846-52.

POYRAZ, O., SCHMIDT, H., SEIDEL, K., DELISSEN, F., ADER, C., TENENBOIM, H., GOOSMANN, C., LAUBE, B., THUNEMANN, A. F., ZYCHLINSKY, A., BALDUS, M., LANGE, A., GRIESINGER, C. & KOLBE, M. 2010. Protein refolding is required for assembly of the type three secretion needle. *Nat Struct Mol Biol,* 17**,** 788-92.

PRINDLE, J. R., WANG, Y., ROCHA, J. M., DIEPOLD, A. & GAHLMANN, A. 2022. Distinct Cytosolic Complexes Containing the Type III Secretion System

ATPase Resolved by Three-Dimensional Single-Molecule Tracking in Live Yersinia enterocolitica. *Microbiol Spectr*, e0174422.

RADICS, J., KONIGSMAIER, L. & MARLOVITS, T. C. 2014. Structure of a pathogenic type 3 secretion system in action. *Nat Struct Mol Biol,* 21, 82-7.

RASCOVAN, N., SJOGREN, K. G., KRISTIANSEN, K., NIELSEN, R., WILLERSLEV, E., DESNUES, C. & RASMUSSEN, S. 2019. Emergence and Spread of Basal Lineages of Yersinia pestis during the Neolithic Decline. *Cell,* 176, 295-305 e10.

RASMUSSEN, S., ALLENTOFT, M. E., NIELSEN, K., ORLANDO, L., SIKORA, M., SJOGREN, K. G., PEDERSEN, A. G., SCHUBERT, M., VAN DAM, A., KAPEL, C. M., NIELSEN, H. B., BRUNAK, S., AVETISYAN, P., EPIMAKHOV, A., KHALYAPIN, M. V., GNUNI, A., KRIISKA, A., LASAK, I., METSPALU, M., MOISEYEV, V., GROMOV, A., POKUTTA, D., SAAG, L., VARUL, L., YEPISKOPOSYAN, L., SICHERITZ-PONTEN, T., FOLEY, R. A., LAHR, M. M., NIELSEN, R., KRISTIANSEN, K. & WILLERSLEV, E. 2015. Early divergent strains of Yersinia pestis in Eurasia 5,000 years ago. *Cell,* 163, 571-82.

RIES, J., KAPLAN, C., PLATONOVA, E., EGHLIDI, H. & EWERS, H. 2012. A simple, versatile method for GFP-based super-resolution microscopy via nanobodies. *Nat Methods,* 9, 582-4.

ROBLIN, P., DEWITTE, F., VILLERET, V., BIONDI, E. G. & BOMPARD, C. 2015. A Salmonella type three secretion effector/chaperone complex adopts a hexameric ring-like structure. *J Bacteriol,* 197, 688-98.

ROCHA, J. M., RICHARDSON, C. J., ZHANG, M., DARCH, C. M., CAI, E., DIEPOLD, A. & GAHLMANN, A. 2018. Single-molecule tracking in live Yersinia enterocolitica reveals distinct cytosolic complexes of injectisome subunits. *Integr Biol (Camb),* 10, 502-515.

ROMANO, F. B., TANG, Y., ROSSI, K. C., MONOPOLI, K. R., ROSS, J. L. & HEUCK, A. P. 2016. Type 3 Secretion Translocators Spontaneously Assemble a Hexadecameric Transmembrane Complex. *J Biol Chem,* 291, 6304-15.

ROSNER, B. M., STARK, K. & WERBER, D. 2010. Epidemiology of reported Yersinia enterocolitica infections in Germany, 2001-2008. *BMC Public Health,* 10, 337.

ROSQVIST, R., MAGNUSSON, K. E. & WOLF-WATZ, H. 1994. Target cell contact triggers expression and polarized transfer of Yersinia YopE cytotoxin into mammalian cells. *EMBO J,* 13, 964-72.

ROSQVIST, R., PERSSON, C., HAKANSSON, S., NORDFELDT, R. & WOLF-WATZ, H. 1995. Translocation of the Yersinia YopE and YopH virulence proteins into target cells is mediated by YopB and YopD. *Contrib Microbiol Immunol,* 13, 230-4.

ROSS, J. A. & PLANO, G. V. 2011. A C-terminal region of Yersinia pestis YscD binds the outer membrane secretin YscC. *J Bacteriol,* 193, 2276-89.

ROTHBAUER, U., ZOLGHADR, K., TILLIB, S., NOWAK, D., SCHERMELLEH, L., GAHL, A., BACKMANN, N., CONRATH, K., MUYLDERMANS, S., CARDOSO, M. C. & LEONHARDT, H. 2006. Targeting and tracing antigens in live cells with fluorescent nanobodies. *Nat Methods,* 3, 887-9.

ROUSHAN, M. R., DE ZEEUW, M. A. M., HOOYKAAS, P. J. J. & VAN HEUSDEN, G. P. H. 2018. Application of phiLOV2.1 as a fluorescent marker for visualization of Agrobacterium effector protein translocation. *Plant J,* 96, 685-699.

RUDOLPH, M., CARSTEN, A., KULNIK, S., AEPFELBACHER, M. & WOLTERS, M. 2022. Live imaging of Yersinia translocon formation and immune recognition in host cells. *PLoS Pathog,* 18**,** e1010251.

RUST, M. J., BATES, M. & ZHUANG, X. 2006. Sub-diffraction-limit imaging by stochastic optical reconstruction microscopy (STORM). *Nat Methods,* 3**,** 793-5.

SABINA, Y., RAHMAN, A., RAY, R. C. & MONTET, D. 2011. Yersinia enterocolitica: Mode of Transmission, Molecular Insights of Virulence, and Pathogenesis of Infection. *J Pathog,* 2011**,** 429069.

SAL-MAN, N., DENG, W. & FINLAY, B. B. 2012. EscI: a crucial component of the type III secretion system forms the inner rod structure in enteropathogenic Escherichia coli. *Biochem J,* 442**,** 119-25.

SCHAAKE, J., DREES, A., GRUNING, P., ULICZKA, F., PISANO, F., THIERMANN, T., VON ALTROCK, A., SEEHUSEN, F., VALENTIN-WEIGAND, P. & DERSCH, P. 2014. Essential role of invasin for colonization and persistence of Yersinia enterocolitica in its natural reservoir host, the pig. *Infect Immun,* 82**,** 960-9.

SCHERMELLEH, L., FERRAND, A., HUSER, T., EGGELING, C., SAUER, M., BIEHLMAIER, O. & DRUMMEN, G. P. C. 2019. Super-resolution microscopy demystified. *Nat Cell Biol,* 21**,** 72-84.

SCHMIDT, R., WEIHS, T., WURM, C. A., JANSEN, I., REHMAN, J., SAHL, S. J. & HELL, S. W. 2021. MINFLUX nanometer-scale 3D imaging and microsecond-range tracking on a common fluorescence microscope. *Nat Commun,* 12**,** 1478.

SCHMIDT, R., WURM, C. A., JAKOBS, S., ENGELHARDT, J., EGNER, A. & HELL, S. W. 2008. Spherical nanosized focal spot unravels the interior of cells. *Nat Methods,* 5**,** 539-44.

SHIM, S. H., XIA, C., ZHONG, G., BABCOCK, H. P., VAUGHAN, J. C., HUANG, B., WANG, X., XU, C., BI, G. Q. & ZHUANG, X. 2012. Super-resolution fluorescence imaging of organelles in live cells with photoswitchable membrane probes. *Proc Natl Acad Sci U S A,* 109**,** 13978-83.

SHIMOMURA, O., JOHNSON, F. H. & SAIGA, Y. 1962. Extraction, purification and properties of aequorin, a bioluminescent protein from the luminous hydromedusan, Aequorea. *J Cell Comp Physiol,* 59**,** 223-39.

SHU, X., LEV-RAM, V., DEERINCK, T. J., QI, Y., RAMKO, E. B., DAVIDSON, M. W., JIN, Y., ELLISMAN, M. H. & TSIEN, R. Y. 2011. A genetically encoded tag for correlated light and electron microscopy of intact cells, tissues, and organisms. *PLoS Biol,* 9**,** e1001041.

SIEBEN, C., BANTERLE, N., DOUGLASS, K. M., GONCZY, P. & MANLEY, S. 2018. Multicolor single-particle reconstruction of protein complexes. *Nat Methods,* 15**,** 777-780.

SIMONET, M. & FALKOW, S. 1992. Invasin expression in Yersinia pseudotuberculosis. *Infect Immun,* 60**,** 4414-7.

SPRETER, T., YIP, C. K., SANOWAR, S., ANDRE, I., KIMBROUGH, T. G., VUCKOVIC, M., PFUETZNER, R. A., DENG, W., YU, A. C., FINLAY, B. B., BAKER, D., MILLER, S. I. & STRYNADKA, N. C. 2009. A conserved structural motif mediates formation of the periplasmic rings in the type III secretion system. *Nat Struct Mol Biol,* 16**,** 468-76.

SPYROU, M. A., TUKHBATOVA, R. I., WANG, C. C., VALTUENA, A. A., LANKAPALLI, A. K., KONDRASHIN, V. V., TSYBIN, V. A., KHOKHLOV, A., KUHNERT, D., HERBIG, A., BOS, K. I. & KRAUSE, J. 2018. Analysis of

3800-year-old Yersinia pestis genomes suggests Bronze Age origin for bubonic plague. *Nat Commun,* 9**,** 2234.

SUKHAN, A., KUBORI, T. & GALAN, J. E. 2003. Synthesis and localization of the Salmonella SPI-1 type III secretion needle complex proteins PrgI and PrgJ. *J Bacteriol,* 185**,** 3480-3.

TAKAO, T., TOMINAGA, N., SHIMONISHI, Y., HARA, S., INOUE, T. & MIYAMA, A. 1984. Primary structure of heat-stable enterotoxin produced by Yersinia enterocolitica. *Biochem Biophys Res Commun,* 125**,** 845-51.

TAMANO, K., AIZAWA, S., KATAYAMA, E., NONAKA, T., IMAJOH-OHMI, S., KUWAE, A., NAGAI, S. & SASAKAWA, C. 2000. Supramolecular structure of the Shigella type III secretion machinery: the needle part is changeable in length and essential for delivery of effectors. *EMBO J,* 19**,** 3876-87.

THORSLUND, S. E., EDGREN, T., PETTERSSON, J., NORDFELTH, R., SELLIN, M. E., IVANOVA, E., FRANCIS, M. S., ISAKSSON, E. L., WOLF-WATZ, H. & FALLMAN, M. 2011. The RACK1 signaling scaffold protein selectively interacts with Yersinia pseudotuberculosis virulence function. *PLoS One,* 6**,** e16784.

TORRES-VARGAS, C. E., KRONENBERGER, T., ROOS, N., DIETSCHE, T., POSO, A. & WAGNER, S. 2019. The inner rod of virulence-associated type III secretion systems constitutes a needle adapter of one helical turn that is deeply integrated into the system's export apparatus. *Mol Microbiol,* 112**,** 918-931.

TREILLE, G.-F. & YERSIN, A. 1894. La peste bubonique à Hong Kong. *VIIIe Congrès international d'hygiène et de démographie.*

TROISFONTAINES, P. & CORNELIS, G. R. 2005. Type III secretion: more systems than you think. *Physiology (Bethesda),* 20**,** 326-39.

TSENG, T. T., TYLER, B. M. & SETUBAL, J. C. 2009. Protein secretion systems in bacterial-host associations, and their description in the Gene Ontology. *BMC Microbiol,* 9 Suppl 1**,** S2.

VAN DE LINDE, S., LOSCHBERGER, A., KLEIN, T., HEIDBREDER, M., WOLTER, S., HEILEMANN, M. & SAUER, M. 2011. Direct stochastic optical reconstruction microscopy with standard fluorescent probes. *Nat Protoc,* 6**,** 991-1009.

VAN ENGELENBURG, S. B. & PALMER, A. E. 2008. Quantification of real-time Salmonella effector type III secretion kinetics reveals differential secretion rates for SopE2 and SptP. *Chem Biol,* 15**,** 619-28.

VAN ENGELENBURG, S. B. & PALMER, A. E. 2010. Imaging type-III secretion reveals dynamics and spatial segregation of Salmonella effectors. *Nat Methods,* 7**,** 325-30.

VAN NHIEU, G. T. & ISBERG, R. R. 1991. The Yersinia pseudotuberculosis invasin protein and human fibronectin bind to mutually exclusive sites on the alpha 5 beta 1 integrin receptor. *J Biol Chem,* 266**,** 24367-75.

VAN PELT, W. W., M. A. S. DE; WANNET, W. J. B.; LIGTVOET, E. J. J.; WIDDOWSON, M. A.; VAN DUYNHOVEN, Y. T. H. P. 2003. Laboratory surveillance of bacterial gastroenteric pathogens in The Netherlands, 1991-2001. *Epidemiology and infection,* 130**,** 431-441.

VIBOUD, G. I. & BLISKA, J. B. 2001. A bacterial type III secretion system inhibits actin polymerization to prevent pore formation in host cell membranes. *EMBO J,* 20**,** 5373-82.

VIBOUD, G. I. & BLISKA, J. B. 2005. Yersinia outer proteins: role in modulation of host cell signaling responses and pathogenesis. *Annu Rev Microbiol,* 59**,** 69-89.

VIBOUD, G. I., MEJIA, E. & BLISKA, J. B. 2006. Comparison of YopE and YopT activities in counteracting host signalling responses to Yersinia pseudotuberculosis infection. *Cell Microbiol,* 8**,** 1504-15.

VIRANT, D., TRAENKLE, B., MAIER, J., KAISER, P. D., BODENHOFER, M., SCHMEES, C., VOJNOVIC, I., PISAK-LUKATS, B., ENDESFELDER, U. & ROTHBAUER, U. 2018. A peptide tag-specific nanobody enables high-quality labeling for dSTORM imaging. *Nat Commun,* 9**,** 930.

WAGNER, S. & DIEPOLD, A. 2020. A Unified Nomenclature for Injectisome-Type Type III Secretion Systems. *Curr Top Microbiol Immunol,* 427**,** 1-10.

WAGNER, S., GRIN, I., MALMSHEIMER, S., SINGH, N., TORRES-VARGAS, C. E. & WESTERHAUSEN, S. 2018. Bacterial type III secretion systems: a complex device for the delivery of bacterial effector proteins into eukaryotic host cells. *FEMS Microbiol Lett,* 365.

WAGNER, S., KONIGSMAIER, L., LARA-TEJERO, M., LEFEBRE, M., MARLOVITS, T. C. & GALAN, J. E. 2010. Organization and coordinated assembly of the type III secretion export apparatus. *Proc Natl Acad Sci U S A,* 107**,** 17745-50.

WALDO, G. S., STANDISH, B. M., BERENDZEN, J. & TERWILLIGER, T. C. 1999. Rapid protein-folding assay using green fluorescent protein. *Nat Biotechnol,* 17**,** 691-5.

WANG, X., HYBISKE, K. & STEPHENS, R. S. 2018. Direct visualization of the expression and localization of chlamydial effector proteins within infected host cells. *Pathog Dis,* 76.

WATTIAU, P., BERNIER, B., DESLEE, P., MICHIELS, T. & CORNELIS, G. R. 1994. Individual chaperones required for Yop secretion by Yersinia. *Proc Natl Acad Sci U S A,* 91**,** 10493-7.

WAUTERS, G., KANDOLO, K. & JANSSENS, M. 1987. Revised biogrouping scheme of Yersinia enterocolitica. *Contrib Microbiol Immunol,* 9**,** 14-21.

WEILL, C. O., BIRI, S. & ERBACHER, P. 2008. Cationic lipid-mediated intracellular delivery of antibodies into live cells. *Biotechniques,* 44**,** Pvii-Pxi.

WESTPHAL, V. & HELL, S. W. 2005. Nanoscale resolution in the focal plane of an optical microscope. *Phys Rev Lett,* 94**,** 143903.

WILSON, W. D., TANIOUS, F. A., BARTON, H. J., JONES, R. L., FOX, K., WYDRA, R. L. & STREKOWSKI, L. 1990. DNA sequence dependent binding modes of 4',6-diamidino-2-phenylindole (DAPI). *Biochemistry,* 29**,** 8452-61.

WOLTERS, M., BOYLE, E. C., LARDONG, K., TRULZSCH, K., STEFFEN, A., ROTTNER, K., RUCKDESCHEL, K. & AEPFELBACHER, M. 2013. Cytotoxic necrotizing factor-Y boosts Yersinia effector translocation by activating Rac protein. *J Biol Chem,* 288**,** 23543-53.

WOLTERS, M., ZOBIAK, B., NAUTH, T. & AEPFELBACHER, M. 2015. Analysis of Yersinia enterocolitica Effector Translocation into Host Cells Using Beta-lactamase Effector Fusions. *J Vis Exp.*

WONG, K. W. & ISBERG, R. R. 2005. Yersinia pseudotuberculosis spatially controls activation and misregulation of host cell Rac1. *PLoS Pathog,* 1**,** e16.

WOOD, S. E., JIN, J. & LLOYD, S. A. 2008. YscP and YscU switch the substrate specificity of the Yersinia type III secretion system by regulating export of the inner rod protein YscI. *J Bacteriol,* 190**,** 4252-62.

WREN, B. W. 2003. The yersiniae--a model genus to study the rapid evolution of bacterial pathogens. *Nat Rev Microbiol,* 1**,** 55-64.

YANG, Q., LI, X., TU, H. & PAN, S. Q. 2017. Agrobacterium-delivered virulence protein VirE2 is trafficked inside host cells via a myosin XI-K-powered ER/actin network. *Proc Natl Acad Sci U S A,* 114**,** 2982-2987.

YANG, X., PAN, J., WANG, Y. & SHEN, X. 2018. Type VI Secretion Systems Present New Insights on Pathogenic Yersinia. *Front Cell Infect Microbiol,* 8**,** 260.

YIP, C. K., KIMBROUGH, T. G., FELISE, H. B., VUCKOVIC, M., THOMAS, N. A., PFUETZNER, R. A., FREY, E. A., FINLAY, B. B., MILLER, S. I. & STRYNADKA, N. C. 2005. Structural characterization of the molecular platform for type III secretion system assembly. *Nature,* 435**,** 702-7.

YOUNG, A. M., MINSON, M., MCQUATE, S. E. & PALMER, A. E. 2017. Optimized Fluorescence Complementation Platform for Visualizing Salmonella Effector Proteins Reveals Distinctly Different Intracellular Niches in Different Cell Types. *ACS Infect Dis,* 3**,** 575-584.

YOUNG, B. M. & YOUNG, G. M. 2002. Evidence for targeting of Yop effectors by the chromosomally encoded Ysa type III secretion system of Yersinia enterocolitica. *J Bacteriol,* 184**,** 5563-71.

ZHANG, Y., LARA-TEJERO, M., BEWERSDORF, J. & GALAN, J. E. 2017. Visualization and characterization of individual type III protein secretion machines in live bacteria. *Proc Natl Acad Sci U S A,* 114**,** 6098-6103.

ZLOKARNIK, G., NEGULESCU, P. A., KNAPP, T. E., MERE, L., BURRES, N., FENG, L., WHITNEY, M., ROEMER, K. & TSIEN, R. Y. 1998. Quantitation of transcription and clonal selection of single living cells with beta-lactamase as reporter. *Science,* 279**,** 84-8.
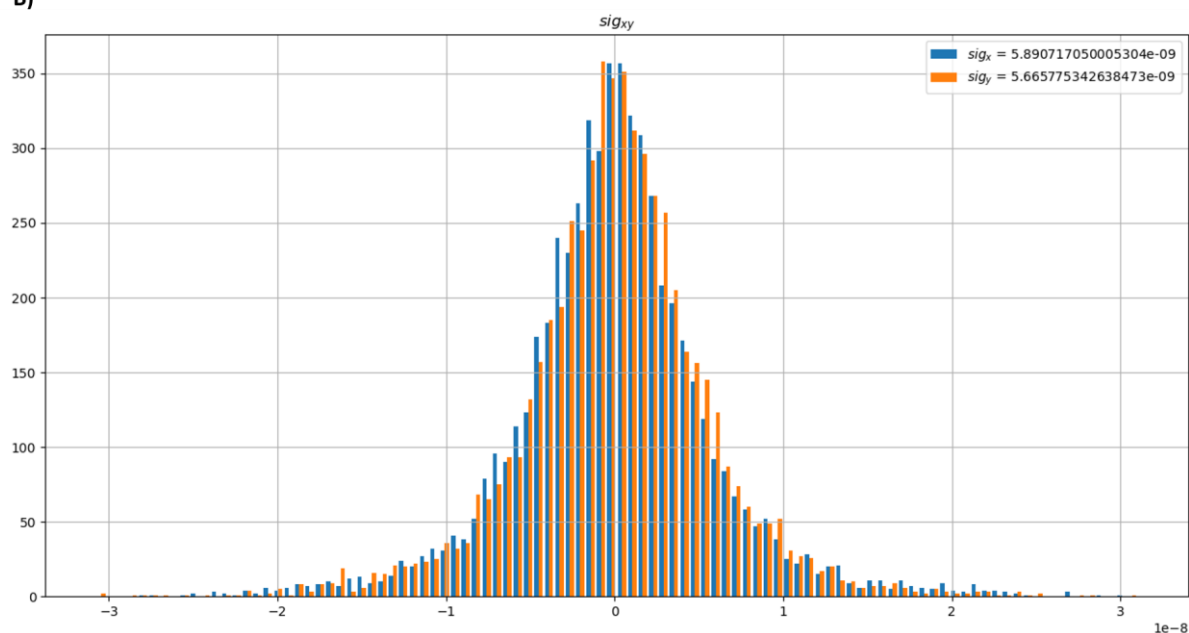
8 Supplement

Supplemental Fig. 1

A)
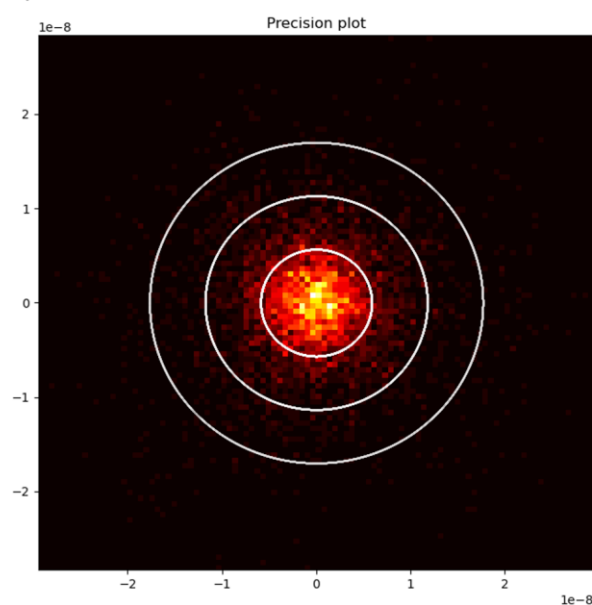
B)

Supplemental Figure 1 Localization precision of YopD-ALFA MINFLUX nanoscopy. Adapted from: Carsten et al., 2022.

(A) Lateral precision of YopD-ALFA localizations.

(B) Histogram of the distance between individual localizations of a single fluorophore and its mean position estimate.

9 List of figures

10 List of tables

11 Abbreviations

Abbreviation	Meaning
°C	degree celsius
µg	microgram
µl	microliter
µm	micrometer
µM	micromolar
µs	mirosecond
2D	two dimensional
2nd	secondary
3D	three dimensional
4Cys	tetracysteine hairpin loop
aa	aminoacid
AF	Alexa Fluor
Ail	attachment invasion locus
APD	avalanche photodiode
APS	ammonium persulfate
Ars	arsenite
ATP	adenosine triphosphate
bla	beta lactamase
BSA	bovine serum albumin
Ca^{2+}	calcium
$CaCl_2$	calcium chloride
cm	centimeter
CO_2	carbon dioxide
DAPI	4',6-diamidino-2-phenylindole
ddH_2O	double distilled water
DMEM	Dulbecco's modified eagle's medium
DMSO	dimethyl sulfoxide
DNA	deoxyribonucleic acid
Dr.	doctor
e.g.	for example (lat.: "exempli gratia")
EDTA	ethylenediamine tetra-acetic acid
eGFP	enhanced green fluorescent protein
EGTA	ethylene glycol-bis(β-aminoethyl ether)-N,N,N',N'-tetraacetic acid
et al.	and others (lat.: "et alteri")
Esc	*Escherichia coli* secretion components
eYFP	enhanced yellow fluorescent protein
FAE	follicle-associated epithelium
FCS	fetal calf serum
Fig.	figure
FlAsH	fluorescein based biarsenical dye
FliN	Flagellar motor switch protein FliN
FWHM	full width at half maximum
g	gram
g	relative centrifugal force
GBP1	guanylate-binding protein 1
GFP	green fluorescent protein

GFP 11	11th beta strand of GFP
GTP	guanosine 5-triphosphate
h	hour
HCl	hydrochloric acid
HCM	host cell membrane
HPI	high pathogenicity island
HRP	horseradish peroxidase
Hz	Hertz
i.e.	that is (lat.: "id est")
IF	immunofluorescence
Ig	immunoglobulin
IM	inner membrane
Inv	invasion
Kan	kanamycin
Kb	kilobase
kDa	kilodalton
l	liter
LB	lysogeny broth
LcrV	low calcium response protein V
LOV	light, oxygen and voltage-sensing domain
m	meter
M	molar
m^2	square meter
mA	milliampere
M-cells	microfold cells
MDa	megadalton
MEA	mercaptoethylamine
$MgCl_2$	magnesium chloride
min	minute
MINFLUX	minimal photon fluxes
ml	milliliter
mm	millimeter
mM	millimolar
MOI	multiplicity of infection
mRNA	messenger RNA
ms	millisecond
Mxi	membrane expression of Ipa
NA	numerical aperture
NaCl	sodium chloride
NaOH	sodium hydroxide
NbALFA	nanobody against the ALFA-tag
nM	nanomolar
nM	nanometer
ns	nanosecond
OD	optical density
OM	outer membrane
Org	oxygen repressed gene
PAGE	polyacrylamide gel electrophoresis
PALM	photoactivated localization microscopy
PBS	phosphate buffered saline
PBS-T	phosphate buffered saline with Tween-20

PFA	paraformaldehyde
PG	peptidoglycan layer
pH	power of/potential for hydrogen
PLC	phospholipase C
POI	protein of interest
Pop	*Pseudomonas* outer protein
Prg	PhoP repressed gene
ps	picosecond
PSF	point spread function
PVDF	polyvinylidendifluoride membrane
pYV	*Yersinia* virulence plasmid
Rac	Ras-related C3 botulinum toxin substrate
Rho	Ras homolog gene family
RNA	ribonucleic acid
Rpm	revolutions per minute
RT	room temperature
Sct	secretion and cellular translocation
SCy5	Sulfo-Cyanin 5
SDS	sodium-dodecylsulfate
Sec	secretion
SIM	structured illumination microscopy
Sip	cell invasion protein
SMLM	single molecule localization microscopy
SOFI	super-resolution optical fluctuation imaging
Sop	Salmonella outer protein
Spa	surface presentation of antigens
SPI-2	Salmonella pathogenicity island 2
Spp.	species
Ssa	secretion system apparatus protein
Sse	secretion system effector
Ste	Salmonella translocated effector
STED	stimulated emission depletion
STORM	stochastic optical reconstruction microscopy
Suppl. Fig.	supplementary figure
Syc	specific Yop chaperone
T3SS	type 3 secretion system
TBS	Tris buffered saline
TBS-T	Tris buffered saline with Tween-20
TCA	trichloroacetic acid
Tir	transfer inhibition protein
TIRF	total internal reflections
UV	ultraviolet
V	volt
v/v	volume per volume
Vir	virulence
W	watt
w/v	weight per volume
WB	western blot
YadA	*Yersinia* adhesion A
Yop	*Yersinia* outer protein
Ysc	*Yersinia* secretion

Yst   *Yersinia* stable toxin
α   anti-

12 Publications

12.1 Publications

Rudolph, M., Carsten, A., Kulnik, S., Aepfelbacher, M., & Wolters, M. (2022). Live imaging of Yersinia translocon formation and immune recognition in host cells. *PLoS pathogens*, *18*(5), e1010251. https://doi.org/10.1371/journal.ppat.1010251

Carsten, A., Rudolph, M., Weihs, T., Schmidt, R., Jansen, I., Wurm, C. A., Diepold, A., Failla, A. V., Wolters, M., & Aepfelbacher, M. (2022). MINFLUX imaging of a bacterial molecular machine at nanometer resolution. *Methods and applications in fluorescence*, *11*(1), 10.1088/2050-6120/aca880. https://doi.org/10.1088/2050-6120/aca880

12.2 Presentations

Carsten, A., Rudolph, M., Weihs, T., Schmidt, R., Wurm, C. A., Diepold, A., Failla, A. V., Wolters, M., & Aepfelbacher, M. Visualization of Type III Secretion System components in *Yersinia enterocolitica* down to the molecular level by MINFLUX microscopy – Focus on Microscopy 2021, Online

Carsten, A., Zobiak, B., Knipp, S., Kreienkamp, H.J., Woike, D., Loreth, D., Meyer-Schwesinger, C., Failla, A.V. Live-STED imaging with outstanding spatio-temporal resolution: Proof of principle applications in biomedical imaging – Focus on Microscopy 2022, Online

Carsten, A., Rudolph, M., Weihs, T., Schmidt, R., Wurm, C. A., Diepold, A., Failla, A. V., Wolters, M., & Aepfelbacher, M. Visualization of Type III Secretion System components in *Yersinia enterocolitica* down to the molecular level by MINFLUX microscopy - DGHM 2022, Berlin, Germany

12.3 Poster

Carsten, A., Rudolph, M., Weihs, T., Schmidt, R., Wurm, C. A., Diepold, A., Failla, A. V., Wolters, M., & Aepfelbacher, M. Visualization of Type III Secretion System components in *Yersinia enterocolitica* down to the molecular level by MINFLUX

microscopy – EMBO Workshop: In situ Structural Biology – From Cryo-EM to Integrative Modelling 2020, Online

Carsten, A., Rudolph, M., Weihs, T., Schmidt, R., Wurm, C. A., Diepold, A., Failla, A. V., Wolters, M., & Aepfelbacher, M. Visualization of Type III Secretion System components in *Yersinia enterocolitica* down to the molecular level by MINFLUX microscopy – EMBO/EMBL symposium: New Approaches and Concepts in Microbiology 2021, Online

Carsten, A., Rudolph, M., Weihs, T., Schmidt, R., Jansen, I., Wurm, C. A., Diepold, A., Failla, A. V., Wolters, M., & Aepfelbacher, M. Two color- and 3D- MINFLUX nanoscopy visualizes elementary type III secretion system proteins in *Yersinia enterocolitica* – Focus on Microscopy 2022, Online

13 Danksagung

Mein erster Dank gilt meinem Doktorvater Prof. Dr. Martin Aepfelbacher. Der Dank gilt nicht nur für die Bereitstellung des Themas und für die Betreuung, Förderung und Unterstützung, sondern auch dafür, dass du mir viele Freiheiten gegeben hast und es mir ermöglicht hast an vielen Konferenzen teilzunehmen, ich jederzeit Dinge ausprobieren konnte und immer ein offenes Ohr für mich hattest, nicht nur im Fachlichen.

Herrn Prof. Dr. Thomas Marlovits danke ich für die Bereitschaft zur Übernahme der Begutachtung meiner Dissertation.

Ein sehr großer, besonderer Dank geht an Virgilio. Du hast mich während der gesamten Zeit über das zu erwartende Maß hinaus gefördert und unterstützt. Immer wenn ich es gebraucht habe, hast du mich motiviert und dir meine Probleme angehört. Ich werde unsere vielen Fahrten nach Göttingen in guter Erinnerung behalten. Ich konnte jederzeit auf deine fachliche und persönliche Meinung zählen, egal in welcher Situation und wie gestresst du selbst zu diesem Zeitpunkt warst. Danke!

Selbstverständlich möchte ich auch den Menschen bei Abberior Instruments und insbesondere Christian, Tobi, Roman und Isabelle für eine tolle Kooperation danken. Es hat mir immer Freude bereitet nach Göttingen zu kommen und das MINFLUX in allen möglichen verschiedenen Entwicklungsstadien nutzen zu können.

Vielen Dank natürlich auch an alle ehemaligen und jetzigen Mitglieder des MiBi-Instituts. Es ist eine wunderbare und –same Arbeitsumgebung. Ich hatte und habe hier immer viel Spaß.

Danke Manuel für tiefgreifende, wissenschaftliche Diskussionen mit dir und für deine Korrekturen. Gesche, danke dir für deinen unermüdlichen Arbeitseinsatz, deine Frusttoleranz und deine Hilfe. Ich hoffe, dass wir noch viele Jahre zusammenarbeiten können. Vielen Dank Gunni für einen tollen gemeinsamen Start im Labor, für gemeinsame Abende mit Nachwirkungen, für die gegenseitige

Offenheit und für den dauerhaften Quatsch und Spaß. Asiri, danke für viele unterhaltsame Monate im Labor und deine fleißige Mitarbeit. Danke Claudia für viele Gespräche über Sinn und Unsinn und dein beeindruckendes Wissen darüber, wer was wann wie wo gemacht hat und in welchem Tiefkühlfach das jetzt zu finden ist. Sören, danke für deine faszinierend entspannte Art und deine „Ach, das wird schon"-Haltung. Für musikalische Unterhaltung und unterhaltsames deutsch-österreichisches Gebrabbel (sowohl sprachlich als auch inhaltlich) vielen Dank an Su. Danke auch an Julie für Korrekturvorschläge, deine ruhige Art und deine Frusttoleranz gegenüber der Forschung.

Paul, unsere Dänemarkurlaube werde ich in guter Erinnerung behalten, genauso wie die zahllosen (!) Siege im Dart gegen dich. Deine Musikauswahl eher nicht.

Für viele gemeinsame Sonntagabende mit immer sehr guter Verpflegung, insbesondere während der Corona-Pandemie, danke an Elena und Matze. Malte, Robert und Felix, vielen Dank für schöne Reisen und Wochenenden. Danke euch allen, ihr seid tolle Freunde und ich bin froh, euch in meinem Leben zu haben!

Ute, danke, dass du dafür sorgst, dass ich mich nicht zu viel stresse, du immer für mich da bist und dass du genau der Mensch bist, der du bist!

Der allerwichtigste Dank gilt meinen Eltern Silke und Uwe. Euch habe ich zu verdanken, dass ich jetzt da bin, wo ich bin und dass ich ein so tolles, glückliches und erfülltes Leben führen darf. Danke, dass ihr mich jederzeit gefördert habt und weiterhin fördert, für euer Interesse an meiner Arbeit, für euer Verständnis und vor allem natürlich für eure unendliche Liebe! Ein Kind kann sich keine besseren Eltern wünschen!

14 Lebenslauf

Zur Person

Name   Alexander Carsten

Geburtsdatum und -ort   10.05.1992, Einbeck

Nationalität   Deutsch

Ausbildungsweg

2004 – 2011:

Allgemeine Hochschulreife mit naturwissenschaftlichem Schwerpunkt an der Goetheschule Einbeck (Gymnasium)

Abschlussnote: 1,9

WS 2011/2012 – SS 2014:

Studiengang Bachelor of Science in Biologie mit dem Schwerpunkt Genetik und organismische Interaktionen an der Philipps-Universität Marburg

Abschlussarbeit: „Identification of aspartyl proteases involved in processing of the signaling mucin Msb2 in *Ustilago maydis*" am Max-Planck-Institut für terrestrische Mikrobiologie, AG Prof. Dr. Regine Kahmann, Marburg

Abschlussnote: 1,9

WS 2014/2015 – WS 2016/2017:

Studiengang Master of Science in „Molecular and Cellular Biology" mit dem Schwerpunkt Genetik und organismische Interaktionen an der Philipps-Universität Marburg

Abschlussarbeit: "Localisation of the repetitive effector protein Rsp3 in *Ustilago maydis*" am

Max-Planck-Institut für terrestrische Mikrobiologie, AG Prof. Dr. Regine Kahmann, Marburg

Abschlussnote: 1,4

Seit Juni 2018:

Doktorandenstelle im Institut für medizinische Mikrobiologie, Virologie und Hygiene am Universitätsklinikum Hamburg-Eppendorf

Veröffentlichungen

Ma LS, Wang L, Trippel C, Mendoza-Mendoza A, Ullmann S, Moretti M, Carsten A, Kahnt J, Reissmann S, Zechmann B, Bange G, Kahmann R. The Ustilago maydis repetitive effector Rsp3 blocks the antifungal activity of mannose-binding maize proteins. Nat Commun. 2018 Apr 27;9(1):1711. doi: 10.1038/s41467-018-04149-0. PMID: 29703884; PMCID: PMC5923269.

Braun F, Lütgehetmann M, Pfefferle S, Wong MN, Carsten A, Lindenmeyer MT, Nörz D, Heinrich F, Meißner K, Wichmann D, Kluge S, Gross O, Pueschel K, Schröder AS, Edler C, Aepfelbacher M, Puelles VG, Huber TB. SARS-CoV-2 renal tropism associates with acute kidney injury. Lancet. 2020 Aug 29;396(10251):597-598. doi: 10.1016/S0140-6736(20)31759-1. Epub 2020 Aug 17. PMID: 32818439; PMCID: PMC7431179.

Rudolph M, Carsten A, Kulnik S, Aepfelbacher M, Wolters M. Live imaging of Yersinia translocon formation and immune recognition in host cells. PLoS Pathog. 2022 May 23;18(5):e1010251. doi: 10.1371/journal.ppat.1010251. PMID: 35604950; PMCID: PMC9173619.

Carsten A, Rudolph M, Weihs T, Schmidt R, Jansen I, Wurm CA, Diepold A, Failla AV, Wolters M, Aepfelbacher M. MINFLUX imaging of a bacterial molecular machine at nanometer resolution. Methods Appl Fluoresc. 2022 Dec 13;11(1). doi: 10.1088/2050-6120/aca880. PMID: 36541558.

15 Eidesstattliche Versicherung

Ich versichere ausdrücklich, dass ich die Arbeit selbständig und ohne fremde Hilfe verfasst, andere als die von mir angegebenen Quellen und Hilfsmittel nicht benutzt und die aus den benutzten Werken wörtlich oder inhaltlich entnommenen Stellen einzeln nach Ausgabe (Auflage und Jahr des Erscheinens), Band und Seite des benutzten Werkes kenntlich gemacht habe.

Ferner versichere ich, dass ich die Dissertation bisher nicht einem Fachvertreter an einer anderen Hochschule zur Überprüfung vorgelegt oder mich anderweitig um Zulassung zur Promotion beworben habe.

Ich erkläre mich einverstanden, dass meine Dissertation vom Dekanat der Medizinischen Fakultät mit einer gängigen Software zur Erkennung von Plagiaten überprüft werden kann.

Unterschrift: